

Characteristics and Modeling of Site Response Using Downhole Seismic Records

Ahmed-W. Elgamal
University of California at San Diego
Department of Applied Mechanics and Engineering Sciences
La Jolla, CA 92093-0411

Mourad Zeghal
Rensselaer Polytechnic Institute
Department of Civil Engineering
Troy, NY 12180

Award Number 1434-97-G-03070
Program Element and Objective number III.3

Research supported by U.S. Geological Survey (USGS),
Department of the Interior, under USGS Award number 1434-97-G-03070.
The views and conclusions contained in this document
are those of the authors and should not be interpreted
as necessarily representing the official policies,
either expressed or implied, of the U.S. Government.

Abstract

Vertical downhole arrays are deployed to record seismic soil (and overall site) behavior. Such arrays have already recorded a large body of benchmark earthquake case histories worldwide. These valuable records document: (1) mechanisms of vertical wave propagation and site resonance, (2) characteristics of site amplification for soft and stiff soil formations, (3) cyclic soil behavior during liquefaction. At present, downhole-array data offer a most effective means for calibration and verification of our predictive computational capabilities.

This report consists of three elements. The first element presents a review focused on seven vertical-array sites that have been widely studied in the last few years. A number of techniques developed for analyses of downhole seismic records are presented. Relevance of each downhole site, characteristics of the installed array, available seismic records, and lessons learned to date are discussed.

In the second element, free-field downhole array seismic records are employed to identify and model the dynamic response at Wildlife Refuge (California, USA), and Port Island (Kobe, Japan) sites. The Wildlife Refuge site was instrumented in 1982 with a two-accelerometer array, and six piezometers that recorded a case of seismically induced site liquefaction. At Port Island, a four-accelerometer downhole array recorded strong motion during the recent 1995 Hyogoken-Nanbu Earthquake. Using this downhole data, the actual seismic shear stress-strain histories are directly evaluated from the recorded downhole accelerations. These histories provide valuable insight into the mechanisms of site liquefaction and associated loss of stiffness and strength. Computational simulations of these case histories are performed based on the identified mechanisms of site response.

In the third element, the process of dynamically induced liquefaction in two centrifuge soil models is analyzed. These models consist of saturated medium-dense sand overlain by a low permeability silt deposit; and represent prototypes of a level site and an embankment. The recorded lateral accelerations are employed to evaluate shear stress and strain histories at different elevations within the tested soil-systems. These histories shed light on the involved liquefaction process, and the associated mechanisms of: (1) lateral deformation, (2) stiffness and strength degradation, and (3) possible densification and regain of stiffness, thereafter. The identified response patterns are found comparable to those documented by laboratory cyclic-loading tests.

Finally, general conclusions are drawn based on the identified soil/site dynamic properties.

Contents

1	Introduction	13
2	Site Response and Vertical Seismic Arrays	15
2.1	Introduction	15
2.2	Scope	15
2.3	Historical Review	16
2.4	Chiba Array, Japan	17
2.4.1	Three dimensional seismic strains ^[24,25]	17
2.5	Lotung, Taiwan	18
2.5.1	Correlation analyses	20
2.5.2	Spectral analyses	21
2.5.3	Shear stress-strain histories	21
2.5.4	System identification and computational model calibration	23
2.6	Hualien, Taiwan	23
2.7	Garner Valley, California, USA	23
2.8	Treasure Island, California, USA	24
2.9	Wildlife-Refuge, California USA	24
2.9.1	Transfer function analyses	25
2.10	Port Island, Kobe Japan	27
2.11	References	28
3	Identification and Modeling of Earthquake Site Liquefaction	37
3.1	Introduction	37
3.2	Scope	37
3.3	Analysis Techniques	38
3.4	Wildlife-Refuge, California USA	38
3.4.1	Instrumentation and seismic records	38
3.4.2	Seismic site response	42
3.5	Port Island, Kobe Japan	53
3.5.1	Instrumentation and seismic records	53
3.5.2	Shear stress-strain histories	53
3.5.3	Computational simulation	57
3.6	References	57

4	Mechanism of Liquefaction Response in Sand-Silt Sites Using Dynamic Centrifuge Tests	67
4.1	Introduction	67
4.2	Testing Procedures	68
4.3	Evaluation Of Shear Stress-Strain Histories	68
4.4	Level Site Response: Model 4a	70
4.4.1	Stress-strain histories	71
4.4.2	Liquefaction mechanism	76
4.5	Embankment Response: Model 6	76
4.5.1	Stress-strain histories	76
4.6	Appendix I: Analysis Approximations	89
4.7	References	90
5	Conclusions	93
6	Acknowledgments	95

List of Figures

2.1	Three-dimensional array at Chiba, Japan ^[14]	19
2.2	Instrumentation of Lotung experiment site ^[15] : (a) downhole array; (b) surface array.	20
2.3	Samples of Lotung site shear stress-strain cycles at 6 m depth ^[41,42,45]	22
2.4	Wildlife Refuge shear stress-strain response at 3.75 m depth ^[77,78]	26
2.5	Port Island shear stress-strain responses midway between accelerometers, at 8.0 m, 24.0 m and 57.5 m depths ^[78,89]	29
3.1	Cross-section and instrumentation at the Wildlife Refuge site (after Bennett <i>et al.</i> 1984).	39
3.2	Wildlife Refuge site NS and EW surface and downhole (at 7.5 m depth) accelerations during the Elmore Ranch 1987 earthquake.	40
3.3	Wildlife Refuge site NS and EW surface and downhole (at 7.5 m depth) accelerations, and associated pore water pressure (at 2.9 m depth) during the Superstition Hills 1987 earthquake.	41
3.4	Wildlife Refuge EW and NS shear stress-strain histories during the Elmore Ranch 1987 earthquake (evaluated from acceleration histories shown in Fig. 3.2).	43
3.5	Wildlife Refuge shear strain histories, and associated stress histories evaluated from recorded acceleration and predicted by the equivalent linear model.	44
3.6	Average shear wave velocity during the SH earthquake (NS and EW directions).	45
3.7	Wildlife-Refuge NS and EW shear stress-strain histories during the Superstition Hills 1987 Earthquake (evaluated from acceleration histories shown in Fig. 3.3).	46
3.8	Wildlife-Refuge NS and EW shear stress-strain histories during the Superstition Hills 1987 Earthquake (evaluated from acceleration and excess pore pressure histories shown in Fig. 3.3).	47
3.9	Shear stress-strain history during selected loading cycles of stages 1, 2 and 3 of the Superstition Hills earthquake.	48
3.10	Wildlife-Refuge shear stress-strain history during selected loading cycles of stages 3 and 4 of the Superstition Hills earthquake.	49
3.11	Wildlife-Refuge computed NS shear stress-strain and effective-stress histories during the Superstition Hills 1987 Earthquake.	50
3.12	Wildlife-Refuge shear stress-strain history during selected loading cycles of stages 3 and 4 of the Superstition Hills earthquake.	51
3.13	Wildlife-Refuge shear stress-strain history during selected loading cycles of stages 3 and 4 of the Superstition Hills earthquake.	52

3.14	Port Island map (showing reclaimed areas completed in 1981, after Nakakita and Watanabe 1981).	54
3.15	Soil profile and instrumentation at the Port Island site (after Iwasaki 1995a).	55
3.16	N44W accelerations at ground surface and downhole stations (at 16 m, 32 m and 83 m depths, after Iwasaki 1995a).	56
3.17	Port Island site shear stress-strain histories at 8.0 m, 16.0 m, 24.0 m, 32.0 m, and 57.5 m depths.	58
3.18	Selected N44W shear stress-strain cycles midway between accelerometers, at 8.0 m, 24.0 m and 57.5 m depths.	59
3.19	Port Island shear stress histories estimated from acceleration histories and corresponding constitutive model prediction (at 8.0 m, 24.0 m, and 57.5 m depths).	60
3.20	Port Island shear stress-strain histories estimated from acceleration histories and corresponding constitutive model prediction (at 8.0 m, 24.0 m, and 57.5 m depths).	61
3.21	Port Island recorded and computed accelerations at surface, 16 m and 32 m depth, and computed excess pore pressure ratio at 8 m depth.	62
4.1	Model configurations: (a) VELACS model 4a, and (b) VELACS model 6 (dimensions in prototype units).	72
4.2	Soil-system model and stress-strain sampling locations (model 4a).	73
4.3	UCD model 4a time histories: (a) accelerations at free surface, 3 m depth, 4.5 m depth, and associated input acceleration; (b) settlement at silt layer surface; and (c) excess pore pressures at 1.5 m, 3.1 m, and 4.5 m depths.	74
4.4	Sample acceleration and settlement records of RPI model 4b and CalTech model 4a.	75
4.5	UCD Model 4a shear stress and strain histories at 1.5 m, 3.0 m, 3.75 m, 4.5 m, and 5.25 m depths.	77
4.6	Selected cycles of UCD model 4a shear stress-strain histories at 1.5 m, 3.0 m, 3.75 m, 4.5 m, and 5.25 m depths.	78
4.7	Selected cycles of RPI model 4b shear stress-strain histories at 1.5 m, 3.0 m, 3.75 m, 4.5 m, and 5.25 m depths.	79
4.8	Shear stress, shear strain and EPP histories of a Nevada sand sample (at $D_r = 60\%$, and 160 kPa confining pressure) subject to a stress-controlled cyclic direct simple shear test [17].	80
4.9	Shear stress, shear strain and EPP histories of a Nevada sand sample (at $D_r = 40\%$, and 160 kPa confining pressure) subject to a stress-controlled cyclic direct simple shear test [17].	81
4.10	Model 6 recorded response: (a) acceleration histories at 0.3 m, 1.5 m, and 3.75 m depths, and associated input acceleration; (b) vertical settlement of the right slope at 1.25 m depth; and (c) excess pore pressure histories at 0.75 m, 1.35 m and 2.10 m depths.	82
4.11	Model 6 shear strain and stress histories at 0.9 m and 2.6 m depths.	84
4.12	Selected cycles of model 6 shear stress-strain histories at 0.9 m and 2.6 m depths.	85
4.13	Model 6 shear stress-strain history at 2.6 m depth (with superposed permanent deformation evaluated from settlement records).	86

4.14 Shear stress, shear strain and EPP histories of two Nevada sand samples (at $D_r = 60\%$ and $D_r = 40\%$) subject to a stress-controlled cyclic direct simple shear test and stress bias [17]. 87

4.15 Selected shear stress-strain cycles of two Nevada sand samples (at $D_r = 60\%$ and $D_r = 40\%$) subject to a stress-controlled cyclic direct simple shear test and stress bias [17]. 88

List of Tables

4.1	Transducer coordinates.	71
4.2	Soil properties.	71
4.3	Characteristics of employed filters.	92

Chapter 1

Introduction

This report consists of three elements. The first element is a review of seven vertical-array sites that have been widely studied in the last few years, by the authors and other researchers. Specifically, the reviewed arrays and studies are those of: the Chiba Site (Japan), the Lotung Site (Taiwan), the Hualien Site (Taiwan), the Garner Valley Site (California, USA), the Treasure Island Site (California, USA), the Wildlife Refuge Site (California, USA), and the Port Island Site (Kobe, Japan). This set of unique instrumented sites has provided valuable insights into the mechanisms of seismic soil response over a broad range of loading condition, including liquefaction and failure.

The second and third elements present new studies pertinent to earthquake induced liquefaction of sites and embankments. Analyses were conducted to investigate the recorded down-hole seismic response at Wildlife Refuge (California, USA), and Port Island (Kobe, Japan) sites. Within a unified framework, this report presents new findings, and summarizes a number of major results. The outcome of these liquefaction studies is supplemented by two centrifuge soil models. These models consist of saturated medium-dense sand overlain by a low permeability silt deposit; and represent prototypes of a level site and an embankment.

Chapter 2

Site Response and Vertical Seismic Arrays

2.1 Introduction

Damage due to seismic excitation is often directly correlated to local site conditions. The effects of surficial soil strata was evident during recent earthquakes in the form of motion amplification and/or liquefaction-induced ground deformations. For instance, the 1964 Niigata, the 1989 Loma Prieta, and the 1995 Kobe earthquakes, demonstrated the damaging effects of liquefaction-induced loss of soil strength and associated lateral spreading.

Currently, there remains a need to further understand and identify such response mechanisms. In this regard, the dynamic characteristics of ground response are being increasingly documented through a growing set of worldwide sites instrumented with vertical downhole seismic arrays. Downhole acceleration and excess-pore-pressure records provide direct insight into the response of instrumented soil layers within the ground. In addition, these records offer a solid basis for: (1) calibration of in-situ and laboratory testing procedures, and (2) refinement of empirical and computational predictive techniques. In the next sections, the selected vertical-array sites are described along with the relevant analysis techniques and identified soil response characteristics.

2.2 Scope

This review is focused on the following set of unique instrumented sites that have provided valuable insights into the mechanisms of seismic soil response.

The Chiba Site (Japan)

A network of 9 vertical arrays was installed to capture the three dimensional aspects of site seismic response. More than 160 earthquakes were recorded by the installed 44 surface and downhole instruments since 1982.

The Lotung Site (Taiwan)

A 1/4 scale model of a nuclear plant containment structure was constructed at this soft soil site. Three surface and two vertical arrays were installed to monitor free-field, structure, and soil-structure responses. Eighteen earthquakes were recorded during the period 1985-1986, including three moderate events (about 0.2 g peak lateral surface acceleration).

The Hualien Site (Taiwan)

Stiff soils prevail at this site. The instrumentation setup is similar to that of Lotung, with 3 downhole-accelerometer arrays. A total of 7 earthquakes were recorded during the period 1993-1995.

The Garner Valley Site (California, USA)

A vertical array consisting of six accelerometers was installed (USA and France sponsorship) at this relatively stiff and seismically-active site. This array has recorded numerous weak seismic events.

The Treasure Island Site (California, USA)

This site was instrumented in 1992 with an array of 6 downhole accelerometers and 8 pore pressure sensors. It is located within a soil-profile setting similar to that of the San Francisco Marina District. The array was installed to monitor the mechanisms associated with soil liquefaction as observed during recent Loma Prieta earthquake. So far, this array has recorded 2 low amplitude earthquakes in 1993 and 1996.

The Wildlife Refuge Site (California, USA)

This site was instrumented in 1982 with a surface and a downhole accelerometers and six pore pressure transducers (by the United States Geological Survey, USGS), in anticipation of a future seismically-induced liquefaction event. A unique set of acceleration and excess pore-water pressure records were obtained during the 1987 Superstition Hills earthquake. These records demonstrated for the first time a number of salient mechanisms associated with site liquefaction.

The Port Island Site (Kobe, Japan)

A five-accelerometer vertical-array was triggered during the 1995 Hyogoken-Nanbu Earthquake. The recorded response documented the observed widespread liquefaction of reclaimed ground.

The above mentioned arrays will be discussed in more detail in the following sections. In addition, a number of techniques for analyses of downhole seismic data will be reviewed. These techniques include:

Correlation and Spectral Analyses

These techniques were used to evaluate shear wave propagation characteristics, variation of shear wave velocity with depth, and site resonant frequencies and modal configurations. They were also used to document evidence of nonlinear site response.

Stress-Strain Imaging

This newly developed technique was employed to evaluate seismic shear stress-strain histories, directly from the recorded downhole accelerations.

System Identification

A number of procedures were employed to estimate soil stiffness and damping parameters, and to calibrate computational models of seismic site response.

2.3 Historical Review

In the United States, early downhole data sets were recorded at the San Francisco Bay area^[1,2,3], and at Union Bay in Seattle, Washington^[4,5,6]. The data was employed to verify site amplification procedures, study the response of Bay sediments for the San Francisco Trans-Bay Tube project, and analyze the response of peat and clay deposits in Seattle. In 1978, Abdel-Ghaffar

and Scott^[7,8] introduced a technique to evaluate stiffness and damping properties of earth dam soils from input-output earthquake response records. In Japan, early downhole array efforts were described by Kanai *et al.*^[9,10], Shima^[11], Akino *et al.*^[12], and Tajimi and Uchida^[13]. On the premises of Tokyo Station, an array of two surface and two downhole seismometers recorded a set of seven earthquakes^[11] in the late 1950's. Using these earthquake records, site resonance and damping characteristics were estimated^[6,11].

These early efforts were followed by more comprehensive array installations, such as at the Chiba^[14], Lotung^[15], Hualien^[16], Port Island^[17], and Treasure Island^[18] sites. Since the 1980's, data from downhole seismic arrays that include pore-pressure piezometers became increasingly available (e.g. Owi Island site in Japan^[19], Wildlife Refuge site in California^[20], and Lotung site in Taiwan^[15]). Such data sets offer a more complete picture of site response, when the potential for soil liquefaction exists. At present, numerous downhole arrays are in operation in seismically active regions worldwide. The data to be collected by these arrays will have a major impact on refining our understanding of seismic site response; and on developing more accurate and appropriate analysis and design tools.

2.4 Chiba Array, Japan

The prospect for conducting 3-dimensional (3D) studies using downhole array data is illustrated by the Chiba 3D dense array, installed by the University of Tokyo, Institute of Industrial Science^[14,21,22,23]. This array (Fig. 2.1) is located at Chiba Experiment Station, Institute of Industrial Science, University of Tokyo, Japan. Ground surface at the array location is essentially flat and the site is dry. Geological material consists of a top loam layer 4-5 m in thickness, followed by a 4 m thick clayey layer. A sand layer lies under this clayey stratum.

Site instrumentation was completed in April 1982, and was expanded with a complementary system to measure relative ground displacement and strains in December 1982. The instrumentation includes a dense network of downhole accelerometers, that constitute a system of 9 vertical arrays. The downhole accelerometers are located at 1 m, 5 m, 10 m, 20 m, and 40 m depth from ground surface.

Extensive data was recorded by the Chiba array (nearly 160 earthquake events). Most of these events produced low shaking levels with amplitudes below 0.05 g. However, peak ground accelerations of about 0.1g were recorded during one event, and 0.3 g during another. The recorded data was used to conduct numerous valuable studies including back-calculation of the 3D seismic strain field^[14,21,24,25], site amplification analyses^[22], and orientation error (also known as azimuthal error) analyses of the buried accelerometers^[23]. The 3D seismic strain analysis technique is outlined below. The entire set of downhole records is publicly available for the purposes of research (from the University of Tokyo, Institute of Industrial Science).

2.4.1 Three dimensional seismic strains^[24,25]

The dense 3D downhole configuration at Chiba allows for evaluation of the seismic strain field. For every tetrahedron, defined by a set on 4 non-coplanar accelerometers (Fig. 2.1), a finite

element interpolation may be used to approximate the displacement field, u_i , as follows:

$$u_i = \sum_{A=1}^4 N_A d_{Ai}, \quad i = 1, 2, 3 \quad (2.1)$$

in which $N_A = N_A(x_i)$ is the finite element shape function^[26] associated with tetrahedron node A , d_{Ai} is the i^{th} displacement component at node A , and x_i ($i = 1, 2, 3$) are the 3D Cartesian coordinate components. At any recording station, the dynamic component of earthquake displacement, d_{Ai} , may be evaluated through double time integration of the recorded accelerations. Thus, the strain field, ϵ_{ij} , within the tetrahedron is given by^[24,25]:

$$\epsilon_{ij} = \sum_{A=1}^4 \frac{1}{2} \left(\frac{\partial N_A}{\partial x_j} d_{Ai} + \frac{\partial N_A}{\partial x_i} d_{Aj} \right) \quad (2.2)$$

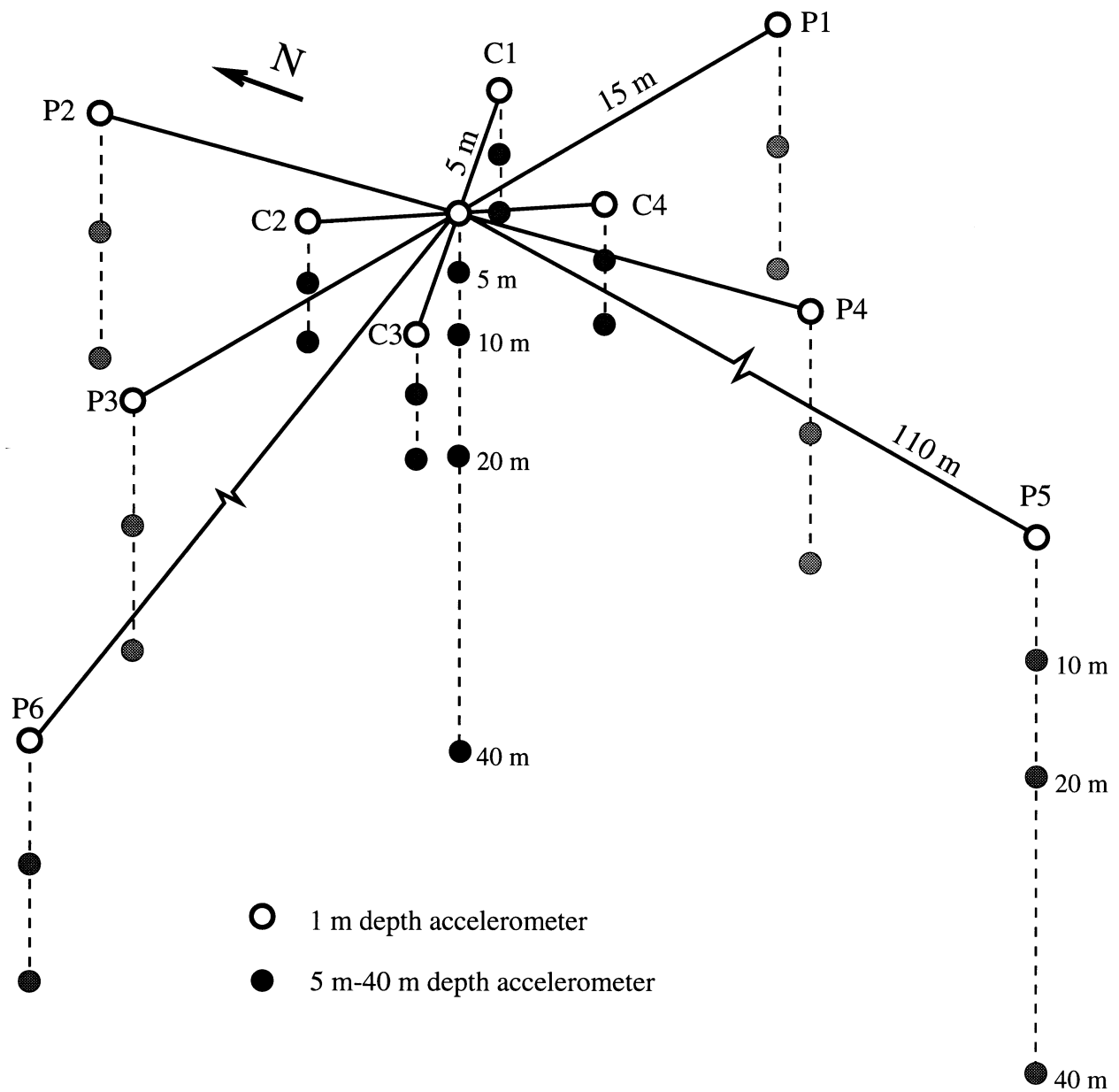
Katayama, Farjoodi, and co-workers^[24,25] evaluated the Chiba site seismic strain field using linear finite element shape functions. In general, the calculated strains were found to be in good agreement with those measured in-situ by the installed complementary displacement and strain instruments.

2.5 Lotung, Taiwan

The U.S. Electric Power Research Institute (EPRI) in cooperation with the Taiwan Power Company (TPC) conducted a Large-Scale Seismic Test (LSST) at a site near Lotung, within the southwestern quadrant of the SMART1 array^[15]. This test was conducted to shed light on the seismic response of nuclear power-plant containment structures founded on soft saturated soils. Two models (1/4-scale and 1/12-scale) of a nuclear-plant containment structure were constructed on a flat plain alluvium basin of vast lateral extent (in the vicinity of seismically active faults). Soil at this site consisted predominantly of inter-layered silty-sand and sandy-silt^[27]; and ground-water level was at or within 1 m of ground surface.

Extensive instrumentation was deployed to record both structural and ground seismic responses. The ground instrumentation included (Fig. 2.2) three linear surface arrays (arms 1, 2, and 3), and two downhole arrays (DHA and DHB) that extended to a depth of 47 m below ground surface^[15].

Eighteen earthquakes were recorded during the period 1985–1986^[15] at the Lotung site. This wealth of data constituted a basis for a number of valuable research efforts. Hadjian *et al.*^[28] compared a number of soil-structure studies and briefly reviewed the site stiffness and damping investigations. Chang *et al.*^[29,30,31,32] evaluated equivalent-linear dynamic shear moduli from the recorded downhole earthquake acceleration records. During each LSST earthquake, a representative equivalent linear shear modulus and effective shear strain were estimated, for each soil layer between consecutive downhole stations. The equivalent-linear shear moduli were identified using Fourier spectral ratios, and the effective shear strains were estimated by linear ground response deconvolution analyses. It was shown that the identified reduction in shear modulus, as a function of effective shear strain, was in agreement with laboratory test data. This reduction was a clear evidence of nonlinear soil behavior during earthquake excitation^[29,30,31,32]. Chang *et al.*^[33] also analyzed the vertical accelerations recorded at Lotung.

Figure 2.1: Three-dimensional array at Chiba, Japan ^[14].

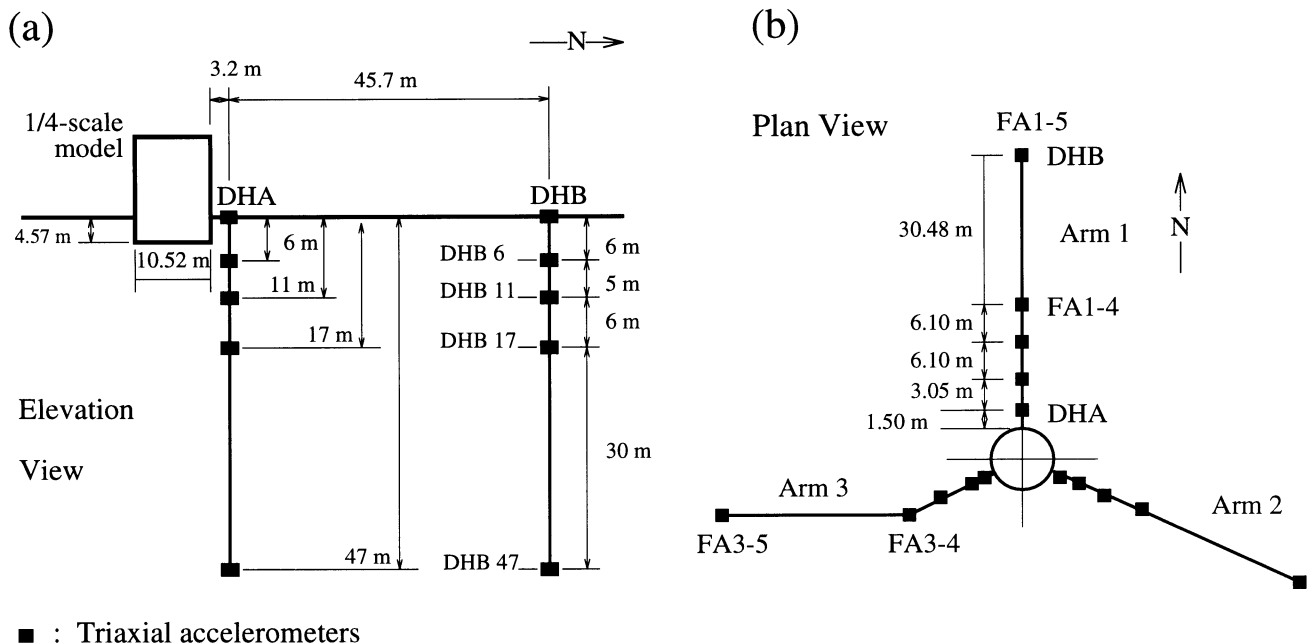


Figure 2.2: Instrumentation of Lotung experiment site ^[15]: (a) downhole array; (b) surface array.

Estimates of compressional-wave velocity profiles were evaluated and compared with geophysical measurements.

A number of other notable studies were also conducted to document nonlinear site amplification at Lotung ^[34,35,36,37,38]. Loh and Yeh ^[34] proposed a system identification method to estimate the hysteresis soil response parameters. Shen *et al.* ^[39] computed the Lotung site seismic response and evaluated excess pore pressures during three different LSST earthquakes. Finally, the authors and co-workers ^[40,41,42] used correlation, spectral and stress-strain imaging techniques, along with nonlinear response modeling to identify the soil dynamic parameters and evaluate the Lotung site seismic performance. In the following sections, some of these analysis procedures are briefly reviewed.

2.5.1 Correlation analyses

Cross correlation techniques were employed to evaluate average shear wave velocity between downhole stations, and to investigate shear-wave vertical propagation characteristics ^[30,40,41]. This type of analysis is based on the notion that the cross-correlation function between two downhole acceleration histories $a_i(t)$ and $a_j(t)$ (recorded at stations i and j) reaches a major peak at a time delay $t = t_d$, where t_d is time for seismic waves to travel from station i to station j . Thus, the apparent velocity v_a of wave propagation between stations i and j may be estimated as:

$$v_a = d/t_d \quad (2.3)$$

in which d is the known distance between stations i and j . For situations of nearly vertical shear wave propagation, the actual shear wave velocity is practically equal to v_a . At Lotung, this commonly adopted assumption of vertical wave propagation (in numerical studies) was found to be valid from a practical point of view ^[40,41].

2.5.2 Spectral analyses

Downhole acceleration records may be used to identify the resonant site characteristics. The amplitude of cross-spectrum energy function $s_{a_i a_j}(f)$ of downhole accelerations $a_i(t)$ and $a_j(t)$, peaks at either a resonant or an input frequency (an excitation spectrum peak). In general, such peaks represent a resonance if the corresponding phase-angle approaches 0° or 180° . The relative displacement of the k^{th} natural mode ϕ_k (of frequency f_k), at the i^{th} sensor location may be approximated by:

$$\phi_k(z_i) = \pm \sqrt{s_{a_i a_i}(f_k)} \quad (2.4)$$

where $s_{a_i a_i}(f_k)$ is a_i auto-spectral density function, and z_i is depth coordinate of a_i (i.e., location of the i^{th} accelerometer). Finally, the phase angle at a resonant frequency may be used to determine the relative direction of motion at each accelerometer location [40,41].

Site stiffness properties may be estimated from downhole accelerations by a notable alternate spectral procedure as reported by Chang *et al.* [30,31]. This procedure is based on the observation that the spectral ratio of surface and downhole accelerations a_s and a_d reaches a peak at the fundamental frequency of the soil layer between the two recording stations. This observation, along with an iterative technique for the evaluation of site resonant frequencies (developed by Dobry *et al.* [43]) were employed to estimate the Lotung site stiffness properties [30,31].

2.5.3 Shear stress-strain histories

A simple identification procedure, proposed in basic form for shake-table studies by Koga and Matsuo [44], was developed and used to evaluate site seismic shear stress-strain histories directly from recorded downhole accelerations [41,42,45]. Using a shear beam model to describe lateral site response, seismic shear stress at level z_i may be expressed as:

$$\tau_i(t) = \tau_{i-1}(t) + \rho_i \frac{\ddot{u}_{i-1} + \ddot{u}_i}{2} \Delta z_{i-1}, i = 2, 3, \dots \quad (2.5)$$

in which subscript i refers to levels z_i (of the i^{th} accelerometer), $\ddot{u}_i = \ddot{u}(z_i, t)$ is acceleration at level z_i , and Δz_i is spacing interval between accelerometers. The corresponding shear strains may be expressed as:

$$\gamma_i(t) = \frac{1}{\Delta z_{i-1} + \Delta z_i} \left((u_{i+1} - u_i) \frac{\Delta z_{i-1}}{\Delta z_i} + (u_i - u_{i-1}) \frac{\Delta z_i}{\Delta z_{i-1}} \right), i = 2, 3, \dots \quad (2.6)$$

in which $u_i = u(z_i, t)$ is absolute displacement (evaluated through double integration of the recorded acceleration history $\ddot{u}(z_i, t)$).

This technique was employed [41,42,45] to evaluate seismic shear stress strain histories at Lotung, for each soil layer located between downhole accelerometers. These histories revealed two salient response features: (1) stiffness reduction due to the increase in shear strain amplitude (Fig. 2.3), and (2) stiffness reduction due to pore pressure buildup.

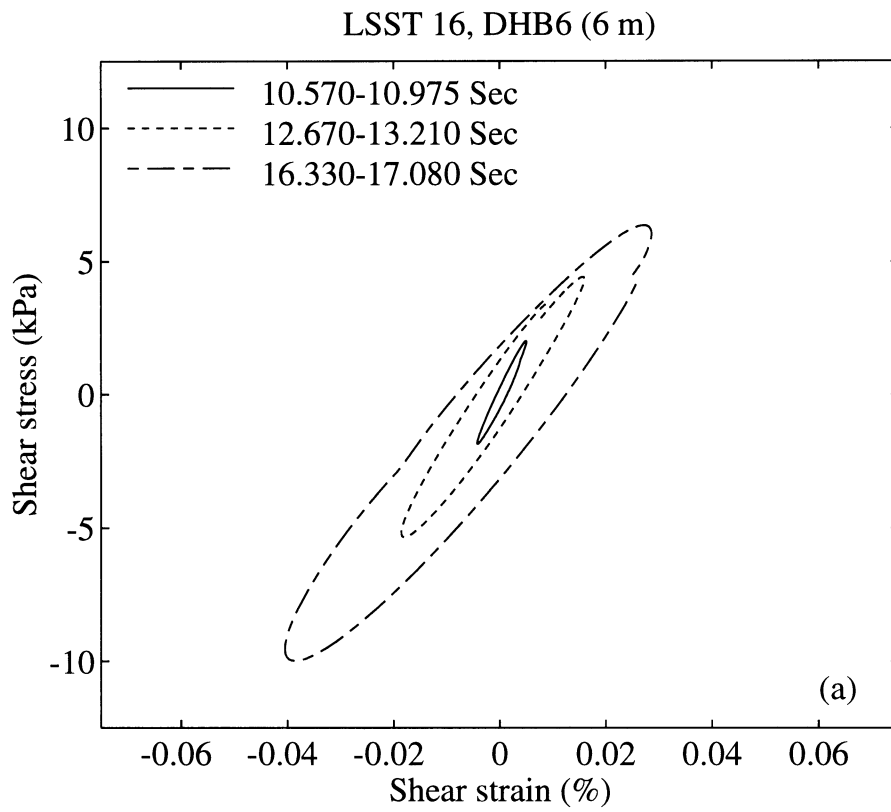


Figure 2.3: Samples of Lotung site shear stress-strain cycles at 6 m depth ^[41,42,45].

2.5.4 System identification and computational model calibration

The Lotung downhole seismic records were employed to calibrate linear^[45], equivalent-linear^[29], and nonlinear^[39,45,46] computational site response models. In this regard, such downhole records are a most valuable means of advancing the state-of-the-art.

2.6 Hualien, Taiwan

Hualien is located south of Lotung on the east coast of Taiwan, in a highly active seismic zone near the Philippine Sea plate boundary. The Hualien LSST was initiated in 1993 by a consortium of industrial and research enterprises from five countries (Japan, USA, Taiwan, France and Korea). In contrast to the Lotung soft soil conditions, the Hualien experiment was located at a relatively stiff site^[47,48]. The site is located within a large region instrumented with the seismic surface array SMART2^[49,50,51]. This region, is marked by the presence of the Meilun fault (and other parallel faults), which strikes northeast and attains an observed length of about 5 kilometers^[49].

Extensive instrumentation was deployed to record seismic structural and ground responses, and to monitor soil pore-water pressure buildup^[16]. The ground instrumentation (installed around a one-quarter scale nuclear power-plant containment structure) included fifteen accelerometer surface stations; and three downhole accelerometer arrays. Each downhole array consisted of accelerometers installed at depths of 0.0 m, 5.3 m, 15.8 m, 26.3 m, and 52.6 m^[16].

During the period July 1993 to May 1995, seven earthquakes were recorded at the Hualien site^[16]. The largest peak lateral acceleration of these events is about 0.1g. However, the instrumentation is still active and available to record an anticipated future stronger earthquake excitation.

The earthquake records at this site revealed a unique mechanism of azimuthal anisotropic soil response. Correlation analyses, and identified seismic stress-strain histories showed lower shear wave velocity estimates in the EW, compared to the NS direction^[52,53]. In addition, a notable study by Ueshima and Okano^[54] arrived at the same conclusion. In their study^[54], a frequency domain system identification technique was employed to analyze the recorded seismic accelerations. Finally, it appears that this azimuthal anisotropic response was also manifested in the analysis of Barros and Luco^[55] who identified foundation impedance functions for the one-quarter-scale nuclear-plant containment model. In this case^[55], the identification process was not based on the recorded seismic motions, but rather on response data obtained from forced vibration tests.

2.7 Garner Valley, California, USA

The Garner Valley experiment^[56] is sponsored jointly by the US Nuclear Regulatory Commission and the French Institut de Protection et de Surete Nucleaire (IPSN). This site is in a seismically active area of southern California 7 km east of the San Jacinto fault^[57]. The array consists of three-component accelerometer stations at the surface and within the ground at depths of 6 m, 15 m, 22 m, 55 m, and 220 m. At this location, the upper 18 m of soil are followed by weathered granite (up to 45 m), with solid granite bedrock thereafter. Shear-wave and P-wave velocity

tests were conducted along with Standard Penetration and laboratory soil sample tests^[58]. The outcome of analyses of 218 recorded weak seismic motions was found to be in agreement with in-situ low-strain shear wave velocity measurements^[57,59]. In addition, a damping mechanism proportional to the power 0.68 of the frequency was identified^[58].

2.8 Treasure Island, California, USA

Treasure Island is a 160 ha reclaimed (man-made) island located in the San Francisco bay. It was constructed in the 1930's^[60,61] of hydraulic fill over natural sand and Bay Mud. The fill (about 12 m thick at the array location) is in a relatively loose condition, and is susceptible to liquefaction. Geologic formation at Treasure Island (including the upper loose hydraulic fill) is similar to that of nearby Marina District in San Francisco^[60,62]. At both locations, widespread liquefaction with devastating consequences was documented during the recent 1989 Loma Prieta Earthquake^[60,61]. In the vicinity of the Treasure Island array, sand boils indicative of site liquefaction were observed^[63,64,65]. This liquefaction and associated loss of soil stiffness and strength was documented by Pease and O'Rourke^[60,62] using the surface accelerations recorded at Treasure Island, and representative bedrock accelerations recorded at the nearby outcrop of Yerba Buena Island.

The array site was instrumented in 1992 by the California Strong Motion Instrumentation Program, and the National Science Foundation^[18]. Among the main goals of installing this array (within a framework of a U.S. Geotechnical Test Site Network^[66]) were: (1) to gather seismic data that would elucidate the mechanisms of rock-motion amplification by deep soil deposits in the San Francisco area, and (2) to document the mechanisms of site liquefaction in the upper hydraulic fill strata^[18]. The Treasure Island Geotechnical Array consists of six triaxial accelerometers located at the surface, 7 m, 16 m, 31 m, 44 m and 104 m depths; and 6 piezometers located within the top 12 m reclaimed hydraulic fill^[18,67,68].

Since the array installation, 2 low amplitude shaking events were recorded in 1993 and 1996. These events provide a source of benchmark information on Treasure Island low amplitude dynamic response characteristics. The 1993 downhole records were employed to evaluate^[45]: (1) shear wave velocity profile, (2) site shear stress-strain response, and (3) low-strain soil dynamic properties. The identified wave velocities and soil properties were found to be in general agreement with measurements from earlier geophysical tests^[69]. The array is currently active in anticipation of a future strong earthquake excitation.

2.9 Wildlife-Refuge, California USA

The Wildlife Refuge site is located on the west side of the Alamo river in Imperial County, southern California. Evidence of liquefaction was observed at or near the site following the 1930, 1950, 1957, 1979, and 1981 Imperial Valley earthquakes^[70]. These observations triggered an interest in Wildlife which in an insightful effort, was instrumented in 1982 by the United States Geological Survey (USGS)^[20]. The instrumentation included a surface and a downhole accelerometer (at 7 m depth, below the liquefiable layer), and a number of pore-pressure transducers.

In 1987, the site was shaken by two main earthquakes ^[20]. On November 23, the Elmore Ranch earthquake occurred with essentially no excess pore pressure rise ($M_W = 6.2$, moment scale of magnitude). The next day, the Superstition Hills earthquake occurred ($M_W = 6.6$), causing a sharp increase in recorded pore-water pressure ^[20]. In addition, subsequent field investigations showed evidence of site liquefaction and ground fissures. The surface records displayed peculiar acceleration spikes ^[20] associated with simultaneous instants of excess pore-pressure drop ^[71,72,73].

Zorapapel and Vucetic ^[74] employed the 1987 seismic records to assess the relationship between lengthening of site fundamental period, motion amplification, and excess pore pressure buildup. Glaser and Chung ^[75,76] used ARMA modeling and system identification techniques to assess the effects of excess-pore-pressure on the site dynamic properties. Variation of average shear wave velocity was evaluated using cross-correlation analyses between overlapping segments of the surface and downhole acceleration records ^[46,77,78]. No significant change in site stiffness was observed throughout the Elmore Ranch shaking event. During the Superstition Hills earthquake, the change in shear wave velocity showed clear evidence of stiffness degradation ^[20] during the window of strong seismic excitation. This degradation clearly coincided with the initial phase of sharp pore-pressure rise.

The dramatic change in site response due to liquefaction was also evident in the stress-strain (evaluated using Eqs. 2.5 and 2.6, Fig. 2.4) history of the Superstition Hills earthquake ^[46,77,78]. During the strong shaking phase, the site experienced a clear and gradual stiffness degradation associated with a sharp increase in recorded pore water pressure (Fig. 2.4). At low effective confining pressures (high excess pore pressures), the effective stress-path clearly exhibited a reversal of behavior from contractive to dilative, as the line of phase transformation was approached ^[79].

Thus, this case history clearly showed (for the first time), an in-situ mechanism of shear stress hardening at large strain excursions during liquefaction (Fig. 2.4). Such a mechanism has been observed in a number of experimental studies ^[44,80,81,82,83], and is a consequence of soil dilation at large strain excursions, which results in associated instantaneous pore-pressure drops ^[84]. This observed phenomenon of hardening at large shear strain excursions (during liquefaction) is of paramount importance in restricting the extent of lateral deformation due to seismic excitation ^[85]. Consequently, constitutive models that capture this phenomenon are essential in analyses of such an important site response mechanism ^[85].

2.9.1 Transfer function analyses

Each surface and downhole lateral acceleration pair constitutes a complete input-output data set. The corresponding input-output relationship is dictated by the site dynamic parameters. This relationship may be estimated in the frequency domain as the non-parametric ratio of output and input Fourier spectra (referred to as the frequency-domain transfer function H_f):

$$H_f = \frac{\mathcal{F}(a_o)}{\mathcal{F}(a_i)} \quad (2.7)$$

in which $\mathcal{F}(a_o)$ and $\mathcal{F}(a_i)$ are the Fourier transforms of the output, a_o , and input, a_i , accelerations. To capture the variation of site dynamic properties during shaking, the transfer function may be evaluated for a succession of short overlapping time windows ^[77]. As proposed

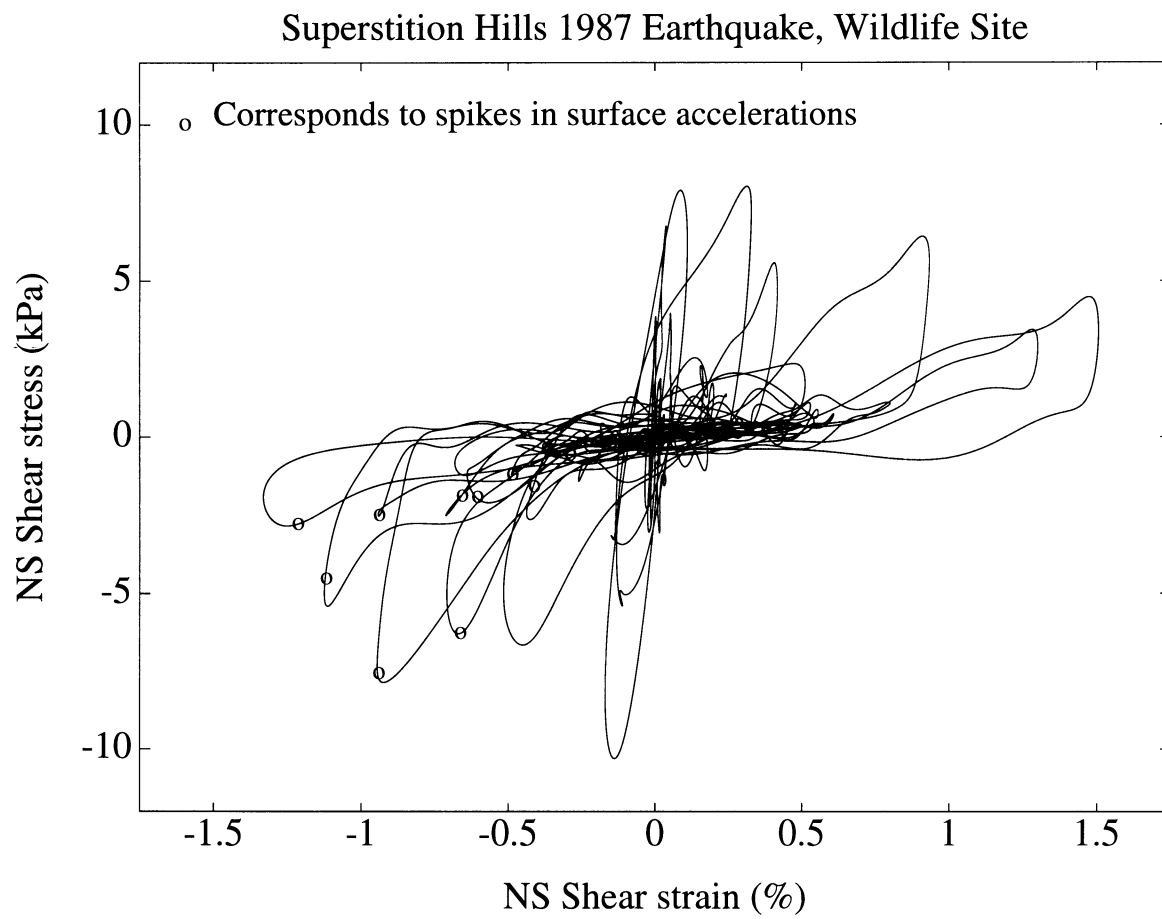


Figure 2.4: Wildlife Refuge shear stress-strain response at 3.75 m depth ^[77,78].

by Glaser ^[75,76], an alternative approach to the evaluation of transfer functions is based on the selection of an a priori input-output general relationship, such as for example an autoregressive moving-average (ARMA) model:

$$a_o(t_l) = \sum_{j=0}^n \alpha_j a_o(t_{l-j}) + \sum_{k=1}^m \beta_k a_i(t_{l-k}) \quad (2.8)$$

in which t_l is the l^{th} time step. The model parameters, α_j , β_k , n , m , are to be evaluated using a least-squares fitting or other optimization techniques (the site resonant frequencies and damping factors are defined by these parameters). Thus, the transfer function is given by:

$$H_f = \frac{\beta_0 + \beta_1 z + \beta_2 z^2 + \dots}{1 - \alpha_1 z - \alpha_2 z^2 - \dots} \quad (2.9)$$

in which $z^k = e^{2\pi k i f}$. If the input-output time histories are non-stationary, such as for earthquake accelerations, the model parameters α_j , β_k , are time dependent. Adaptive filtering along with a recursive non-stationary model are employed to handle such non-stationary input-output data set. Glaser ^[76] thoroughly reviewed and used these techniques to evaluate the performance of Wildlife site during the Elmore Ranch and Superstition Hills earthquakes.

2.10 Port Island, Kobe Japan

Port Island is an artificial (reclaimed) island located on the south-west side of Kobe, Japan. In the phase completed by 1981, 436 ha were reclaimed by bottom-dumping from barges ^[86]. Soil in the artificial reclaimed layer ^[87,88] consisted of decomposed weathered granite fill (Masa soil mined from the nearby Rokko mountains) with grain sizes ranging from gravel and cobble-sized particles, to fine sand (2 mm mean particle size, with silt-sized particles or smaller of less than 10% by weight). A downhole accelerometer array was installed at the North-West corner of Port Island in August 1991 ^[17]. The array consisted of triaxial accelerometers located at the surface, 16 m, 32 m, and 83 m depths.

The downhole array site consists of: (1) an artificial, reclaimed, loose surface layer down to about 19 m depth, (2) an alluvial clay layer between 19 m and 27 m depth, (3) sand and sand with gravel strata interlayered with clay between 27 and 61 m depth, (4) a diluvial clay layer between 61 m and 82 m depth, and (5) sand with gravel layers interlayered with clay starting at about 82 m depth. The water table was located at a depth of 4 m approximately.

Using the recorded downhole accelerations, shear stress-strain response (Eqs. 2.5 and 2.6) was evaluated ^[89,78], as shown in Fig. 2.5. Two remarkably different response patterns were exhibited at the site. Below 32m depth, the shear stress-strain histories showed an essentially linear soil response, with no appreciable reduction in soil stiffness. On the other hand, at shallow depths, the stress-strain histories indicated: (1) a noticeable reduction in stiffness with a slight shear strain hardening at elevation 24m, and (2) an abrupt sharp loss of stiffness and reduction of yield strength near the surface at 8m depth, evidently associated with site liquefaction. This liquefaction response mechanism was marked by the virtual absence of hardening at large strains, in contrast to the Wildlife case (Figs. 2.4 and 2.5).

The Port Island records have been the subject of numerous recent studies (e.g., see references [90,91]). These records along with the 1987 Superstition Hills record at Wildlife have provided valuable insight into the mechanisms associated with site liquefaction.

2.11 References

Special interest *

Outstanding interest **

1. Aisiks, E. G. and Tarshansky, I. W. (1969). "Soil Studies for Seismic Design of San Francisco Transbay Tube," *Vibration Effects of Earthquakes on Soils and Foundations*, ASTM STP 450, 138-166.
2. Joyner, W. B., Warrick R. E., and Oliver A. A. (1976). "Analysis of Seismograms from a Downhole Array in Sediments Near San Francisco Bay," *Bulletin of the Seismological Society of America*, Vol. 66, 937-958.
3. Johnson, L. R. and Silva, W. (1981). "The Effects of Unconsolidated Sediments Upon the Ground Motion During Local Earthquakes," *Bulletin of the Seismological Society of America*, Vol. 71, No. 1, 127-142.
4. Seed, H. B. and Idriss I. M. (1970). "Analyses of Ground Motion at Union Bay, Seattle During Earthquakes and Distant Nuclear Blasts," *Bulletin of the Seismological Society of America*, Vol. 60, No. 1, 125-136.
5. Tsai, N. C. and Housner, G. W. (1970). "Calculation of Surface Motions of a Layered Half-Space," *Bulletin of the Seismological Society of America*, Vol. 60, No. 5, 1625-1651.
6. ** Dobry, R., Whitman R. V. and Roesset J. M. (1971). "Soil Properties and the One-Dimensional Theory of Earthquake Amplification," *Research Report R71-18*, School of Engineering Massachusetts Institute of Technology.

Contains early rigorous analyses of site response using downhole array data.

7. Abdel-Ghaffar, A. M. and Scott, R. F. (1978). "Investigation of the Dynamic Characteristics of an Earth Dam," Report No. EERL 78-02, Earthquake Engineering Laboratory, California Institute of Technology, Pasadena, California.
8. * Abdel-Ghaffar, A. M. and Scott, R. F. (1979). "Shear Moduli and Damping Factors of Earth Dam," *Journal of the Geotechnical Engineering Division*, ASCE Vol. 105, No. Gt12, 1405-1426.

Pioneering effort to estimate soil dynamics properties from seismic response.

9. Kanai, K., Tanaka, T. and Yoshizawa, S. (1959). "Comparative Studies of Earthquake Motions on the Ground and Underground," *Bulletin of Earthquake Research Institute*, Tokyo, Vol. 37, 53-87.
10. Kanai, K., Tanaka, T., Yoshizawa, S., Morishita, T., Osada, K., and Suzuki, T. (1966). "Comparative Studies of Earthquake Motions on the Ground and Underground II," *Bulletin of Earthquake Research Institute*, Tokyo, Vol. 44, 609-643.

Port Island, Kobe (Japan). Hyogoken-Nanbu Earthquake, Jan. 17, 1995

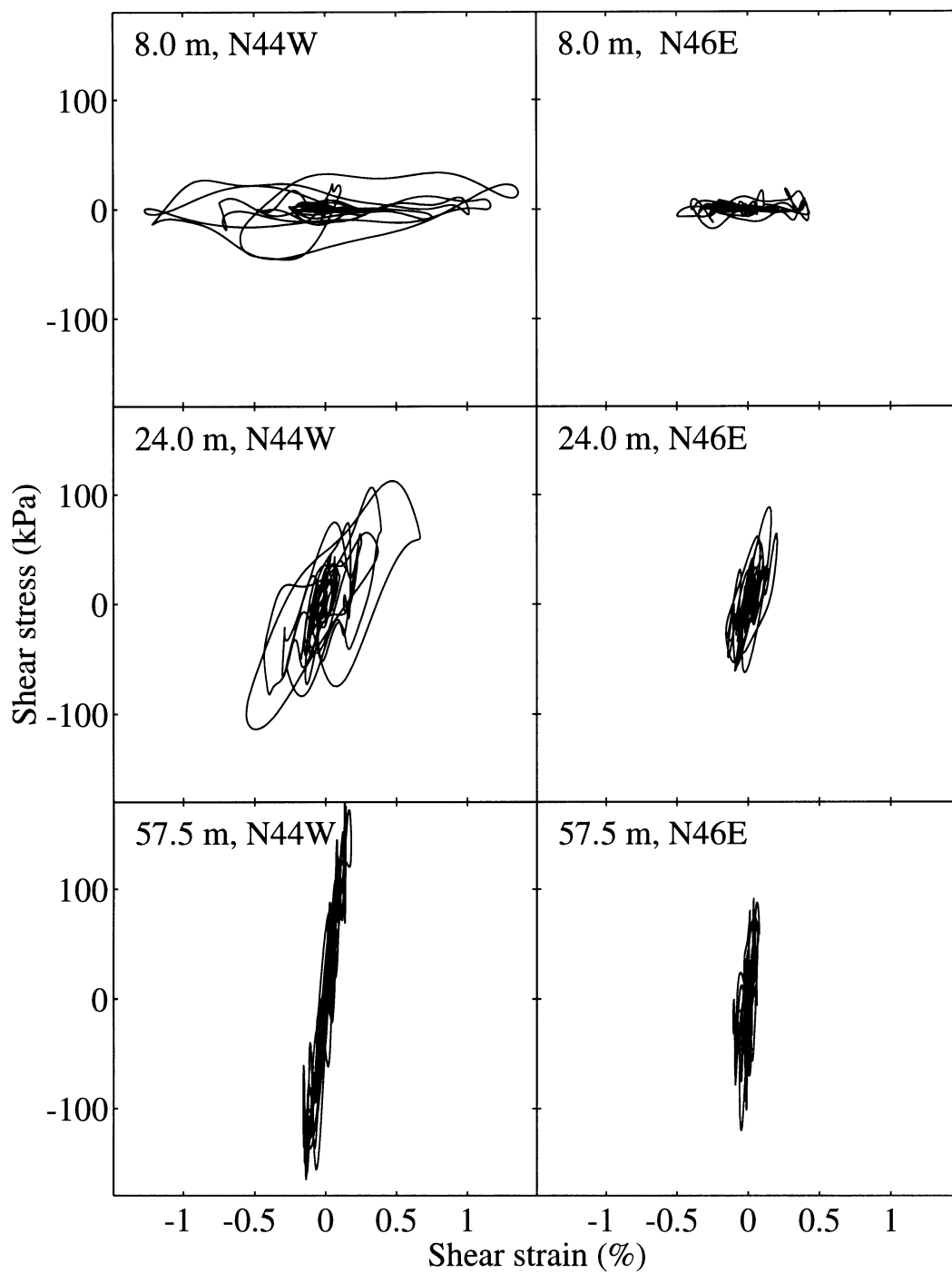


Figure 2.5: Port Island shear stress-strain responses midway between accelerometers, at 8.0 m, 24.0 m and 57.5 m depths ^[78,89].

11. Shima, E. (1962). "Modification of Seismic Waves in Superficial Layers as Verified by Comparative Observations on and Beneath the Surface," *Bulletin of Earthquake Research Institute*, Tokyo, Vol. 40, 187-259.
12. Akino, K., Ohta, T., and Yamahara, H. (1969). "Vibration Test of Models for Reactor Building Constructed on Different Soil Conditions and Excited by Natural Earthquakes," *IAEA Meeting on Aseismic Design and Testing of Nuclear Facilities*, The Japan Earthquake Engineering Promotion Society, Tokyo.
13. Tajimi, H. and Uchida, T. (1969). "Vibration Test of a Full-Scale Reactor Building (JPDR) Excited by Natural Earthquakes," *IAEA Meeting on Aseismic Design and Testing of Nuclear Facilities*, The Japan Earthquake Engineering Promotion Society, Tokyo.
14. ** Katayama, T., Yamazaki, F., Nagata, S., Lu L. and Turker, T. (1990). "A Strong Motion Data Base For the Chiba Seismometer Array and Its Engineering Analysis" *Earthquake Engineering and Structural Dynamics*, Vol. 19, 1089-1106.

A key representative reference about one of the most extensive downhole databases available nowadays; and associated novel research.

15. * Tang, H. T. (1987). "Large-Scale Soil Structure Interaction," Report No. NP-5513-SR, Electric Power Research Institute, Palo Alto, California.

Contains descriptive information on a valuable vertical-array site and data set.

16. Yang, Y. C., Huang, W. G., Liu, C. C., Cheng, S. N., and Yeh, Y. T. (1995). "Strong-Motion Earthquake Records on the 23 February, 1995, in LSST Array, Hualien," Reports IESER 95-001 and -002, Institute of Earth Sciences, Academia Sinica, Republic of China.
17. Iwasaki, Y. (1995). "Geological and Geotechnical Characteristics of Kobe Area and Strong Ground Motion Records by 1995 Kobe Earthquake, Tsuchi-to-Kiso," *Japanese Society of Soil Mechanics and Foundation Engineering*, Vol. 43, No. 6, 15-20 (in Japanese).
18. de Alba, P., Benoit, J., Youd, T. L., Shakal, A. F., Pass, D. G., and Carter, J. L. (1994). "Deep instrumentation Array at Treasure Island Naval Station," in *The Loma Prieta, California Earthquake of October 17, 1989 - Strong Ground Motion and Ground Failure*, Borchardt, R. E., ed. *U. S. Geological Survey Professional Paper*, Washington, D. C., A155-A168.
19. * Ishihara, K., Anazawa, Y., and Kuwano, J. (1987). "Pore Water Pressures and Ground Motions Monitored During the 1985 Chiba-Ibaragi Earthquake," *Soils and Foundations*, Vol 27, No. 3, 13-30.

Pioneering effort to record and analyze site liquefaction.

20. ** Holzer, T. L., Youd T. L. and Hanks T. C. (1989). "Dynamics of Liquefaction During the 1987 Superstition Hills, California, Earthquake," *Science*, Vol. 244, 56-59.

Insightful analysis of one of the most valuable case histories of documented site liquefaction.

21. Nagata, S., Katayama, T., Yamazaki, F., Lu L. and Turker, T. (1990). "A Dense Seismograph Array in Chiba, Japan and Its Strong Motion Database," *Proceedings of Fourth U.S. National Conference on Earthquake Engineering* May 20-24, Palm Springs, California.

22. Lu, L., Yamazaki, F, and Katayama, T. (1992). "Soil Amplification Based on Seismometer Array and Microtremor Observations in Chiba, Japan," *Earthquake Engineering and Structural Dynamics*, Vol 21, 95-108.
23. Yamazaki, F., Lu, L., and Katayama, T. (1992). "Orientation Error Estimation of Buried Seismographs in Array Observation," *Earthquake Engineering and Structural Dynamics*, Vol 21, 679-694.
24. Farjoodi, J., Katayama, T., and Sato, N. (1983). "Estimation of Seismic-Induced Ground Strains by Dense Seismometer Array Observation," *Proceedings of the 17th JSCE Conference on Earthquake Engineering*, pp. 69-72, Tokyo, Japan.
25. Katayama, T., Farjoodi, J., and Sato, N. (1984). "Measurement of Seismic Ground Strain by a Dense Seismometer Array," *Proceedings of the 8th World Conference on Earthquake Engineering*, Vol. 2, pp. 207-214.
26. Hughes, T. J. R. (1987). *The Finite Element Method*, Prentice Hall, New Jersey.
27. EPRI (1993). Guidelines for Determining Design Basis Ground Motions, Vol. 1: Method and Guidelines for Estimating Earthquake Ground Motion in Eastern North America," Report No. TR-102293, Electric Power Research Institute, Palo Alto, California.
28. * Hadjian A. H., Tseng, W. S., Chang, C. Y., Anderson, D., Tsai, N. C., Tang, Y. K., Tang, H. T., and Stepp, J. C. (1991). "The Learning from the Large Scale Lotung Soil-Structure Interaction Experiment," *Proceedings, Second International Conference on Recent Advances in Geotechnical Earthquake Engineering and Soil Dynamics*, St. Louis, Missouri.

A review of the impact of Lotung site downhole seismic records on soil-structure interaction analyses.

29. ** Chang, C.-Y. Mok, C. M. Tang, H.-T. (1996). Inference of Dynamic Shear Modulus From Lotung Downhole Data," *Journal of Geotechnical Engineering*, 122, 8, Aug., 657-665

A comprehensive coverage of innovative techniques applicable to vertical array analyses.

30. Chang, C.-Y., Mok, C. M., Power, M. S. and Tang, Y. K. (1991a). "Analysis of Ground Response Data at Lotung Large-Scale Soil-Structure Interaction Experiment Site," Report No. NP-7306-SL, Electric Power Research Institute, Palo Alto, California.
31. Chang, C.-Y., Mok, C. M., Power, M. S., Tang, Y. K., Tang, H. T. and Stepp, J. C. (1991b). "Development of Shear Modulus Reduction Curves Based on Lotung Downhole Ground Motion Data," *Proceedings Second International Conference on Recent Advances in Geotechnical Earthquake Engineering and Soil Dynamics*, Prakash, S., ed., St. Louis, Missouri, 111-118.
32. Chang, C.-Y., Power, M. S., Tang Y. K. and Mok, C. M. (1989). "Evidence of Nonlinear Soil Response During a Moderate Earthquake," *Proceedings, Twelfth International Conference on Soil Mechanics and Foundation Engineering*, Vol. 3, Rio de Janeiro, Brazil.
33. Chang, C. Y., Mok, C. M., Tang, Y. K., and Tang, H. T. (1994). "Analysis of Seismic Vertical Motion Using Lotung Downhole Array Data," *Proceedings of the Fifth US National Conference on Earthquake Engineering*, July 10-14, 1994, Chicago, Illinois. Earthquake Engineering Research Institute, Oakland, CA, 149-158.

34. Loh, C. H. Yeh, C. S. (1992). "Identification of Site Response Using 3-D Array Records," *Proceedings of the Tenth World Conference on Earthquake Engineering*, Madrid, 19-24 July 19, A A Balkema, Rotterdam, Vol. 1, 259-263.
35. Wen, K.-L., Yeh, Y. T., Huang, W.-G. (1992). "Effects of an Alluvial Basin on Strong Ground Motions," *Bulletin of the Seismological Society of America*, Vol. 82, number 2, April, 1124-1133.
36. Wen, K. L., Beresnev, I. A., Yeh, Y. T. (1994). "Nonlinear Soil Amplification Inferred From Downhole Strong Seismic Motion Data," *Geophysical Research Letters*, Vol. 21, number 24, Dec. 1, 2625-2628.
37. Wen, K. L., Beresnev, I. A., Yeh, Y. T. (1995). "Investigation of Non-Linear Site Amplification at two Downhole Strong Ground Motion Arrays in Taiwan," *Earthquake engineering and structural dynamics*, Vol. 24, number 3, March, 313-324.
38. Beresnev, I. A. Wen, K.-L. Yeh, Y. T. (1995). "Ground Behavior During Large Earthquakes," *Soil Dynamics and Earthquake Engineering*, 14, 2, 103-114
39. Shen, C. K., Wang, Z. and Li, X. S. (1991). "Pore Pressure Response During 1986 Lotung Earthquakes," *Proceedings, Second International Conference on Recent Advances in Geotechnical Earthquake Engineering and Soil Dynamics*, St. Louis, Missouri.
40. * Elgamal, A.-W., Zeghal, M., Tang, H. T., and Stepp, J. C. (1995). "Lotung Downhole Seismic Array. I: Evaluation of Site Dynamic Properties," *Journal of Geotechnical Engineering*, ASCE, Vol. 121, No. 4, April.

Thorough analysis of low-strain seismic site response.

41. ** Zeghal, M. and Elgamal, A.-W. (1993). "Lotung Site: Downhole Seismic Data Analysis," *Report*, Department of Civil Engineering Rensselaer Polytechnic Institute, Troy, New York.

A comprehensive coverage of innovative techniques applicable to vertical array analyses.

42. * Zeghal, M., Elgamal, A.-W., Tang, H. T. and Stepp J. C. (1995). "Lotung Downhole Array: Evaluation of Soil Nonlinear Properties," *Journal of Geotechnical Engineering* ASCE, Vol 121, No. 4, April.

Thorough analysis of Lotung nonlinear seismic site response.

43. Dobry R., Oweis, I. and Urzua, A. (1976). "Simplified Procedures for Estimating the Fundamental Period of Soil Profile," *Bulletin of the Seismological Society of America*, Vol. 66, No. 4, August 1976.
44. * Koga, Y. and Matsuo, O. (1990). "Shaking Table Tests of Embankments Resting on Liquefiable Sandy Ground," *Soils and Foundations*, Vol. 30, No. 4, 162-174.

Introduces a simple identification technique to estimate shear stress-strain histories from recorded downhole accelerations.

45. ** Elgamal, A.-W., Zeghal, M., Parra, E., Gunturi, R., Tang, H.T., and Stepp, C.J. (1996). "Identification and Modeling of Earthquake Ground Response I: Site Amplification," *Soil dynamics and Earthquake Engineering*, Vol. 15, No. 8, 499-522.

An overall coverage of a large body of work on site amplification as inferred from vertical array data.

46. ** Elgamal, A.-W., Zeghal, M., and Parra, E. (1995). "Identification and Modeling of Earthquake Ground Response," *First International Conference on Earthquake Geotechnical Engineering, IS-TOKYO'95*, Vol. 3, 1369-1406, Ishihara, K., Ed., Balkema, Tokyo, Japan, Nov. 14-16.

A comprehensive set of identification and modeling techniques using down-hole array data.

47. Ansary, M. A., Yamazaki, F., Kokusho, T. and Ueshima, T. (1995). "Micrometer Observation at Hualien LSST Array Site, Taiwan," *First Intl. Conf. on Earthquake Geotechnical Engineering*, November, Japan, 357 - 362.
48. Tang, H. T., Kokusho, T., Nishi, K., Kataoka, T., and Cheng, Y. H. (1991). "The Hualien Large-scale Seismic Test for Soil-Structure Interaction Research," *SMiRT 11 Transactions*, K04/4, 69-74.
49. Yeh, Y. T. and Chiu, H. C. (1994). "Two New Strong-Motion Arrays in Hualien, Taiwan," *Proceedings of the 10th World Conference on Earthquake Engineering*, Jul 19-24, Madrid, Spain, p 6947.
50. Beresnev, I. A., Wen, K. L., and Yeh, Y. T. (1995). "Nonlinear Soil Amplification: Its Corroboration in Taiwan," *Bulletin of the Seismological Society of America*, Vol. 85, 496 - 515.
51. Chiu, H. C., Amirbekian, R. V., and Bolt, B. A. (1995). "Transferability of Strong Ground Motion Coherency Between the SMART1 and SMART2 Arrays," *Bulletin of the Seismological Society of America*, Vol. 85, 342 - 348.
52. Gunturi, V. R., and Elgamal, A.-W. (1996). "Hualien Seismic Downhole Data Analysis," *Report*, Department of Civil Engineering, Rensselaer Polytechnic Institute, Troy, NY.
53. Gunturi, V. R., and Elgamal, A.-W., and Tang, H.-T. (1998). "Hualien Seismic Downhole Data Analysis," accepted for journal publication.
54. ** Ueshima, T. and Okano, H. (1996). "Further Investigation of Seismic Response of Soil and Embedded Structure in Hualien LSST Program," *Proceedings of Eleventh World Conference on Earthquake Engineering*, Acapulco, Mexico, 1996.

Useful system identification technique that documented azimuthal site anisotropy.

55. ** Barros, F. C. P. and Luco, J. E. (1995). "Identification of Foundation Impedance Functions and Soil Properties From Vibration Tests of the Hualien Containment Model," *Soil Dynamics and Earthquake Engineering*, Vol. 14, 229 - 248.

A study about identification of dynamic site properties from forced vibration response; and documentation of possible azimuthal anisotropic site response.

56. Mohammadioun, B. and Gariel, J. C. (1996). "An Analysis of Soil Effects on Earthquake Bed-rock Motion: A Cooperative NRC/IPSN Downhole Experiment at Garner Valley (California)," 11 WCEE, Paper No. 903, Acapulco, Mexico, Elsevier Science Ltd.
57. Archuleta, R. J., Seale, S. H., Sangas, P. V., Baker, L. M., and Swain, S. T. (1992). "Garner Valley Array of Accelerometers: Instrumentation and Preliminary Data Analysis", *Bulletin of the Seismological Society of America*, No. 82, 1592-1621.

58. Pecker, A. (1995). "Variation of Small-strain Properties From Recorded Weak Seismic Motions", *Soil Dynamics and Earthquake Engineering*, Vol. 14, 399-408.
59. Mohammadioun, B. and Pecker, A. (1994). "Low Frequency Transfer of Energy by Superficial Soil Deposits and Soft Rocks," *Soil Dynamics and Earthquake Engineering*, Vol. 12, 537-564.
60. Pease, J. W. and O'Rourke, T. D., (1995). "Liquefaction Hazards in the San Francisco Bay Region: Site Investigation, Modeling, and Hazard Assessment at Areas Most Seriously Affected by the 1989 Loma Prieta Earthquake," *Final Report*, School of Civil and Environmental Engineering, Cornell University, Ithaca, NY.
61. Power, M. S., Egan, J. A., *et al.* (1995). "Analysis of Liquefaction-Induced Stress at Treasure Island," in *The Loma Prieta, California Earthquake of October 17, 1989 - Liquefaction*, Holzer, T. ed., Professional Paper 1551-B, U. S. Geological Survey, Washington D. C.
62. Pease, J. W. and O'Rourke, T. D. (1997). "Seismic Response of Liquefaction Sites," *Journal of Geotechnical and Geoenvironmental Engineering*, 123, 1, 37-45, January.
63. Hryciw, R. D., Rollins, K. M., Homolka, M., Shewbridge, S. E., and McHood, M. (1991). "Soil Amplification at Treasure Island During the Loma Prieta Earthquake," *Proceedings, 2nd International Conference on Recent Advances in Geotechnical Earthquake Engineering and Soil Dynamics*, St. Louis, MO, 1679-1695.
64. Darragh R., Huang, M., and Shakal A., (1993). "Processed Strong-Motion Records from the CSMIP/NSF Treasure Island Geotechnical Array for the Gilroy Earthquake of 16 January 1993," *Report NO. OSMS 93-09*, California Division of Mines and Geology.
65. Finn, W. D. L., Ventura, C. CE., and Wu, G. (1993). "Analysis of Ground Motions at Treasure Island Site During the 1989 Loma Prieta Earthquake," *Soil Dynamics and Earthquake Engineering* Vol. 12, No. 7, 383-390.
66. Benoit, J. and de Alba, Eds. (1988). "Designated Sites For Geotechnical Experimentation in the United States," Proc. of Workshop at the University of New Hampshire.
67. Shakal, A.f. and Petersen, C.P. (1992). "Downhole Strong-Motion Accelerometry: Objectives and Techniques," *Seismological Research Letters*, Vol. 63, No. 30.
68. Hushmand, B. and Scott, R. F. (1996). "In Situ Dynamic Testing of Pore Pressure Transducers at Treasure Island, California Using "Caltech Piezometer"," 11 WCEE, Paper No. 1080, Acapulco, Mexico, Elsevier Science Ltd.
69. Gibbs, J. F., Fumal, T. E., Boore, M. D., and Joyner, W. B. (1992). "Seismic Velocities and Geologic Logs from Borehole Measurements at Seven Strong-Motion Stations that Recorded the Loma Prieta Earthquake," *U. S. Geological Survey Open File Report 92-287*.
70. Youd, T. L., and Wiczorek, G. F. (1984). "Liquefaction During 1981 and Previous Earthquakes Near Westmorland California," U.S. Geological Survey Open-File Report 84-680.
71. Hushmand, B., Scott, R. F., and Crouse, C. B. (1992). "In-Place Calibration of USGS Pore Pressure Transducers at Wildlife Liquefaction Site, California, USA," 10th WCEE, Vol. 3, 1263-1267.
72. Youd, T. L. and Holzer, T. L. (1994). "Piezometer Performance at Wildlife Liquefaction Site, California," *J. of Geotechnical Engineering, ASCE*, Vol. 120, No. 6. 975-995, June.

73. Scott, R. F. and Hushmand, B. (1995). "Discussion on Technical Paper 6044 of Geotechnical Engr. Journal, ASCE, Piezometer Performance at Wildlife Liquefaction Site, California by T.L. Youd and T.L. Holzer," ASCE, J. of Geotechnical Engineering, Vol. 21, No. 12, Dec., 912-919.
74. Zorapapel, G. T., and Vucetic, M. (1994). "The effect of Pore-Pressure on Ground Motion," *Earthquake Spectra*, Vol. 10, No. 2, 403-438.
75. Glaser S. and Chung, R. (1995). "Evaluation of Liquefying Soil Through Time Using System Identification," *Proceedings of the 5th U.S.-Japan Workshop on Earthquake Resistant Design of Lifeline Facilities and Countermeasures Against Soil Liquefaction*, O'Rourke T. and Hamada, M. eds., NCEER.
76. Glaser S. (1996). "Insight into Liquefaction by System Identification," *Geotechnique*, Vol. 46, No. 4, 641-655.
77. * Zeghal, M. and Elgamal, A.-W. (1994). "Analysis of Site Liquefaction Using Earthquake Records," *Journal of Geotechnical Engineering*, ASCE, Vol. 120, No. 6, 996-1017.

Thorough analysis of the one of the most valuable site liquefaction case histories.

78. ** Zeghal, M., Elgamal, A.-W. and Parra, E. (1996). "Identification and Modeling of Earthquake Ground Response II: Site Liquefaction," *Soil Dynamics and Earthquake Engineering*, Vol. 15, No. 8., 523-547.

An overall coverage of a large body of work on site liquefaction as inferred from vertical array data.

79. National Research Council (1985). *Liquefaction of Soils During Earthquakes*, Committee on Earthquake Engineering, National Academy press, Washington D. C.
80. Castro, G. (1975). "Liquefaction and Cyclic Mobility of Saturated Sand," *Journal of Geotechnical Engineering Division*, ASCE, Vol. 101, No. 6, 555-569.
81. Ishihara, K. (1985). "Stability of Natural Deposits During Earthquakes," *Proceedings of 11th International Conference on Soil Mechanics and Foundation Engineering*, San Francisco, Vol. 1, 327-376.
82. Arulmoli, K., Muraleetharan, K. K., Hossain, M. M. and Fruth, L. S. (1992). "Verification of Liquefaction Analyses by Centrifuge Studies Laboratory Testing Program Soil Data Report," Report, The Earth Technology Corporation.
83. Taboada, V. M. and Dobry, R. (1993). "Experimental Results of Model 1 at RPI," *Proceedings of the International Conference on the Verification of Numerical Procedures for the Analysis of Soil Liquefaction Problems*, Arulanandan, K. and Scott, R. F., eds., Vol. 1, Davis, CA, 3-17, Balkema.
84. * Vucetic, M. and Dobry, R. (1988). "Cyclic Triaxial Strain-Controlled testing of Liquefiable Sands," *Amer. Soc. Testing Mat.*, Spec. Tech. Publ. 977, 475-485.

Thorough investigation of dilative soil response during liquefaction.

85. * Elgamal, A.-W., Dobry, R., Parra, E., and Yang, Z. (1998). "Soil Dilation and Shear Deformations During Liquefaction," *Proc. 4th Intl. Conf. on Case Histories in Geotechnical Engineering*, S. Prakash, Ed., March 8-15, St. Louis, Missouri.

Compilation of documented evidence about dilative soil response during liquefaction.

86. Nakakita, Y., and Watanabe, Y. (1981). "Soil stabilization by Preloading in Kobe Port Island," *Proceedings of the 9th International Conference on Soil Mechanics and Foundation Engineering*, Tokyo, Japan, 611-622.
87. O'Rourke, T. D. (1995). "Geotechnical Effects," *Preliminary Report from the Hyogoken-Nambu Earthquake of January 17, 1995*, National Center for Earthquake Engineering Research Bulletin, SUNY, Buffalo, Vol. 9, No. 1.
88. Sitar, N., Ed. (1995). "Geotechnical Reconnaissance of the Effects of the January 17, 1995, Hyogoken-Nambu Earthquake Japan," *Report No. UCB/EERC-95/01*, Earthquake Engineering Research Center, Berkeley, California.
89. Elgamal, A.-W., Zeghal, M. and Parra, E. (1996). "Liquefaction of an Artificial Island in Kobe, Japan," *Journal of Geotechnical Engineering*, ASCE Vol. 122, No. 1.
90. ** Ishihara, K., ed. (1995). *Earthquake Geotechnical Engineering*, Proceedings of the First International Conference on Earthquake Geotechnical Engineering, Tokyo, Japan, November.

Contains a number of recent studies on vertical array analyses.

91. ** Soils and Foundations (1996). "Special Issue on Geotechnical Aspects of the January 17, 1995 Hyogoken Nambu Earthquake," *Soils and Foundations*, Japan Geotechnical Society, January.

Contains a number of important studies on vertical array data from the recent Hyogoken-Nambu earthquake.

Chapter 3

Identification and Modeling of Earthquake Site Liquefaction

3.1 Introduction

A near-catastrophe resulted from a major liquefaction-induced slide in the lower San Fernando dam (Southern-California) during the February 9, 1971 earthquake (Seed *et al.* 1975). Eighty thousand people living downstream of the dam were evacuated, and the reservoir level was promptly lowered to a safe elevation. Recent major seismic events such as the 1964 Niigata, the 1989 Loma Prieta, and the 1995 Kobe earthquakes, continue to demonstrate the damaging effects of liquefaction-induced loss of soil strength and associated lateral spreading (Seed 1966, Ishihara 1985, Seed *et al.* 1990, Bardet *et al.* 1995, Comartin *et al.* 1995, Soils and Foundations 1996). Experimental laboratory research on soil liquefaction has provided valuable insight concerning excess pore-pressure buildup in saturated loose granular soils (National Research Council 1985). However, for engineering applications, there remains a need to further understand and identify the mechanisms of seismically induced soil deformation due to liquefaction, and associated stiffness and strength degradation.

In-situ seismic records of site liquefaction are scarce. Currently, downhole seismic records are only available for: (1) the Wildlife Refuge site (Imperial County, CA) during the 1987 Superstition Hills earthquake (accelerations and pore-pressures), and (2) the Port Island site (Kobe, Japan) during the 1995 Hyogoken-Nanbu earthquake. Such downhole acceleration and excess-pore-pressure records provide direct information on the mechanisms of site liquefaction; and associated stiffness degradation and lateral spreading. This valuable information is of paramount importance to the development of empirical and computational predictive techniques.

In the following sections, two downhole array studies are reported. In both cases, evidence of liquefaction was documented. The downhole data was used herein to identify the associated response mechanisms, and to calibrate appropriate computational models.

3.2 Scope

Studies were conducted to investigate the recorded downhole seismic response at Wildlife Refuge (California, USA), and Port Island (Kobe, Japan) sites. Simple identification procedures were

employed to estimate the associated seismic shear stress-strain histories; and to evaluate the changes in shear wave propagation velocity during seismic excitation. The stress-strain histories were used to: (1) assess the effects of soil stiffness and strength degradation due to liquefaction, and (2) analyze the involved mechanisms of large strain soil deformations. A detailed description of the conducted studies was reported in Zeghal and Elgamal (1994), and Elgamal *et al.* (1996a). Within a unified framework, this report presents additional information, and summarizes a number of major findings. Moreover, the predictions of an effective stress computational model, calibrated by the available downhole data and identified soil properties, are presented and discussed.

3.3 Analysis Techniques

The techniques described in Elgamal *et al.* 1996b were used herein to evaluate: (1) shear wave velocities, (2) site seismic shear stress and strain histories, and (3) optimal shear stiffness and damping parameters. Soil constitutive behavior was modeled using the multi-surface plasticity technique. New modeling capabilities were developed to represent the response mechanisms during liquefaction, as identified from available seismic acceleration and pore-pressure records. This constitutive model was incorporated in a general purpose two-dimensional effective stress finite-element formulation. The salient features of this formulation are presented in Ragheb 1994 and Parra 1996.

3.4 Wildlife-Refuge, California USA

3.4.1 Instrumentation and seismic records

The Wildlife Refuge site is located on the west side of the Alamo river, Imperial County in Southern California. Evidence of liquefaction was observed at or near the site following the 1930, 1950, 1957, 1979, and 1981 Imperial Valley (Youd and Wieczorek 1984) earthquakes.

These observations triggered an interest in Wildlife which in an insightful effort, was instrumented in 1982 (Fig. 3.1, Youd and Wieczorek 1984) by the United States Geological Survey (USGS). In 1987, the Wildlife site was shaken by two main earthquakes (Holzer *et al.* 1989). On November 23, the Elmore Ranch earthquake (Fig. 3.2) occurred with essentially no excess pore pressure rise ($M_W = 6.2$ moment scale of magnitude). The next day, the Superstition Hills earthquake occurred ($M_W = 6.6$), causing a sharp increase in recorded pore-water pressure (Holzer *et al.* 1989). In addition, subsequent field investigations showed evidence of site liquefaction and ground fissures. Fig. 3.3 depicts the NS and EW components of the recorded accelerations at ground surface and 7.5 m depth; and the associated excess pore-water pressure measured at 2.9 m depth (piezometer P5, Fig. 3.1). As shown in Fig. 3.3, the surface records displayed peculiar acceleration spikes (Holzer 1989) associated with simultaneous instants of pore-pressure drop.

Zorapapel and Vucetic (1994) employed the 1987 Wildlife Refuge seismic records to assess the relationship between lengthening of site fundamental period, amplification factors, and excess pore pressure buildup. Glaser and Chung (1995) used ARMA modeling and system iden-

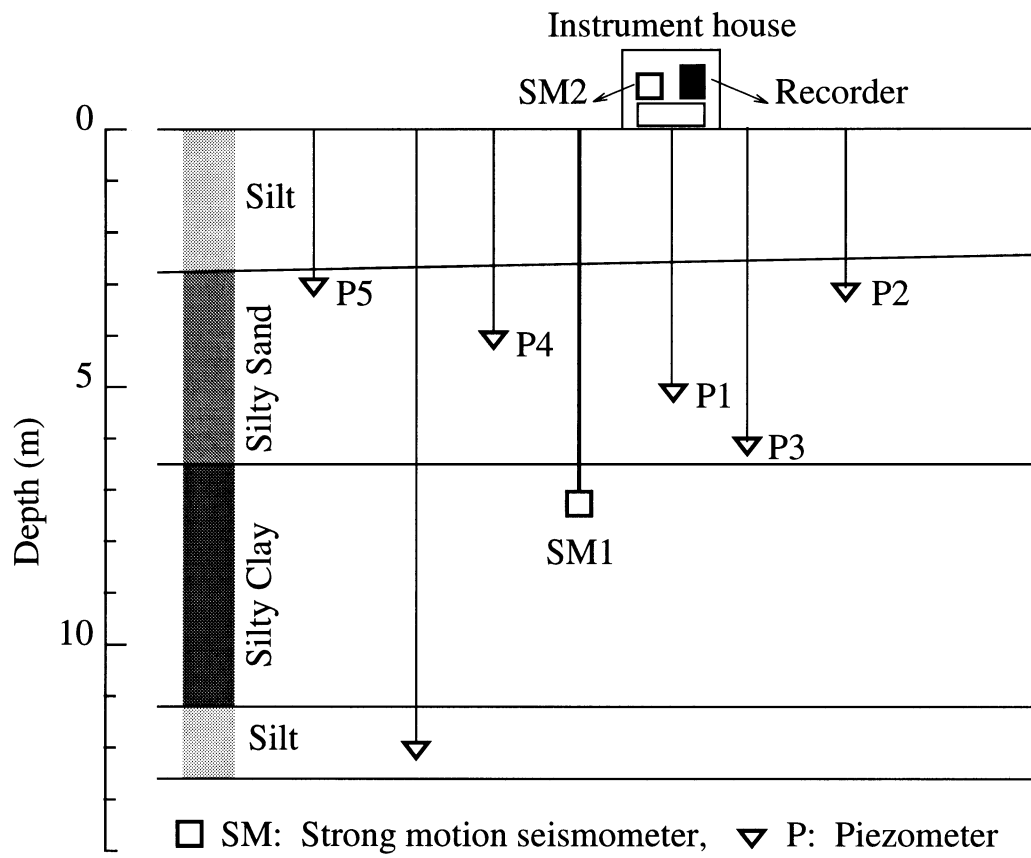


Figure 3.1: Cross-section and instrumentation at the Wildlife Refuge site (after Bennett *et al.* 1984).

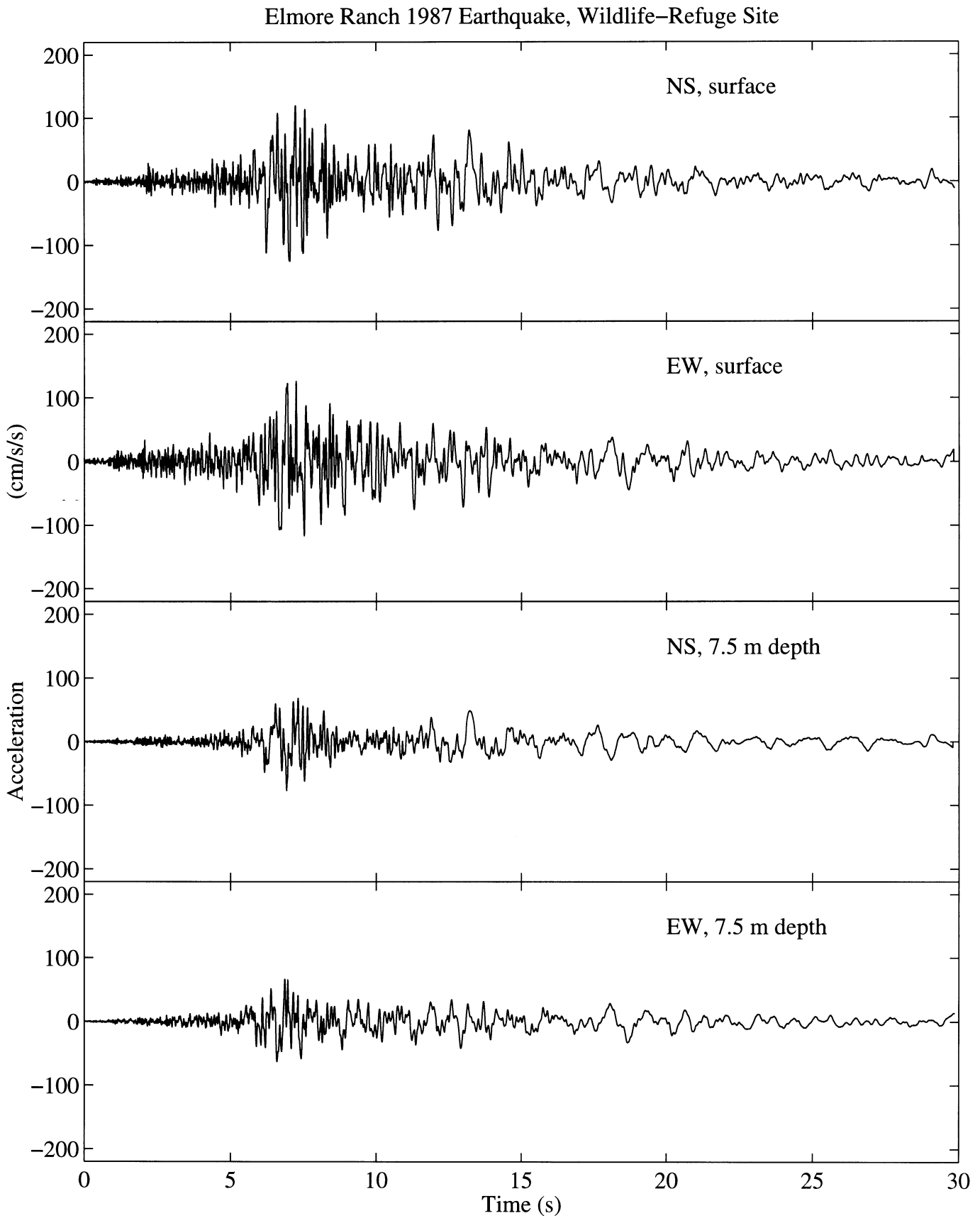


Figure 3.2: Wildlife Refuge site NS and EW surface and downhole (at 7.5 m depth) accelerations during the Elmore Ranch 1987 earthquake.

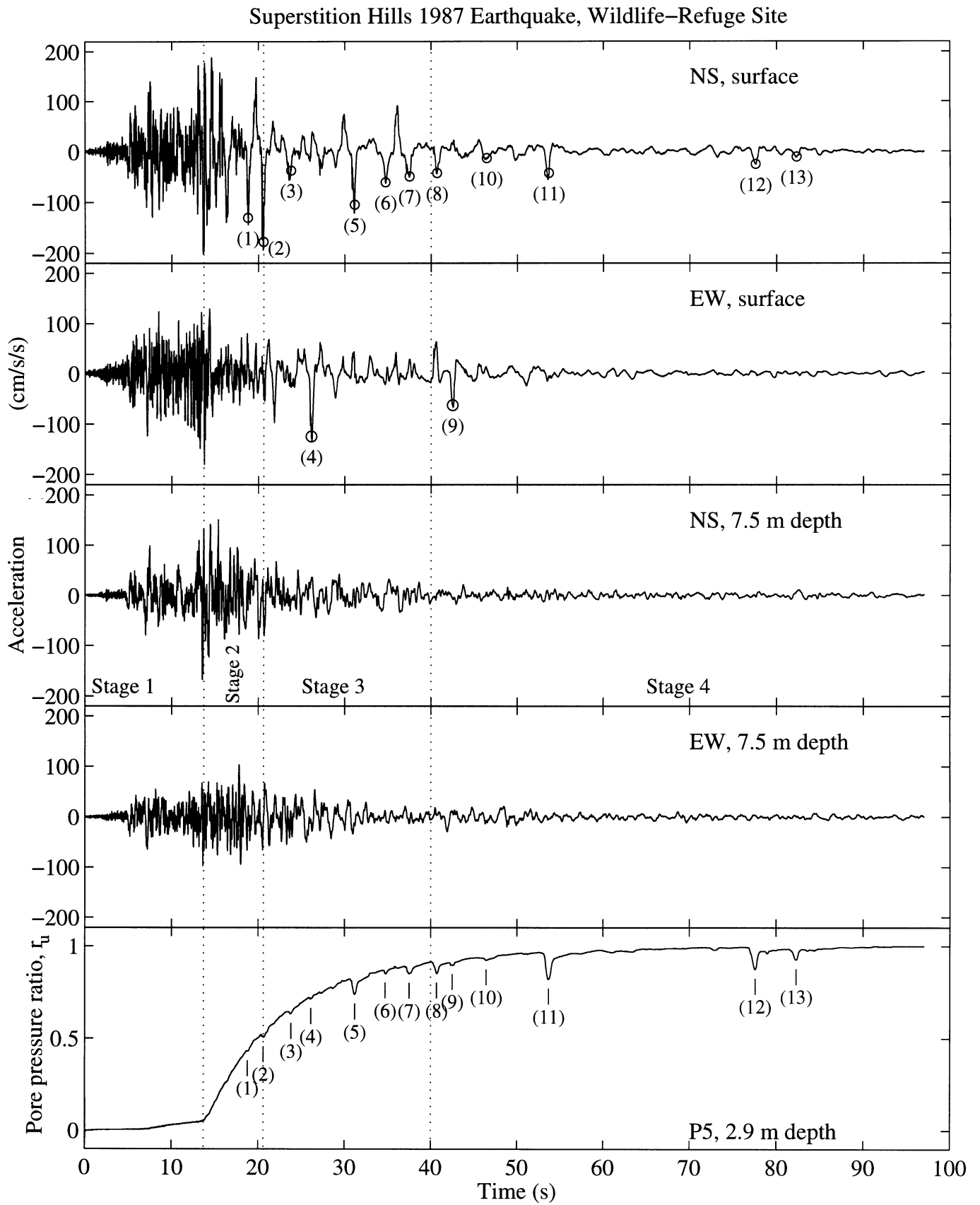


Figure 3.3: Wildlife Refuge site NS and EW surface and downhole (at 7.5 m depth) accelerations, and associated pore water pressure (at 2.9 m depth) during the Superstition Hills 1987 earthquake.

tification techniques to assess the effects of excess-pore-pressure on the Wildlife site dynamic properties.

3.4.2 Seismic site response

Using Eqs. 2.5 and 2.6, Figs. 3.4 and 3.5 display the NS and EW shear stress-strain histories during the Elmore Ranch earthquake ($\rho = 2000 \text{ kg/m}^3$). As shown, no significant change in site stiffness is observed throughout this shaking event. In fact, following the principals of linear optimization as described in Elgamal *et al.* 1996b (Eqs. 11 and 12), the Elmore Ranch response (Fig. 3.5) identified a shear modulus $G = 21.44 \text{ MPa}$ ($v_s = 104 \text{ m/s}$), and a damping ratio $\eta/G = 1.0\%$ (average values for 7.5m stratum between surface and downhole accelerometers). These values are in the neighborhood of those identified at the Lotung, Taiwan site (Elgamal *et al.* 1996b).

During the Superstition Hills earthquake, variation of average shear wave velocity (v_s) was evaluated using cross-correlation analyses between overlapping segments (Chang *et al.* 1991) of the surface and downhole acceleration records (Fig. 3.6). As may be observed, shear wave velocity started with a value in the neighborhood of that estimated during the Elmore Ranch earthquake. However, change in shear wave velocity during shaking showed clear evidence of stiffness degradation (Holzer *et al.* 1989) during the 12 to 18 s window of strong seismic excitation (stage 2, Fig. 3.3). This reduction clearly coincided with the initial phase of sharp pore-pressure rise (stage 2, Fig. 3.3).

The dramatic difference in site response due to liquefaction was also immediately evident in the stress-strain histories of the Superstition Hills earthquake (Fig. 3.7). This was further manifested by the effective stress histories at 2.9 m depth (location of piezometer P5, Fig. 3.1), evaluated from the acceleration and excess pore pressure records of Fig. 3.3. Shear stress versus effective vertical stress ($\sigma'_v = \sigma_v - p$, where p is excess pore pressure measured by P5, and σ_v is total vertical stress at P5) may be interpreted as an effective stress path.

Selected cycles of shear stress-strain response are shown in Figs. 3.9 and 3.10. During the initial phase (stage 1 [0 s to 13.7 s], Fig. 3.3), the site showed no evidence of significant stiffness degradation (Figs. 3.7, 3.9); and no appreciable rise in pore pressure was recorded by piezometer P5 (Fig. 3.3). During the strong shaking phase (stage 2 [13.7 s to 20.6 s], Figs. 3.3, 3.7, 3.9, and 3.10), the site experienced a clear and gradual stiffness degradation associated with a sharp increase in pore water pressure. Soil stiffness and yield strength continued to decrease during stages 3 and 4 ([20.6 s to 96.0 s], Figs. 3.3, 3.7, 3.9, and 3.10). Cycles of large shear strain were developed during these stages, with a peak strain of 1.5 % at 36 s (Figs. 3.7 and 3.10).

During stages 2-4, site response was marked by shear stress-strain hardening at large strains (Figs. 3.7, 3.9, and 3.10). This hardening was more pronounced in the negative direction where negative acceleration spikes occurred along with instantaneous pore pressure drops (Fig. 3.3). Such asymmetric hardening was most probably associated with the presence of a nearby free slope towards which permanent ground deformations were observed (Holzer *et al.* 1989). At low effective confining pressures (high excess pore pressures, stage 4), the effective stress-path (Fig. 3.8) clearly exhibited a reversal of behavior from contractive to dilative as the line of phase transformation was approached (National Research Council 1985).

Thus, this case history clearly showed (for the first time), an in-situ mechanism of shear

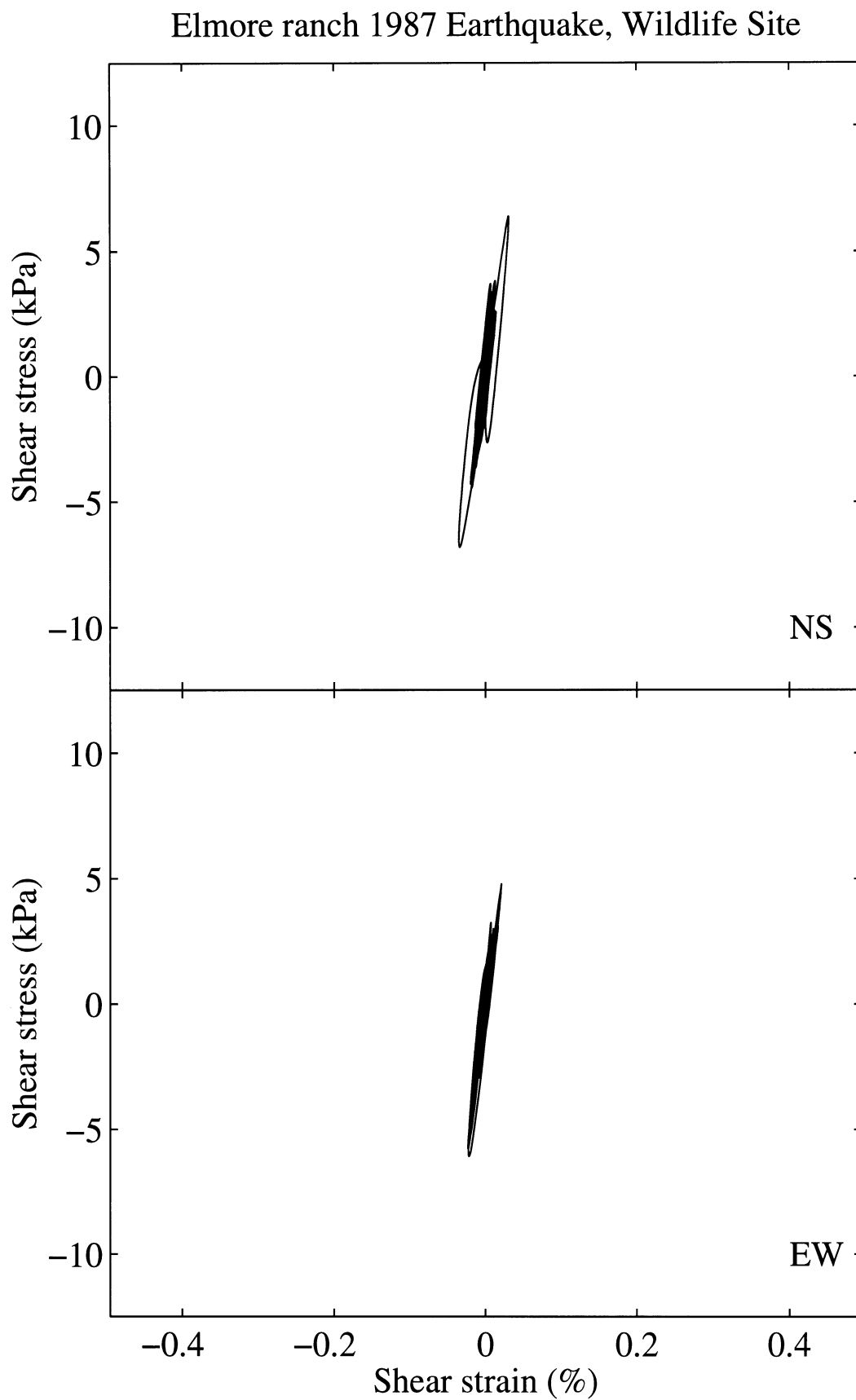


Figure 3.4: Wildlife Refuge EW and NS shear stress-strain histories during the Elmore Ranch 1987 earthquake (evaluated from acceleration histories shown in Fig. 3.2).

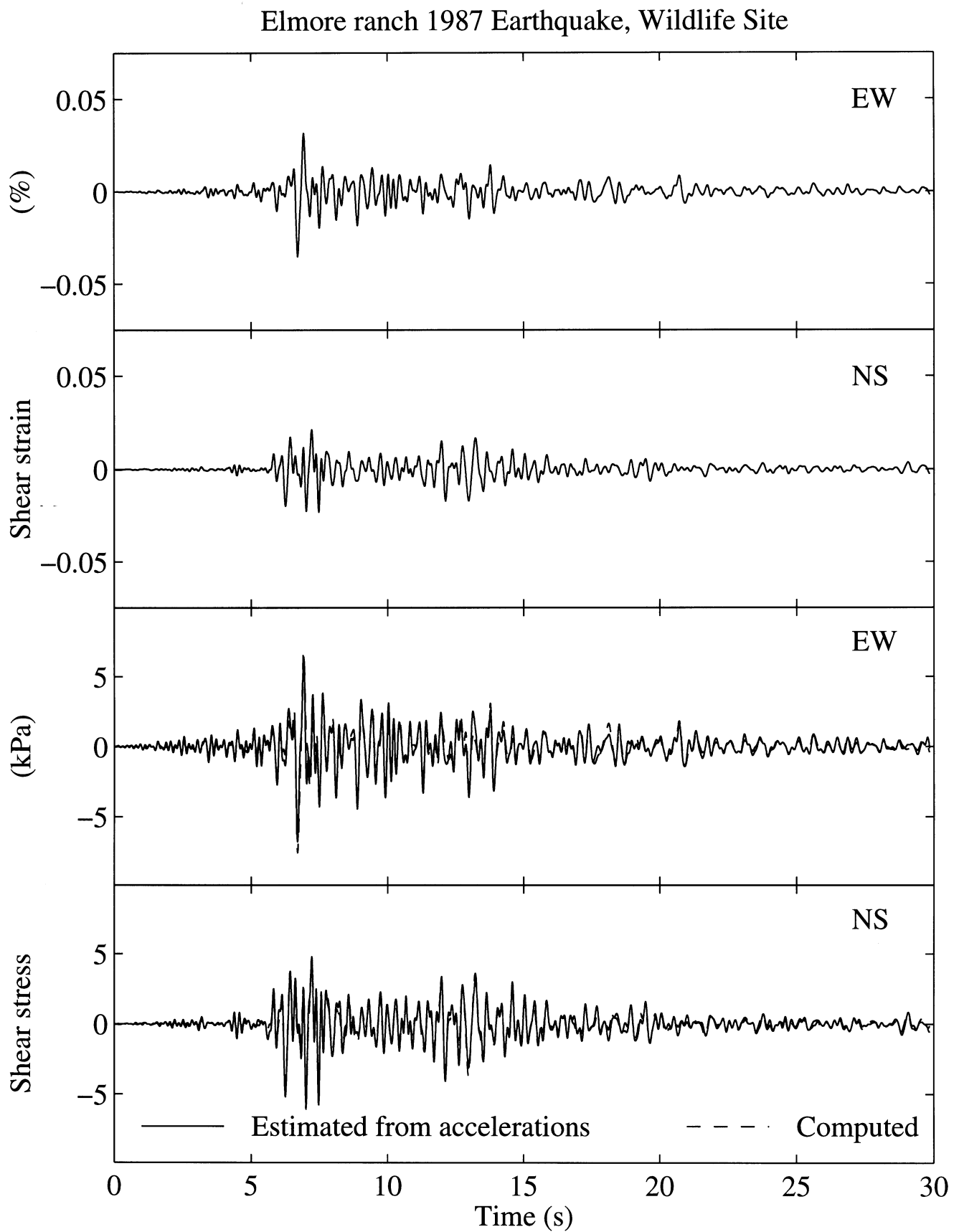


Figure 3.5: Wildlife Refuge shear strain histories, and associated stress histories evaluated from recorded acceleration and predicted by the equivalent linear model.

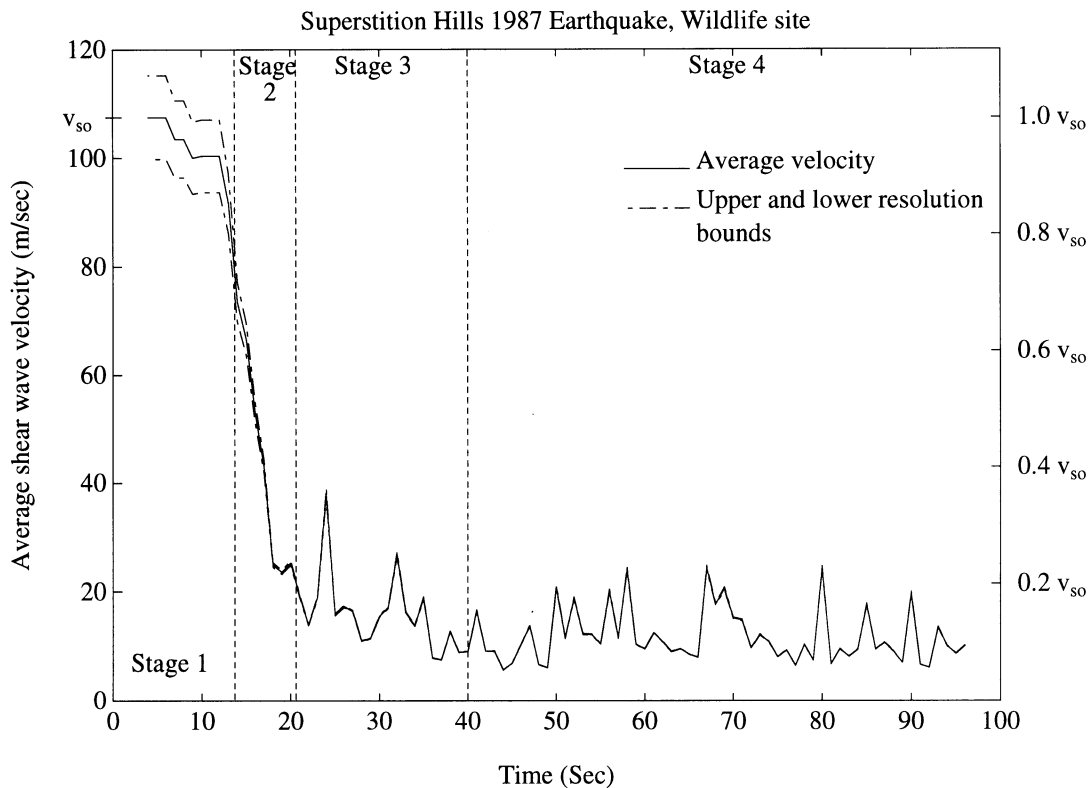


Figure 3.6: Average shear wave velocity during the SH earthquake (NS and EW directions).

stress-strain hardening at large strain excursions during liquefaction. Such a mechanism has been observed in a number of experimental studies (e.g., Castro 1975, Ishihara 1985, Koga and Matsuo 1990, Arulmoli *et al.* 1992, Taboada and Dobry 1993), and is a consequence of soil dilation at large strain excursions, which results in associated instantaneous pore-pressure drops (Vucetic and Dobry 1988).

The observed phenomenon of hardening at large shear strain excursions (during liquefaction) is of paramount importance in restricting the extent of lateral deformation due to seismic excitation. Consequently, constitutive models that capture this phenomenon are essential in analyses of such an important site response mechanism. Currently, this aspect has only received serious attention in a small number of computational studies (Nakai 1989, Kabilamany and Ishihara 1990, Byrne 1991, Iai 1991, Iai *et al.* 1995, Sasaki *et al.* 1992, Towhata and Toyota 1994, Parra 1996) and additional research is necessary. A preliminary computational simulation of the identified response (Figs. 3.7 and 3.8, NS direction) using the constitutive model of Parra 1996 is shown in Fig. 3.11. In addition to the loss of stiffness and strength associated with pore-pressure buildup, this model is seen (Fig. 3.11) to capture the regain in stiffness and strength at large strain excursions. The associated dilative response during these instants occurs near the condition of liquefaction (r_u about 1.0), along the phase transformation line. In order to computationally model this response, a special loading-unloading non-associative flow rule (above the phase transformation line) was specifically developed (Parra 1996), and calibrated by the observed stress-strain response of Fig. 3.7.

Intervals of such dilative behavior (points 1-13 in Figs. 3, 10 and 11) appear to have been

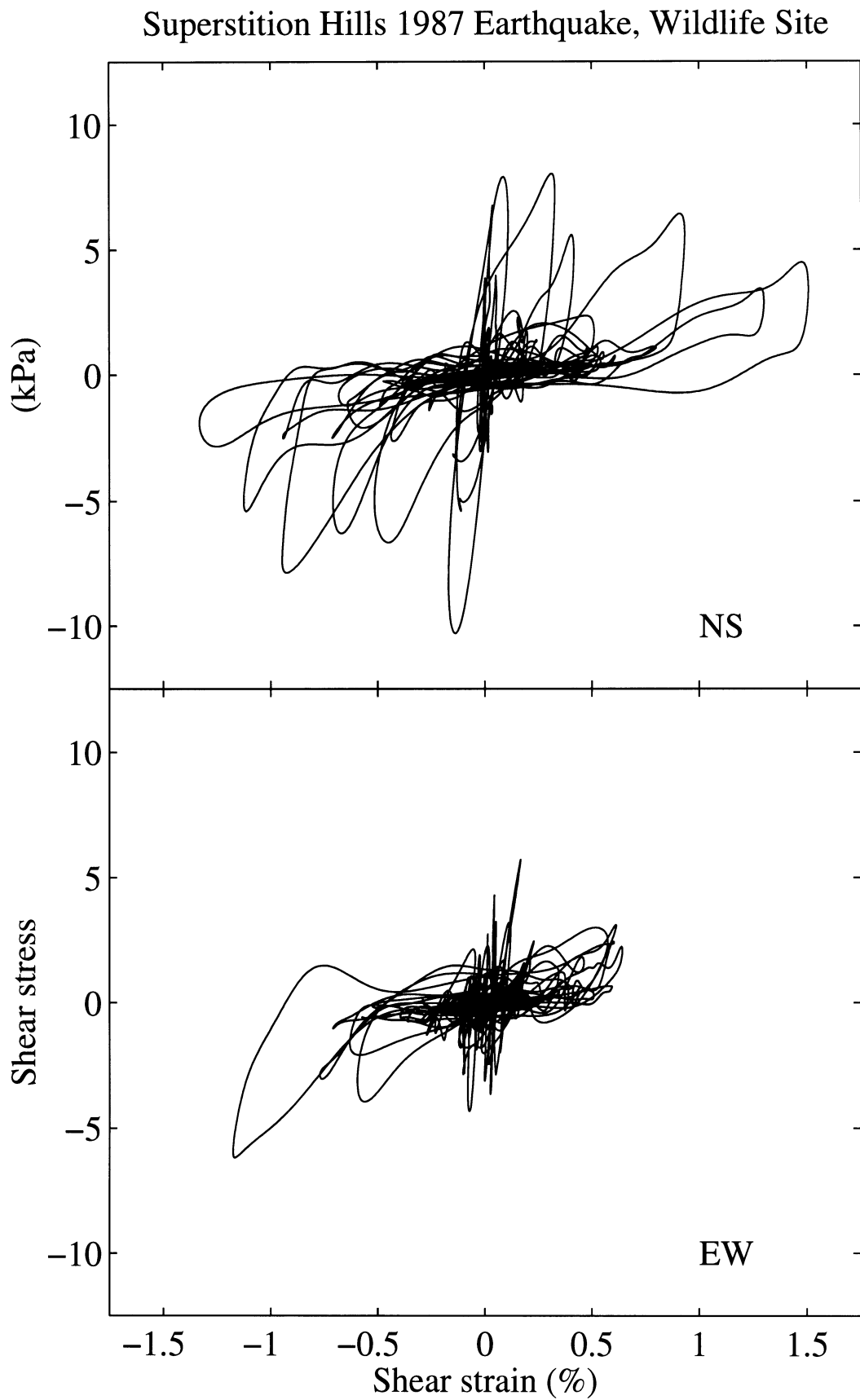


Figure 3.7: Wildlife-Refuge NS and EW shear stress-strain histories during the Superstition Hills 1987 Earthquake (evaluated from acceleration histories shown in Fig. 3.3).

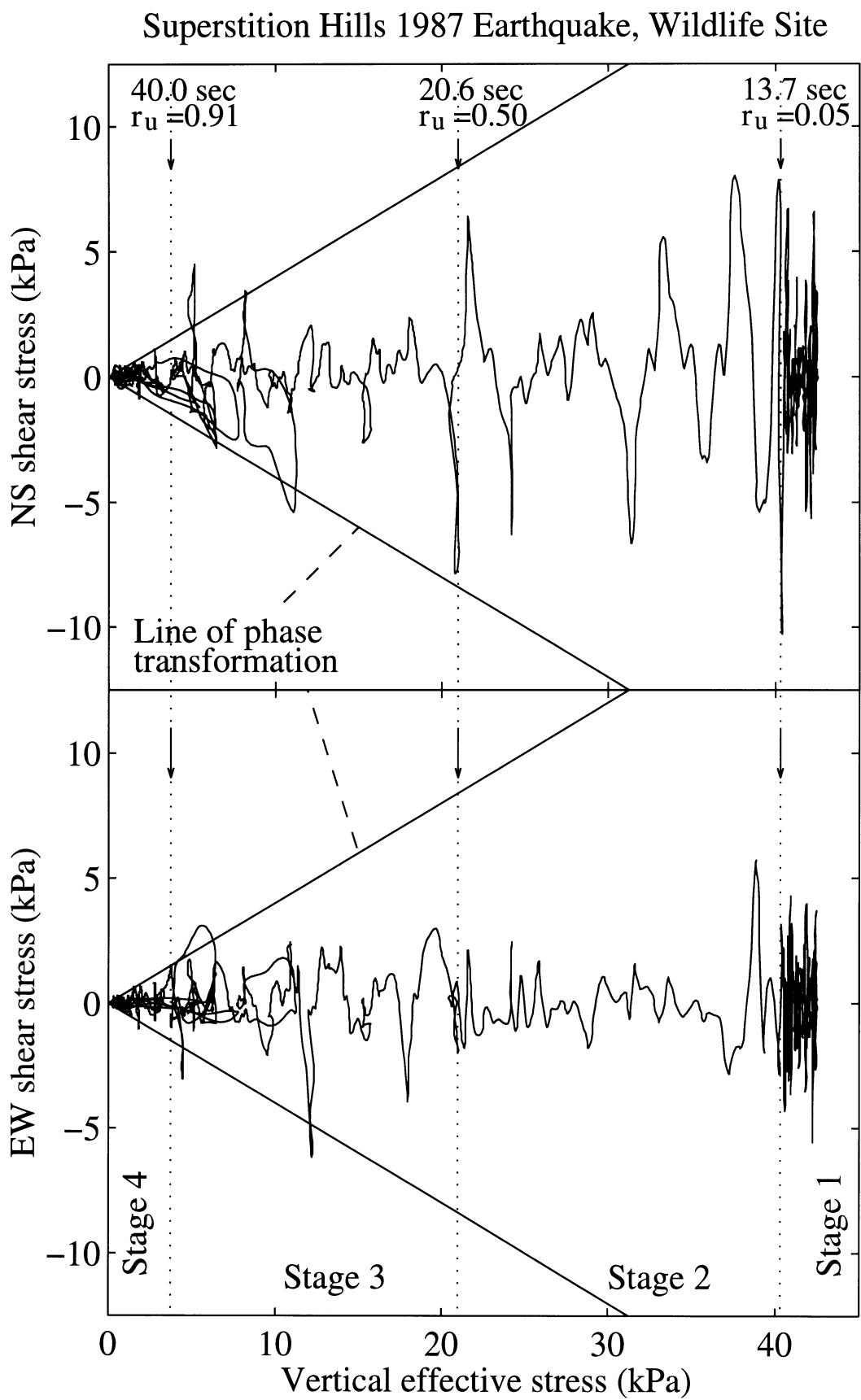


Figure 3.8: Wildlife-Refuge NS and EW shear stress-strain histories during the Superstition Hills 1987 Earthquake (evaluated from acceleration and excess pore pressure histories shown in Fig. 3.3).

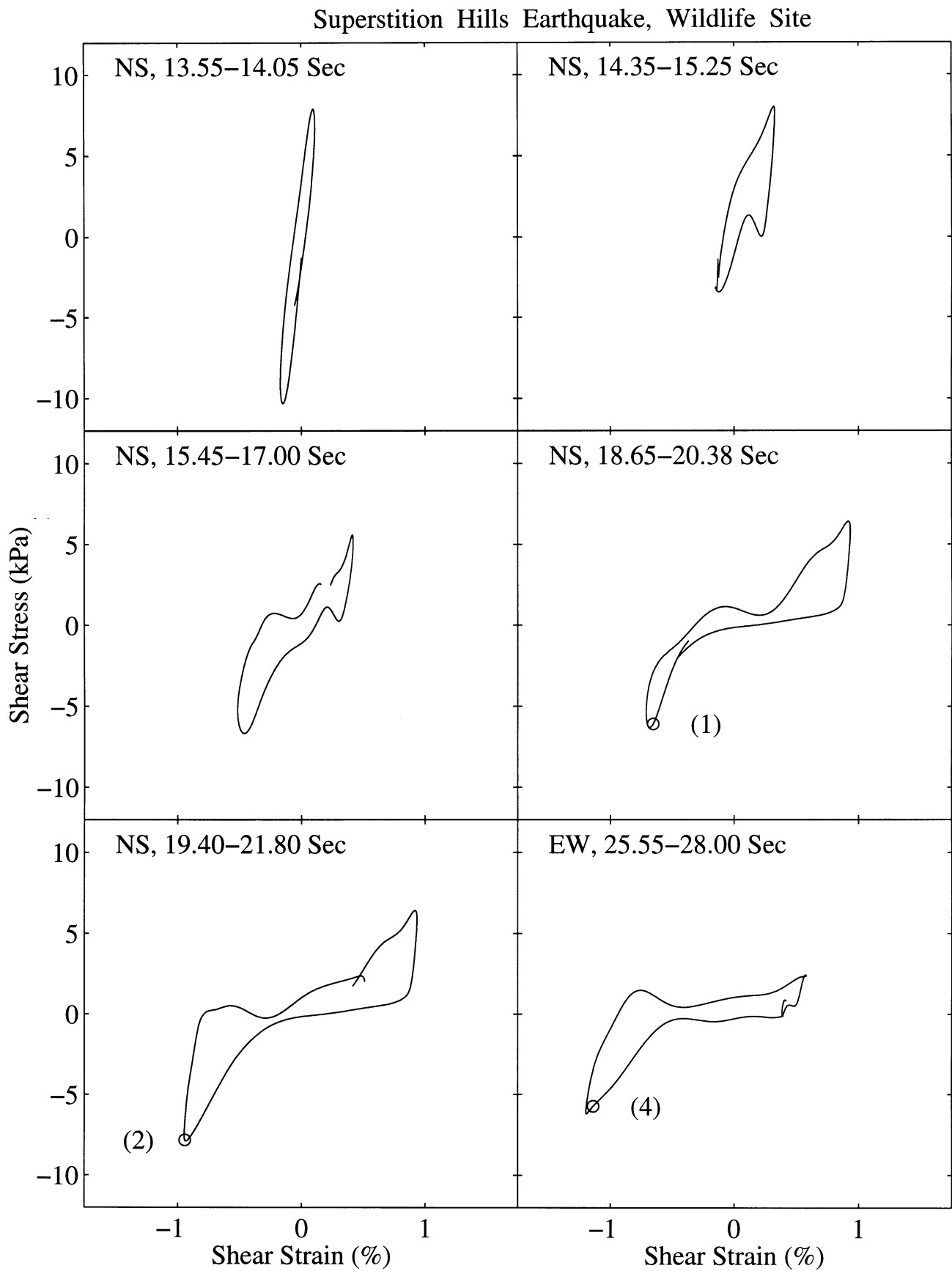


Figure 3.9: Shear stress-strain history during selected loading cycles of stages 1, 2 and 3 of the Superstition Hills earthquake.

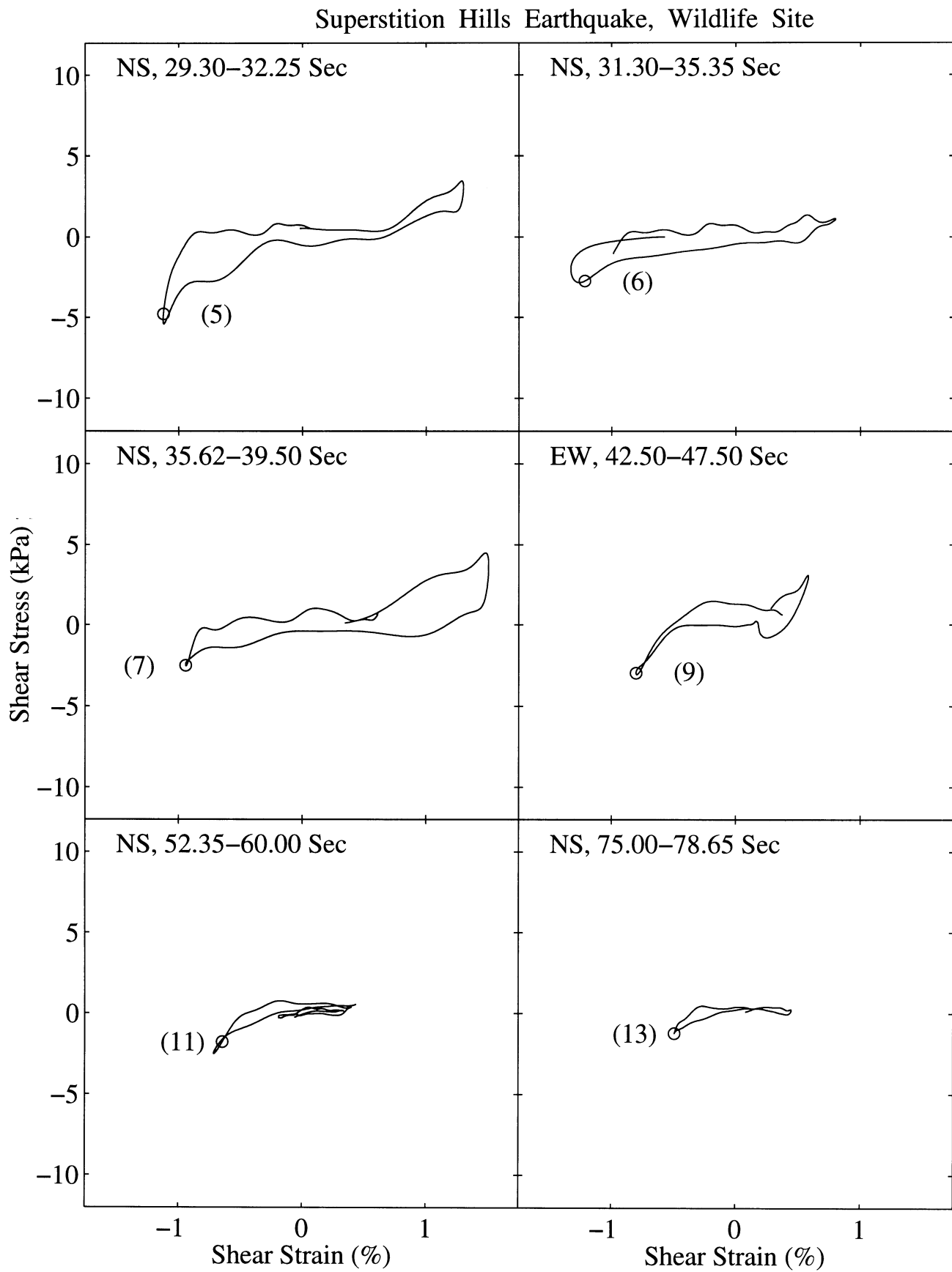


Figure 3.10: Wildlife-Refuge shear stress-strain history during selected loading cycles of stages 3 and 4 of the Superstition Hills earthquake.

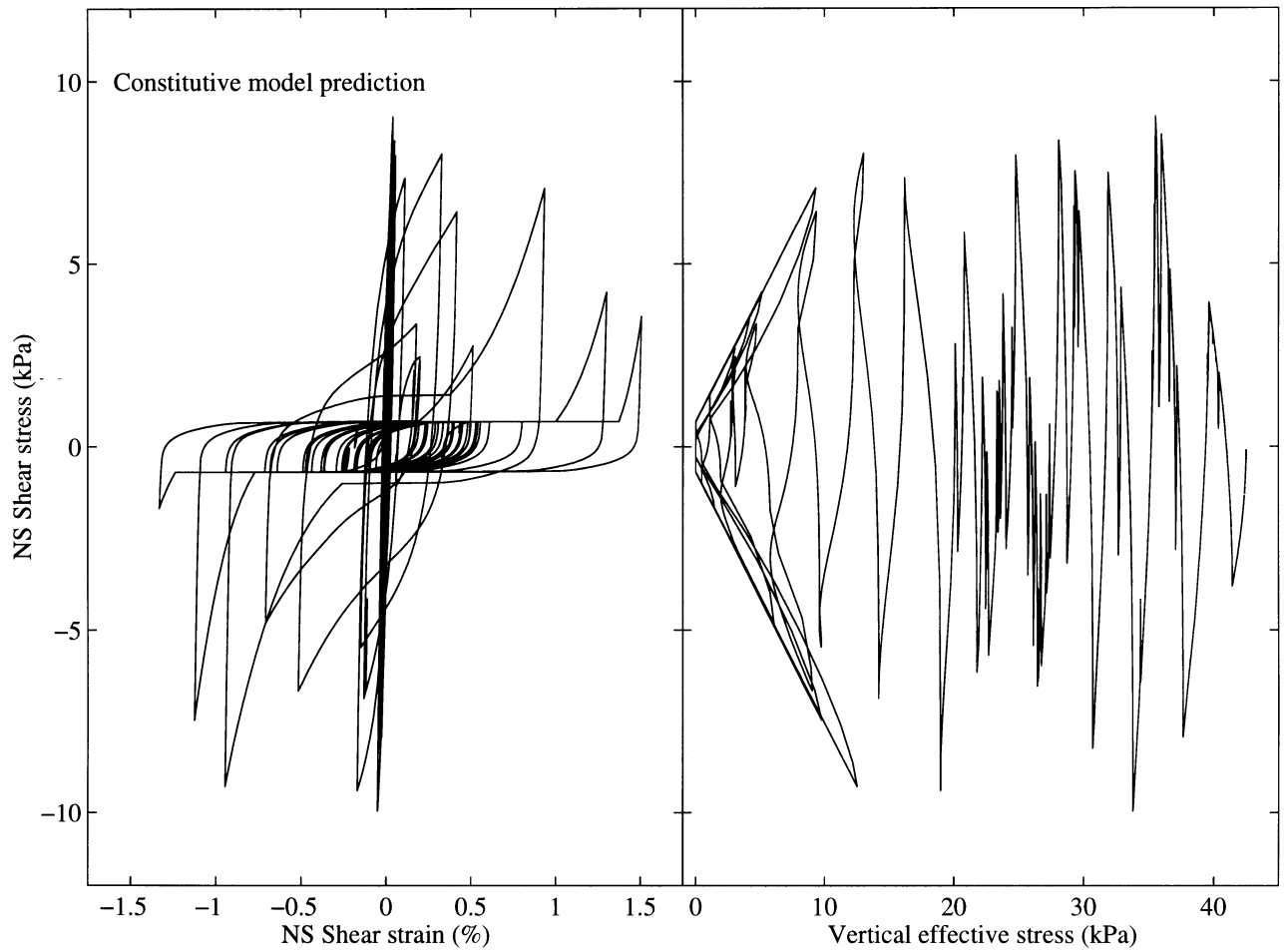


Figure 3.11: Wildlife-Refuge computed NS shear stress-strain and effective-stress histories during the Superstition Hills 1987 Earthquake.

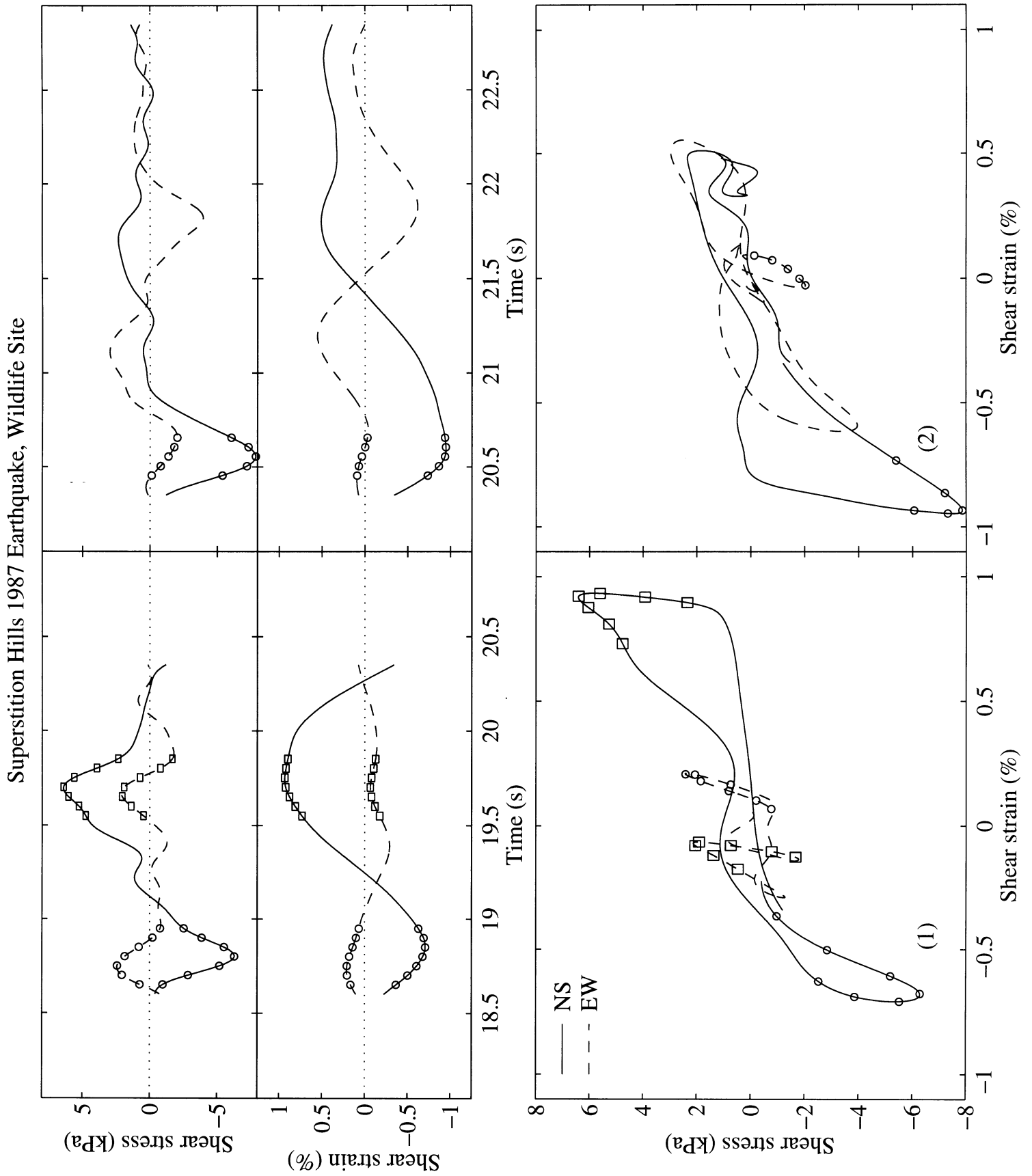


Figure 3.12: Wildlife-Refuge shear stress-strain history during selected loading cycles of stages 3 and 4 of the Superstition Hills earthquake.

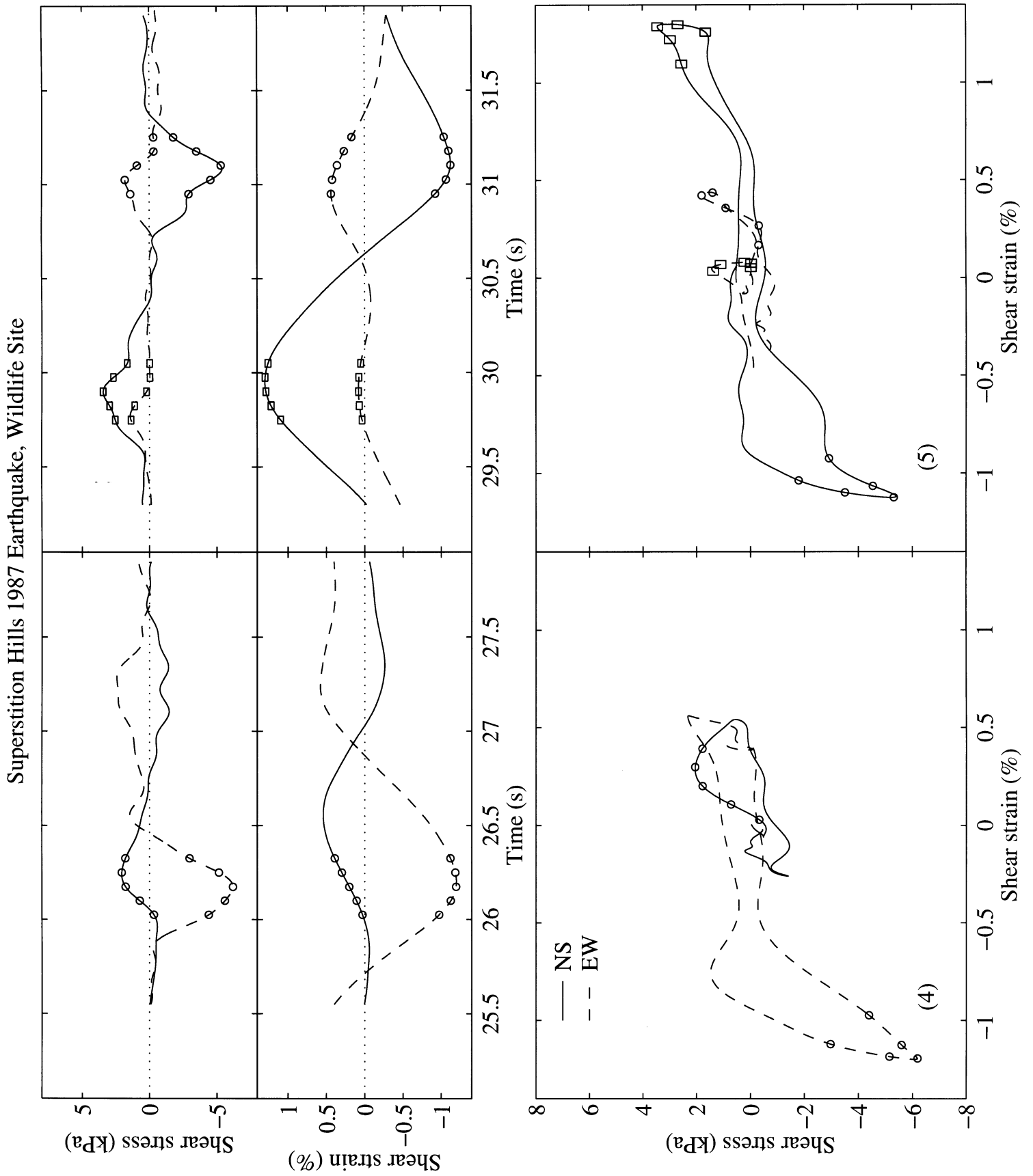


Figure 3.13: Wildlife-Refuge shear stress-strain history during selected loading cycles of stages 3 and 4 of the Superstition Hills earthquake.

manifested in an additional response characteristic. This is illustrated by Figs. 13 and 14 in which selected stress-strain time windows are shown in the NS and EW directions. In these windows (Figs. 13 and 14), it may be observed that during any large strain phase associated with dilation and regain in stiffness and strength (points 1, 2, 4, and 5), a corresponding stiff response phase also appears in the other shaking direction. In other words, the stiffness caused by large strains in a certain direction of shear, is reflected on the overall soil response during this time window. Thus, during such instants, stiff shear response prevails, even in the shearing directions with small shear strain.

3.5 Port Island, Kobe Japan

3.5.1 Instrumentation and seismic records

Port Island is an artificial (reclaimed) island located on the west-south side of Kobe, Japan. In the phase completed by 1981 (Fig. 3.14), 436 ha were reclaimed by bottom-dumping from barges (Nakakita and Watanabe 1981). Soil in the artificial reclaimed layer (O'Rourke 1995, Sitar 1995) consisted of decomposed weathered granite fill (Masa soil mined from the nearby Rokko mountains) with grain sizes ranging from gravel and cobble-sized particles, to fine sand (2 mm mean particle size, with silt-sized particles or smaller of less than 10% by weight). A downhole accelerometer array was installed at the North-West corner of Port Island (Figs. 3.14 and 3.15) in August 1991 (Iwasaki 1995a). The array consisted of triaxial accelerometers located at the surface, 16 m, 32 m, and 83 m depths. All instruments were linked to a common triggering mechanism, and hence the recorded earthquake data were synchronized. The array location is close to an improved-ground warehouse site (Fig. 3.14). Soil treatment at the warehouse site was performed using the vibro-rod method, and covered most of the reclaimed layer thickness (Sitar 1995).

As shown in Fig. 3.15, the downhole array site consists of: (1) an artificial, reclaimed, loose surface layer down to about 19 m depth, (2) an alluvial clay layer between 19 m and 27 m depth, (3) sand and sand with gravel strata interlayered with clay between 27 and 61 m depth, (4) a diluvial clay layer between 61 m and 82 m depth, and (5) sand with gravel layers interlayered with clay starting at about 82 m depth. The water table was located at 4 m depth approximately. A Standard Penetration Test (SPT) and a geophysical shear wave velocity profile of the soil strata around the downhole array are also shown in Fig. 3.15 (Iwasaki 1995a, b). In the upper 20 m layer (Fig. 3.15), low Standard Penetration Test (SPT) blow counts prevailed (average uncorrected N-values of about 6 blows/ft). Such low values in a granular fill are indicative of high liquefaction susceptibility (Seed *et al.* 1983).

3.5.2 Shear stress-strain histories

Using the recorded downhole accelerations (Fig. 3.16) and Eqs. 5-9 of Elgamal *et al.* 1996b, shear stress-strain response was evaluated as shown in Fig. 3.17. Selected representative cycles of this response are shown in Fig. 3.18. Two remarkably different response patterns were exhibited at the site. Below 32m depth, the shear stress-strain histories showed an essentially

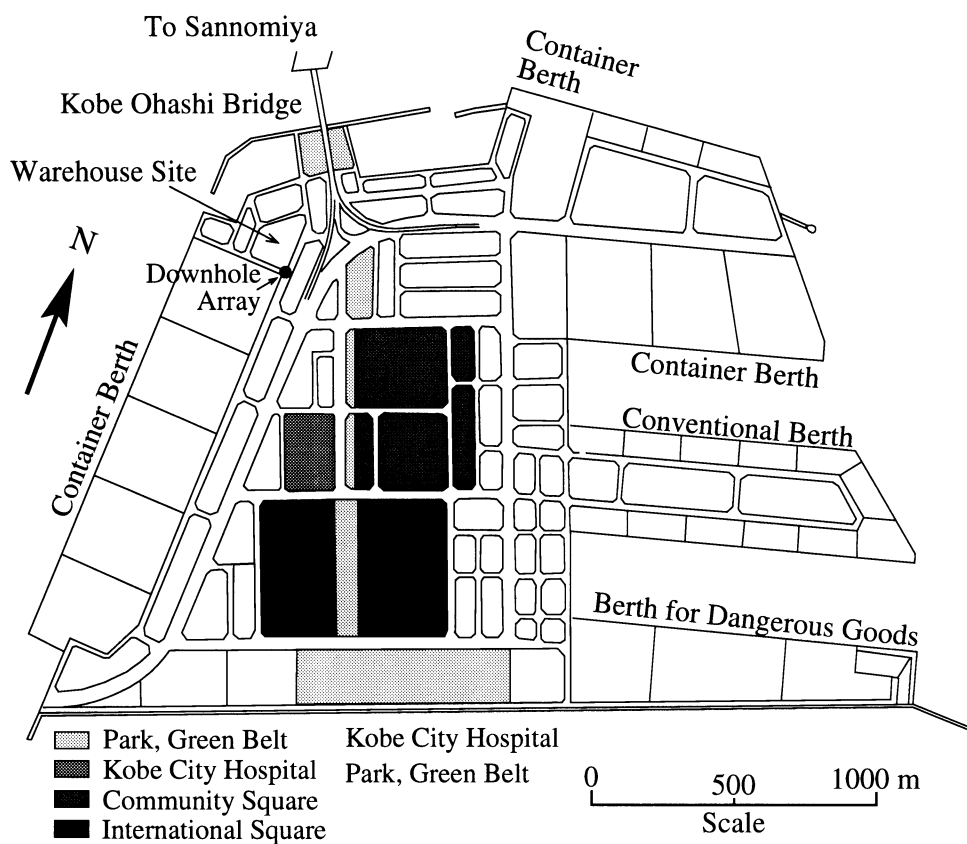


Figure 3.14: Port Island map (showing reclaimed areas completed in 1981, after Nakakita and Watanabe 1981).

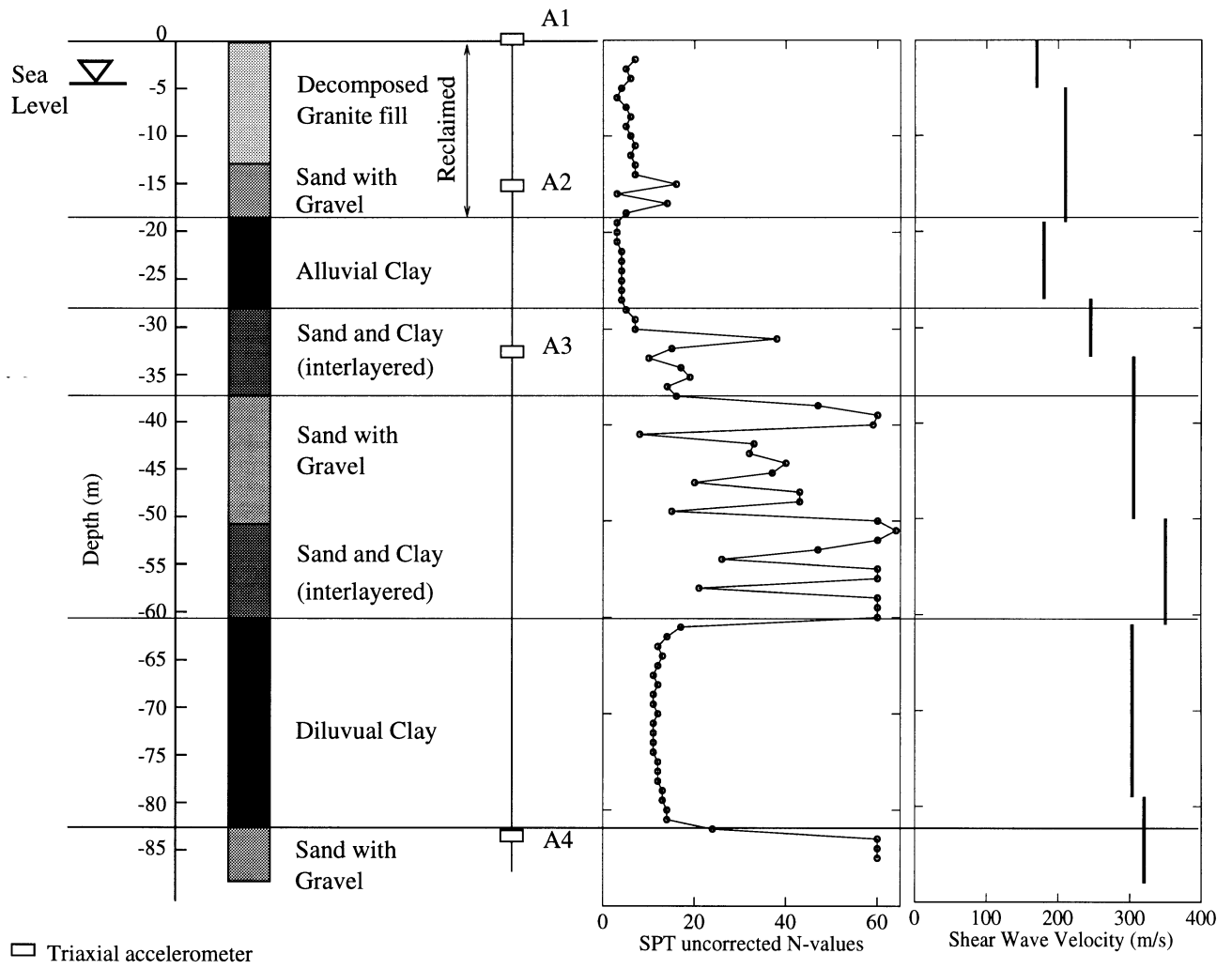


Figure 3.15: Soil profile and instrumentation at the Port Island site (after Iwasaki 1995a).

Port Island, Kobe (Japan). Hyogoken-Nanbu Earthquake, Jan. 17, 1995

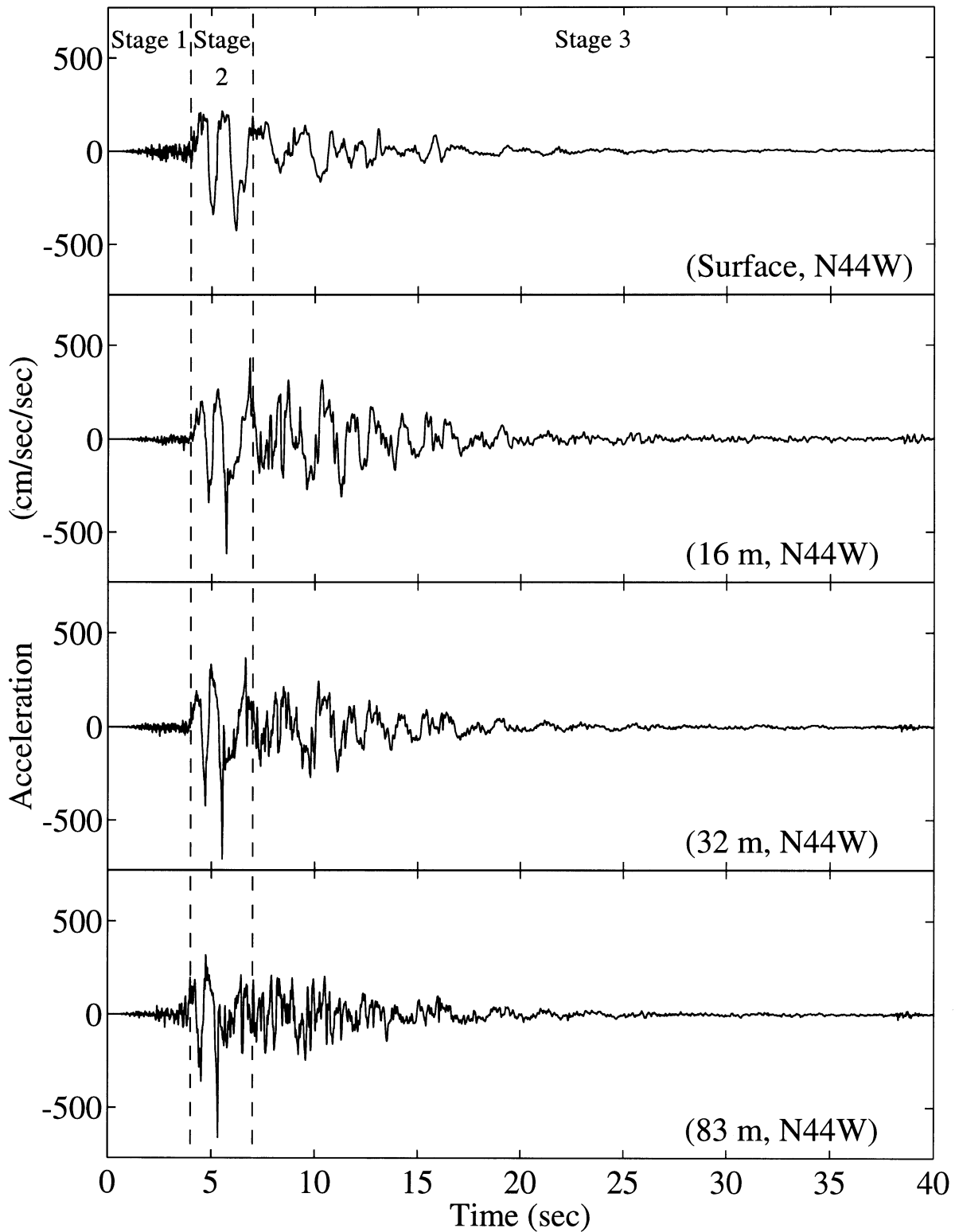


Figure 3.16: N44W accelerations at ground surface and downhole stations (at 16 m, 32 m and 83 m depths, after Iwasaki 1995a).

linear soil response, with no appreciable reduction in soil stiffness. On the other hand, at shallow depths, the stress-strain histories indicated: (1) a noticeable reduction in stiffness with a slight shear strain hardening at elevation 24m (Fig. 3.18), and (2) an abrupt sharp loss of stiffness and reduction of yield strength near the surface at 8m depth.

3.5.3 Computational simulation

The employed soil model parameters were derived through a nonlinear optimization technique (Bard 1974, Gill 1981, NAG 1991), so as to achieve the best possible match between the identified stress-strain responses (selected cycles shown in Fig. 3.18), and the computed counterparts. Optimization was performed in a weighted manner where: (1) the initial phase of response before pore-pressure buildup was used primarily to identify the low amplitude soil properties, (2) the next phase of pore-pressure buildup was employed for calibrating the associated modeling parameters, and (3) the remaining response was used to calibrate the corresponding post-liquefaction model response. Based on the above, the optimized model stress-strain response is shown in Figs. 20 and 21, along with the counterpart evaluated earlier from seismic response. The main optimal modeling parameters were: $v_s = 167$ m/s and friction angle = 34 degrees (0-16m layers), $v_s = 242$ m/s and friction angle = 36 degrees (16-32m layers); and $v_s = 342$ m/s and friction angle = 40 degrees (32-83m layers). These parameters represent average dynamic properties of the soil layers between the accelerometers located at elevations 0 m, 16 m, 32 m, and 83 m (Fig. 16).

Using the effective stress finite element model of Parra 1996, one-dimensional site response was conducted with lateral earth pressure coefficient $K_0 = 1.0$ (during application of own weight) and Bulk modulus $B = (2/3)G$ during dynamic excitation (Parra 1996). An essentially undrained dynamic soil response resulted from using a permeability coefficient $k = 1 \times 10^{-5}$ m/sec. The N44W earthquake record at 83 m depth was employed as input excitation. As may be expected, close agreement was found between the computed and recorded accelerations (Fig. 3.21). The computed excess pore pressure time history at 8 m depth showed that an abrupt rise occurred mainly during the phase of strongest excitation (stage 2, 4-7 s), causing the upper soil layers to lose stiffness and strength (Fig. 3.18).

3.6 References

- Arulmoli, K., Muraleetharan, K. K., Hossain, M. M. and Fruth, L. S. (1992). "Verification of Liquefaction Analyses by Centrifuge Studies Laboratory Testing Program Soil Data Report," Report, The Earth Technology Corporation.
- Bard, Y. (1974). *em Nonlinear Parameter Estimation*, Academic Press, New York, 1974.
- Bardet, J. P., Oka, F., Sugito, M., and Yashima, A. (1995). *The Great Hanshin Earthquake Disaster*, Prelim. Investigation Report, University of Southern California, Los Angeles, CA.
- Bennett, M. J., McLaughlin, P. V., Sarmiento, J. S., and Youd, T. L. (1984). "Geotechnical Investigation of Liquefaction Sites, Imperial Valley, California," *U.S. Geological Survey Open-File Report* 84-252.

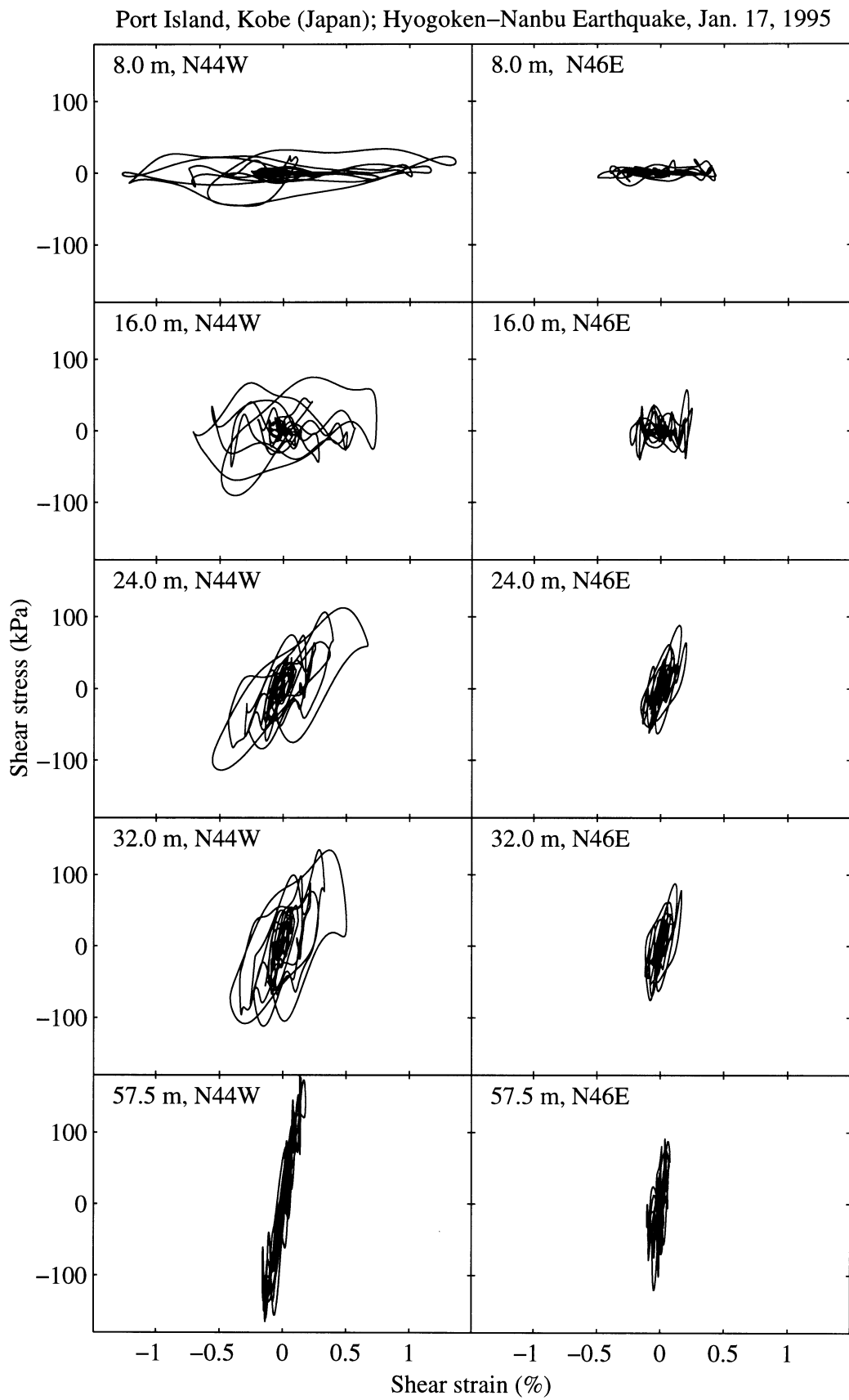


Figure 3.17: Port Island site shear stress-strain histories at 8.0 m, 16.0 m, 24.0 m, 32.0 m, and 57.5 m depths.

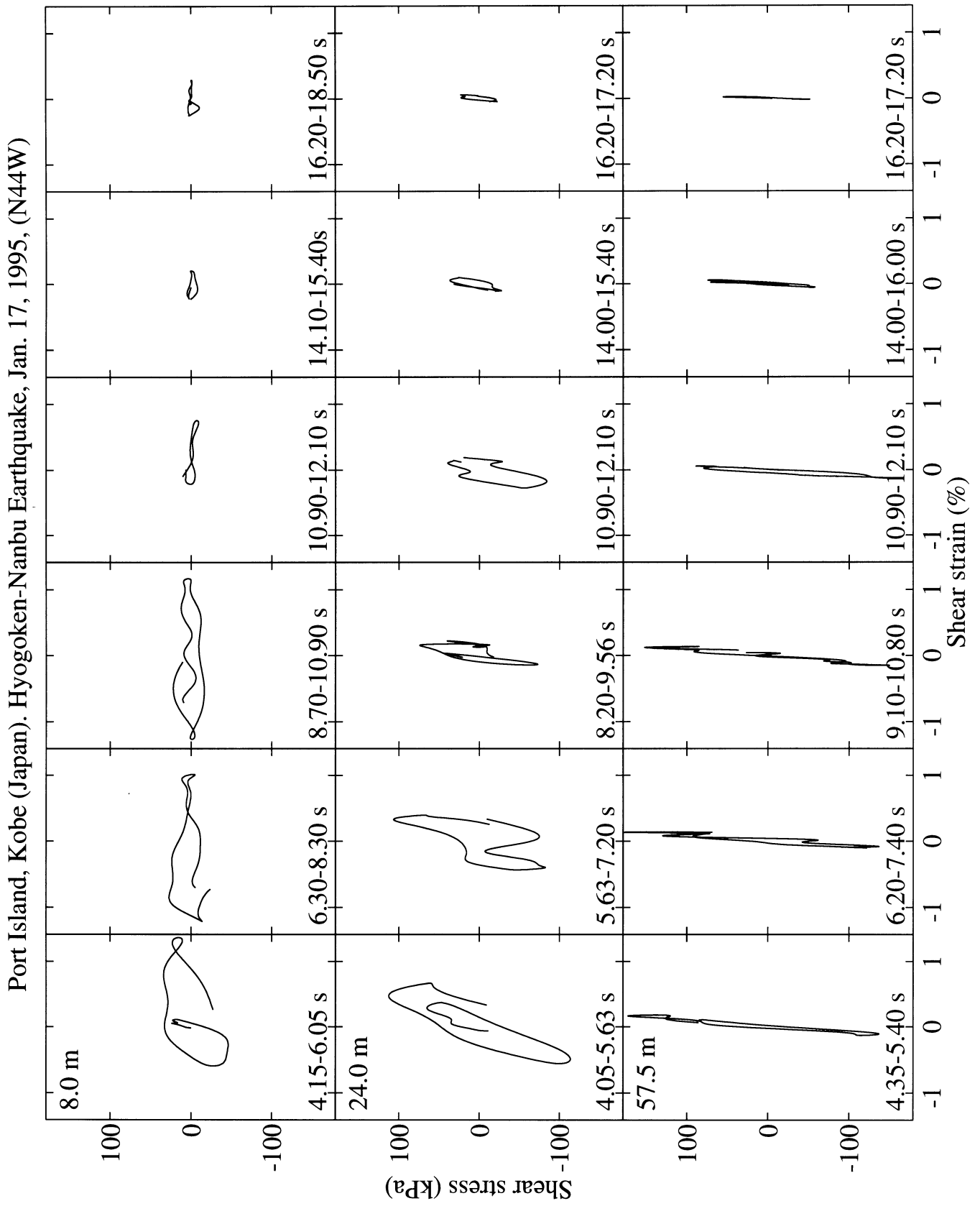


Figure 3.18: Selected N44W shear stress-strain cycles midway between accelerometers, at 8.0 m, 24.0 m and 57.5 m depths.

Port Island, Kobe (Japan); Hyogoken–Nanbu Earthquake, Jan. 17, 1995

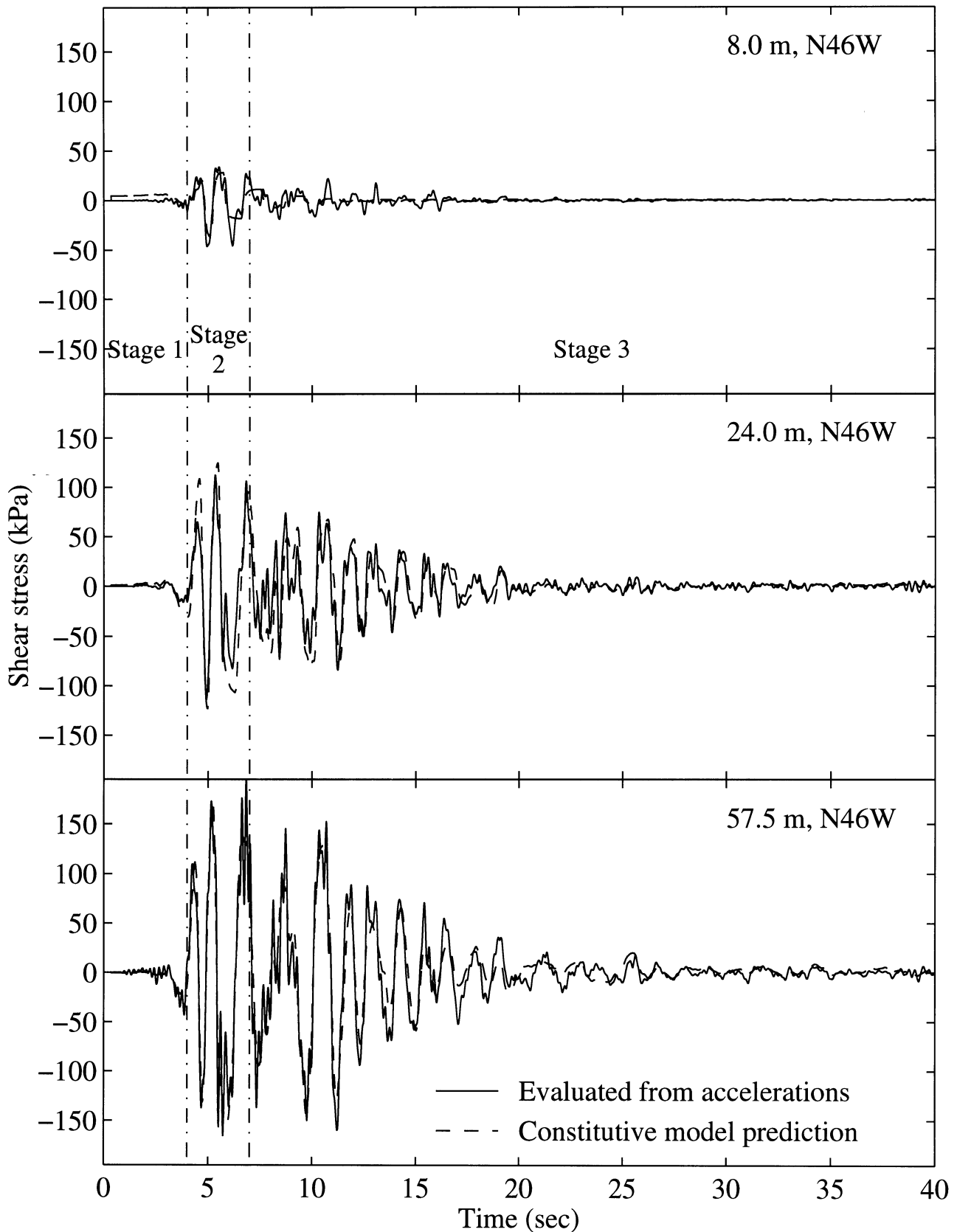


Figure 3.19: Port Island shear stress histories estimated from acceleration histories and corresponding constitutive model prediction (at 8.0 m, 24.0 m, and 57.5 m depths).

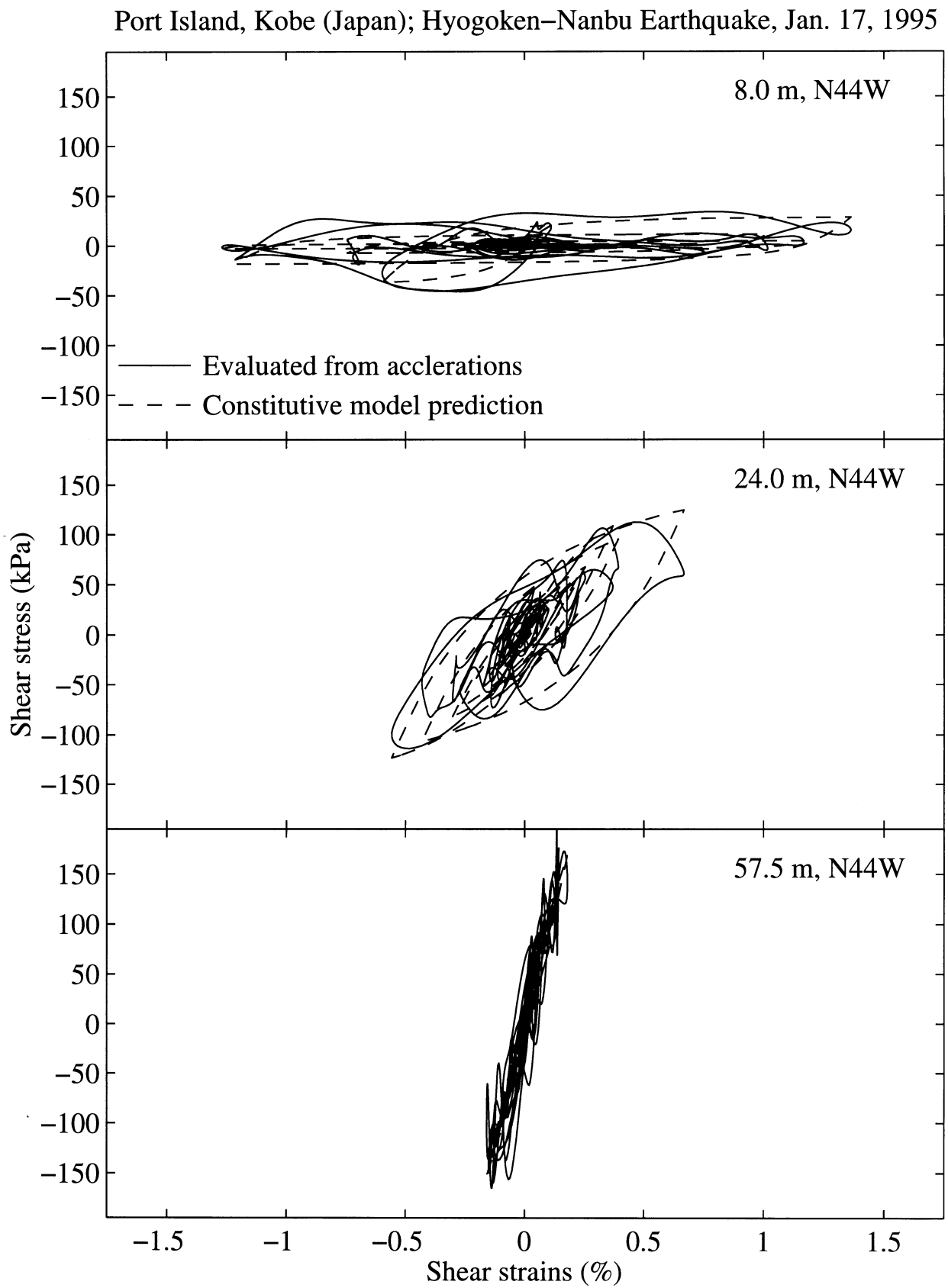


Figure 3.20: Port Island shear stress-strain histories estimated from acceleration histories and corresponding constitutive model prediction (at 8.0 m, 24.0 m, and 57.5 m depths).

Port Island, Kobe (Japan). Hyogoken-Nanbu Earthquake, Jan. 17, 1995

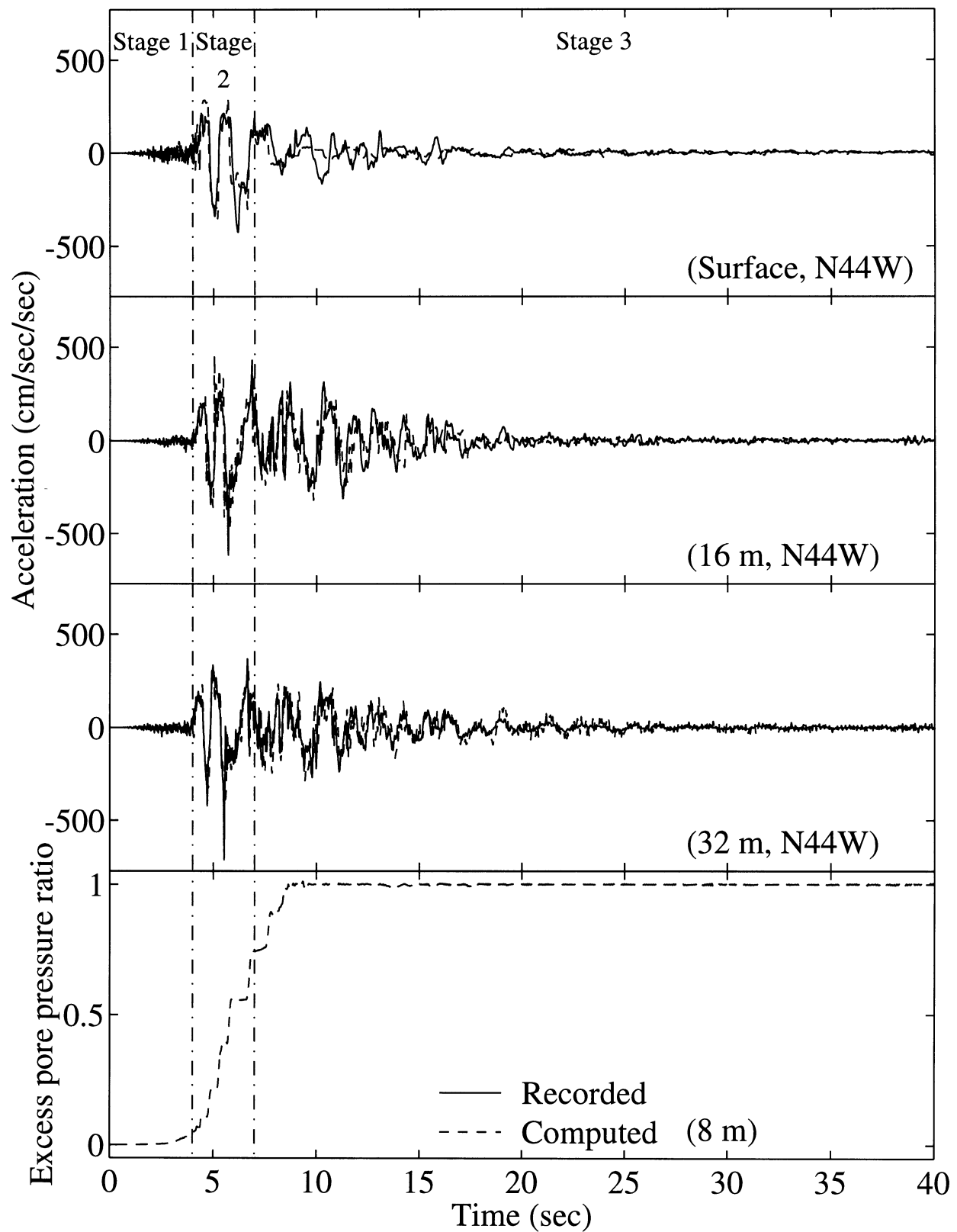


Figure 3.21: Port Island recorded and computed accelerations at surface, 16 m and 32 m depth, and computed excess pore pressure ratio at 8 m depth.

- Biot, M. A. (1962). "The Mechanics of Deformation and Acoustic Propagation in Porous Media", *J. Appl. Phys.*, Vol. 33, No. 4, 1482-1498.
- Byrne, P. M. (1991). "A Cyclic Shear Volume-Coupling and Pore-water Pressure Model for Sand," *Proceeding, 2nd International Conference on Recent Advances in Geotechnical Earthquake Engineering and Soil Dynamics*, St. Louis Missouri. Vol 1, 47-56.
- Castro, G. (1975). "Liquefaction and Cyclic Mobility of Saturated Sand," *Journal of Geotechnical Engineering Division, ASCE*, Vol. 101, No. 6, 555-569.
- Chang, C.-Y., Mok, C. M., Power, M. S., Tang, Y. K. (1991). "Analysis of Ground Response Data at Lotung Large-Scale Soil-Structure Interaction Experiment Site," Report No. NP-7306-SL, Electric Power Research Institute, Palo Alto, California.
- Comartin, C. D., Greene, M., and Tubbesing, S. K., eds. (1995). *The Hyogo-Ken Nanbu Earthquake, Great Hanshin Earthquake Disaster, January 17, 1995*, Preliminary Reconnaissance Report, Earthquake Engineering Research Institute, CA.
- Elgamal, A.-W., Zeghal, M. and Parra, E. (1996a). "Liquefaction of an Artificial Island in Kobe, Japan," *Journal of Geotechnical Engineering, ASCE* Vol. 122, No. 1.
- Elgamal, A.-W., Zeghal, M., Parra, E., Gunturi, R., Tang, H.T., and Stepp, C.J. (1996b). "Identification and Modeling of Earthquake Ground Response I: Site Amplification," Companion paper.
- Gill, P. E., Murray, W., and Wright, M. H. (1981). *Practical Optimization*, Academic Press, London and New York.
- Glaser S. and Chung, R. (1995). "Evaluation of Liquefying Soil Through Time Using System Identification," *Proceedings of the 5th U.S.-Japan Workshop on Earthquake Resistant Design of Lifeline Facilities and Countermeasures Against Soil Liquefaction*, O'Rourke T. and Hamada, M. eds., NCEER.
- Holzer, T. L., Youd T. L. and Hanks T. C. (1989). "Dynamics of Liquefaction During the 1987 Superstition Hills, California, Earthquake," *Science*, Vol. 244, 56-59.
- Iai, S. (1991). "A Strain Space Multiple Mechanism Model for Cyclic Behavior of Sand and Its Application," *Earthquake Engineering Research Note No. 43*, Port and Harbor Research Institute, Japan.
- Iai, S., Morita, T., Kameoka, T., Matsunaga, Y., and Abiko, K., (1995). "Response of a Dense Sand Deposit During 1993 Kushiro-Oki Earthquake," *Soils and Foundations*, Vol 35, No. 1, 115-131.
- Ishihara, K., Anazawa, Y., and Kuwano, J. (1987). "Pore Water Pressures and Ground Motions Monitored During the 1985 Chiba-Ibaragi Earthquake," *Soils and Foundations*, Vol 27, No. 3, 13-30.
- Ishihara, K. (1985). "Stability of Natural Deposits During Earthquakes," *Proceedings of 11th International Conference on Soil Mechanics and Foundation Engineering*, San Francisco, Vol. 1, 327-376.
- Iwasaki, Y. (1995a). Georesearch Institute, Osaka, Japan, Personal communication.
- Iwasaki, Y. (1995b). "Geological and Geotechnical Characteristics of Kobe Area and Strong Ground Motion Records by 1995 Kobe Earthquake, Tsuchi-to-Kiso," *Japanese Society of Soil Mechanics and Foundation Engineering*, Vol. 43, No. 6, 15-20 (in Japanese).
- Kabilamany, K. and Ishihara, K. (1990). "Stress Dilatancy and hardening laws for Rigid Granular Model of Sand," *Soil Dynamics and Earthquake Engineering*, Vol. 9, No. 2, 66-77.

- Koga, Y. and Matsuo, O. (1990). "Shaking Table Tests of Embankments Resting on Liquefiable Sandy Ground," *Soils and Foundations*, Vol. 30, No. 4, 162-174.
- Lacy, S. (1986). "Numerical Procedures for Nonlinear Transient Analysis of Two-phase Soil Systems", *Ph.D. dissertation*, Princeton University, NJ, U.S.A.
- Numerical Analysis Group (1991). "Minimizing or Maximizing a Function," NAG Fortran Library, Mark 16, Downers Grove, IL, USA.
- Nakai, T. (1989). "An Isotropic Hardening Elastoplastic Model for Sand Considering the Stress Path Dependency in Three-Dimensional Stresses," *Soils and Foundations*, Vol 29, No. 1, 119-137.
- Nakakita, Y., and Watanabe, Y. (1981). "Soil stabilization by Preloading in Kobe Port Island," *Proceedings of the 9th International Conference on Soil Mechanics and Foundation Engineering*, Tokyo, Japan, 611-622.
- National Research Council (1985). *Liquefaction of Soils During Earthquakes*, Committee on Earthquake Engineering, National Academy press, Washington D. C.
- O'Rourke, T. D. (1995). "Geotechnical Effects," *Preliminary Report from the Hyogoken-Nanbu Earthquake of January 17, 1995*, National Center for Earthquake Engineering Research Bulletin, SUNY, Buffalo, Vol. 9, No. 1.
- Parra, E. (1996). "Numerical Modeling of Liquefaction and Lateral Ground Deformation Including Cyclic Mobility and Dilation Response in Soil Systems", *Ph.D. dissertation*, Dept. of Civil Engineering, Rensselaer Polytechnic Institute.
- Ragheb, A. (1994) "Numerical Analysis of Seismically Induced Deformations in Saturated Granular Soil Strata", *Ph.D. dissertation*, Dept. of Civil Engineering, Rensselaer Polytechnic Institute, Troy, NY.
- Sasaki, Y., Towhata, I., Tokida, K., Yamada, K., Matsumoto, H., Tamari, Y., and Saya, A. (1992). "Mechanism of Permanent Displacement of Ground Caused by seismic Liquefaction," *Soils and Foundations*, Vol. 32, No. 3, pp.79-96.
- Seed, H. B. (1966). "Landslides During Earthquakes Due to Soil Liquefaction," *Journal of Soil Mechanics and Foundations Division*, ASCE, Vol. 94, No. SM5, Sept., 1053-1122.
- Seed, H. B., Idriss, I., Lee, K. L., and Makdisi, F. (1975). "Dynamic Analysis of the Slide in the Lower San Fernando Dam During the Earthquake of February 9, 1971," *Journal of Geotechnical Engineering*, ASCE, Vol. 101, No. GT9, Sept., 889-911.
- Seed, H. B., Idriss, I. M., and Arango, I. (1983). "Evaluation of Liquefaction Potential Using Field Performance Data," *Journal of Geotechnical Engineering*, ASCE, Vol. 109, No. 3, 458-482.
- Seed, R. B., Dickenson, S. E., Riemer, M. F., Bray, J. D., Sitar, N., Mitchell, J. K., Idriss, I. M., Kayen, R. E., Kropp, A., Hander, L.F. Jr., and Power, M. S. (1990). "Preliminary Report on the Principal Geotechnical Aspects of the October 17, 1989, Loma Prieta Earthquake," Report No. EERC-90-05, Earthquake Engineering Research Center, University of California, Berkeley.
- Soils and Foundations (1996). "Special Issue on Geotechnical Aspects of the January 17, 1995 Hyogoken Nambu Earthquake," *Soils and Foundations*, Japan Geotechnical Society, January 1996.
- Sitar, N., Ed. (1995). "Geotechnical Reconnaissance of the Effects of the January 17, 1995, Hyogoken-Nanbu Earthquake Japan," *Report No. UCB/EERC-95/01*, Earthquake Engineering Research Center, Berkeley, California.

- Taboada, V. M. and Dobry, R. (1993). "Experimental Results of Model 1 at RPI," *Proceedings of the International Conference on the Verification of Numerical Procedures for the Analysis of Soil Liquefaction Problems*, Arulanandan, K. and Scott, R. F., eds., Vol. 1, Davis, CA, 3-17, Balkema.
- Towhata, I. and Toyota, H. (1994). "Dynamic Analysis of Lateral Flow of Liquefied Ground," *Proceedings of the 5th U.S.-Japan Workshop on Earthquake Resistant Design of Lifeline Facilities and Countermeasures Against Soil Liquefaction*, O'Rourke T. and Hamada, M. eds., NCEER.
- Vucetic, M. and Dobry, R. (1988). "Cyclic Triaxial Strain-Controlled testing of Liquefiable Sands," *Amer. Soc. Testing Mat., Spec. Tech. Publ. 977*, 475-485.
- Youd, T. L., and Wicczorek, G. F. (1984). "Liquefaction During 1981 and Previous Earthquakes Near Westmorland California," U.S. Geological Survey Open-File Report 84-680.
- Zeghal, M. and Elgamal, A.-W. (1994). "Analysis of Site Liquefaction Using Earthquake Records," *Journal of Geotechnical Engineering*, ASCE, Vol. 120, No. 6, 996-1017.
- Zorapapel, G. T., and Vucetic, M. (1994). "The effect of Pore-Pressure on Ground Motion," *Earthquake Spectra*, Vol. 10 No. 2, 403-438.

Chapter 4

Mechanism of Liquefaction Response in Sand-Silt Sites Using Dynamic Centrifuge Tests

4.1 Introduction

A near-catastrophe resulted from a major liquefaction-induced slide in the lower San Fernando dam (Southern California) during the February 9, 1971 earthquake [1]. Eighty thousand people living downstream of the dam were evacuated, and the reservoir level was promptly lowered to a safe elevation. Recent major seismic events such as the 1989 Loma Prieta and the 1995 Kobe earthquakes, continue to demonstrate the damaging effects of liquefaction-induced loss of soil strength and associated lateral spreading [2,3,4,5,6,7]. Experimental laboratory research on soil liquefaction has provided valuable insight concerning excess pore-pressure buildup in saturated loose granular soils [8]. However, for engineering applications, there remains a need to further understand and identify the mechanisms of seismically induced soil deformation due to liquefaction, and associated stiffness and strength degradation.

In-situ records of site or embankment liquefaction are scarce. The Wildlife Refuge site seismic records (Imperial County, CA) during the 1987 Superstition Hills earthquake are currently the only such data set (surface and downhole accelerations, and pore-pressures) in the United States, and possibly worldwide [9]. A number of sites have been instrumented throughout California to capture anticipated liquefaction during future earthquakes [10]. Centrifuge tests provide an alternative source of information to assess liquefaction and lateral spreading mechanisms of various soil-systems under a broad range of loading conditions at a relatively low cost. In this regard, the VELACS (Verification of Liquefaction Analysis by Centrifuge Studies) project is unique [11,12]. Within this project, ten saturated soil-systems with well defined boundary conditions and soil properties were tested.

Stratified non-cohesive soils of different permeabilities, such as sand-silt systems, are of common occurrence and are prone to liquefaction and formation of sand boils during seismic excitation [13,14]. Herein, the recorded dynamic response of two VELACS centrifuge models composed of a medium-dense sandy layer overlain by a low permeability silt deposit were analyzed. These models (Fig. 4.1) consist of a two-layer level site [15], and an earth embank-

ment [16]. A simple identification procedure was employed to estimate shear stress and strain histories within the soil layers, directly from the recorded accelerations. These histories were then utilized to assess the layered soil-system response mechanisms during liquefaction. The identified stress-strain histories showed: (1) the typical reduction in soil stiffness and strength associated with liquefaction, and (2) a subsequent gradual regain in stiffness during cyclic excitation. Similar response patterns were observed during simple shear laboratory tests [17].

The following section briefly describes the centrifuge testing procedures. Thereafter, the employed stress-strain identification procedure is presented, and the analysis results are described and discussed in detail. This identification procedure was proposed in basic form for shake-table studies [18], and was further developed and used for analyses of downhole seismic site response [19,20,21].

4.2 Testing Procedures

A Shaevitz centrifuge with a 1 m radius was employed at the University of California Davis (UCD). The level site test was performed in a one dimensional (1D) laminated container [22]. This container (Fig. 4.1a) allows relative slip between laminates in order to simulate 1D shear response. The embankment test was performed in a rigid container (Fig. 4.1b). Instrumentation included pore pressure transducers, accelerometers, and LVDTs (Linear Variable Differential Transducers) to measure settlements (Fig. 4.1).

The soil models were built and instrumented at 1 g (g = acceleration of gravity) with transducers installed at the specified locations; and saturated with water under vacuum. Thereafter, the model containers were placed on the centrifuge and spun to a 50 g gravitational field. At this gravitational field, the analyzed models represent prototypes of: (1) a 6 m thick level site (model 4a), and (2) a 4 m high earth embankment (model 6). In view of the scaling laws applicable to centrifuge experiments [23], prototype permeability of the employed sand corresponds to that of coarse sand or fine gravel.

One-dimensional shaking was imparted along the model base using an electro-hydraulic shaker [24]. Acceleration, pore pressure and displacement time histories were recorded by the installed sensors (Fig. 4.1). The results of these tests have been documented by Arulanandan *et al.* [15,16]. In the following sections, prototype units [23] will be employed when discussing these results.

4.3 Evaluation Of Shear Stress-Strain Histories

Within the setting of a laminar box subjected to lateral input motion, the soil system of model 4a undergoes an essentially 1D shear loading. Thus, the three-dimensional equations of motion reduce to that of a one-dimensional shear beam [25,26]. The governing equations are (Fig. 4.2):

$$\frac{\partial \tau}{\partial z} = \rho \ddot{u}, \quad \text{with the boundary conditions } u(h, t) = u_g(t), \quad \text{and } \tau(0, t) = 0 \quad (4.1)$$

in which t is time, z is depth coordinate, $\tau = \tau(z, t)$ is lateral shear stress, $\ddot{u} = \ddot{u}(z, t)$ is absolute lateral acceleration, $u = u(z, t)$ is absolute lateral displacement, $u_g(t)$ is input (base) lateral displacement, $\rho = \rho(z)$ is mass density, and h is total depth of soil stratum.

Integrating the equation of motion and using the surface stress-free boundary condition (Eq. 4.1), shear stress at any level z within the ground may be expressed as [19,21]:

$$\tau(z, t) = \int_0^z \rho \ddot{u}(\zeta, t) d\zeta \quad (4.2)$$

If linear interpolation is employed between downhole accelerations, discrete counterparts of shear stresses (Eq. 4.2) at levels z_i and $(z_{i-1} + z_i)/2$ may be expressed as (Fig. 4.2):

$$\tau_i(t) = \tau_{i-1}(t) + \rho_{i-1} \frac{\ddot{u}_{i-1} + \ddot{u}_i}{2} \Delta z_{i-1}, \quad i = 2, 3, \dots \quad (4.3)$$

$$\tau_{i-1/2}(t) = \tau_{i-1}(t) + \rho_{i-1} \frac{3\ddot{u}_{i-1} + \ddot{u}_i}{8} \Delta z_{i-1}, \quad i = 2, 3, \dots \quad (4.4)$$

in which subscripts i and $(i - 1/2)$ refer to levels z_i (of the i^{th} accelerometer) and $(z_{i-1} + z_i)/2$ (halfway between accelerometers $(i - 1)$ and i) respectively, $\tau_i(t) = \tau(z_i, t)$, $\tau_{i-1/2}(t) = \tau((z_{i-1} + z_i)/2, t)$, $\tau_1(t) = \tau(0, t) = 0$ at the stress free ground surface, $\ddot{u}_i = \ddot{u}(z_i, t)$, ρ_{i-1} is average mass density for the soil layer between levels z_{i-1} and z_i , and Δz_i is spacing interval as shown in Fig. 4.2. These stress estimates (Eqs. 4.3 and 4.4) are second-order accurate [19]. A corresponding set of second-order accurate shear strains at levels z_i and $(z_{i-1} + z_i)/2$ may be expressed as [27]:

$$\gamma_i(t) = \frac{1}{\Delta z_{i-1} + \Delta z_i} \left((u_{i+1} - u_i) \frac{\Delta z_{i-1}}{\Delta z_i} + (u_i - u_{i-1}) \frac{\Delta z_i}{\Delta z_{i-1}} \right), \quad i = 2, 3, \dots \quad (4.5)$$

$$\gamma_{i-1/2}(t) = \frac{u_i - u_{i-1}}{\Delta z_{i-1}}, \quad i = 2, 3, \dots \quad (4.6)$$

in which $u_i = u(z_i, t)$ is displacement evaluated through double integration of the corresponding acceleration histories.

For an earth embankment (Fig. 4.1b), the equation of motion of 1D shear-wedge response is [28,29]:

$$\frac{\partial(b\tau)}{\partial z} = \rho b \ddot{u}, \quad \text{with the boundary conditions } u(h, t) = u_g(t), \quad \text{and } \tau(0, t) = 0 \quad (4.7)$$

in which $b = b(z)$ is width of embankment base at level z . Thus, the discrete counterpart of shear stress at level $(z_{i-1} + z_i)/2$ between any two accelerometers is given by [27]:

$$\tau_{2/3}(t) = \frac{[\ddot{u}_1(7b_1 + 2b_2) + \ddot{u}_2(2b_1 + b_2)] \Delta m_1}{12(b_1 + b_2)} \quad (4.8)$$

$$\tau_{i+1/2}(t) = \tau_{i-1/2} \frac{(b_{i-1} + b_i)}{b_i + b_{i+1}} + \frac{\ddot{u}_{i-1}(b_{i-1} + 2b_i) \Delta m_{i-1} + \ddot{u}_{i+1}(2b_i + b_{i+1}) \Delta m_i}{12(b_i + b_{i+1})} + \frac{\ddot{u}_i [2b_{i-1} \Delta m_{i-1} + 7b_i (\Delta m_{i-1} + \Delta m_i) + 2b_{i+1} \Delta m_i]}{12(b_i + b_{i+1})}, \quad i = 2, 3, \dots \quad (4.9)$$

in which $b_i = b(z_i)$ and $\Delta m_i = \rho_i \Delta z_i$.

The identification algorithm presented above (Eqs. 2.5-4.6, 4.8 and 4.9) is based only on the equations of motion and the definition of shear strains. Thus, the algorithm is valid regardless of the type of constitutive relationship that links shear stresses and strains; and the identified stresses and strains reflect all dynamic stiffness and damping mechanisms during the conducted tests. The various approximations involved in the above procedures are discussed in Appendix I. In general, these approximations have no significant influence on the identified salient soil response characteristics, as discussed below.

4.4 Level Site Response: Model 4a

Model 4a consisted of a saturated 3 m layer of Bonnie silt overlaying a 3 m saturated medium-dense Nevada sand stratum (Fig. 4.1, and Tables 4.1 and 4.2). It was proposed and tested by Arulanandan *et al.* at UCD [15]. This test was also independently replicated by RPI [30], and by CalTech [31]. The soil profile of model 4a was also studied within VELACS in three additional tests as model 4b (at UCD [32], the University of Colorado at Boulder [33], and RPI [34]). These additional tests were conducted using rigid containers. All six tests (models 4a and 4b) were to be subjected to the same input excitation as specified by VELACS [11,12]. In the following sections, the UCD model 4a results will be thoroughly analyzed.

Fig. 4.3 displays the recorded UCD model 4a accelerations, vertical settlement and excess pore pressures (u_e). Input accelerations were composed primarily of a 1 Hz signal. The shaking lasted for about 20 seconds, with nearly uniform acceleration amplitudes of about 330 cm/s^2 (A8, Fig. 4.3a). In the sand layer, the excess pore water pressure (u_e) rapidly increased, and reached high values in about one cycle of dynamic excitation. This high u_e which approached the initial effective vertical stress ($r_u = 1.0$) at 3.1 m depth, clearly denoted a process of liquefaction that was sustained throughout the shaking event ($r_u = u_e/\sigma'_v$ is excess pore pressure ratio, where σ'_v is effective vertical stress). Upon the onset of liquefaction, acceleration amplitudes decreased and nearly vanished within the entire soil stratum (Fig. 4.3a). This response pattern is a typical characteristic [35] associated with liquefaction, and loss of soil stiffness and strength (e.g., Niigata, Japan 1964, as reported by Ishihara [36]; Treasure Island, CA 1989, as reported by Hryciw *et al.* [37]; and Kobe, Japan 1995, as reported by Elgamal *et al.* [38]).

During liquefaction, the overlaying surface silt layer remained in isolation from base excitation (A2 and A4, Fig. 4.3a). Thus, it may be concluded that a loss of stiffness and strength was sustained somewhere within (and possibly throughout) the silt stratum. However, within the sand layer, the recorded acceleration (A6, Fig. 4.3) exhibited two distinct response patterns during the phase of high u_e : (1) the typical reduction in acceleration amplitudes upon liquefaction, due to pore-pressure buildup and the resulting decrease in effective confining stresses, and thus in soil stiffness and strength; and (2) a subsequent phase of gradual increase in acceleration amplitudes, possibly denoting a progressive regain of stiffness and strength (A6, Fig. 4.3). This unexpected pattern of regain in stiffness and strength during liquefaction ($r_u = 1$) was clearly observed in: (1) four of the six model 4a and 4b (Fig. 4.4) tests (at 7 out of 12 locations A4 and A6, [39]), and (2) laboratory cyclic shear test results on the employed Nevada Sand [17; as will be discussed in detail in the following sections. The disparity in observed responses in the six tested centrifuge models [39] may be attributed to differences in the employed testing equipment and imparted input motions, as well as to the usual margins of experimental error

Table 4.1: Transducer coordinates.

Model 4a (prototype units)					
Transducer	x (m)	z (m)	Transducer	x (m)	z (m)
A 2	2.54	0.00	P A	0.00	1.50
A 4	2.54	3.00	P B	0.00	3.10
A 6	2.54	4.50	P C	0.00	4.50
A 8	-6.35	6.63			

Model 6 (prototype units)					
Transducer	x (m)	z (m)	Transducer	x (m)	z (m)
A 1	0.00	0.30	P E	0.00	0.75
A 2	0.00	1.50	P A	0.00	1.35
A 3	-4.15	2.10	P B	0.00	2.10
A 4	0.00	3.75	L 1	0.00	0.00
A 5	-6.36	5.63	L 2	-4.15	1.25
			L 3	4.15	1.25

Table 4.2: Soil properties.

Model	Mass density (kg/m ³)		Relative density of sand	Water content of silt
	Sand	Silt		
4a	2000	1927	62.0 %	30 %
6	2000	1927	62.0 %	30 %

and instrumentation malfunction.

4.4.1 Stress-strain histories

Centrifuge model response

Using the recorded accelerations (Fig. 4.3a) in Eqs. 2.5–4.6, Fig. 4.5 displays model 4a shear strain and stress histories at 1.5 m, 3.0 m, 3.75 m, 4.5 m and 5.25 m depths. Representative stress-strain cycles at these locations during selected time windows are shown in Fig. 4.6.

Very large strains are seen to occur during the first cycle of loading (Fig. 4.5). The largest strains were within the sand lower-most strata, and reached amplitudes of 2.5 %, 3.5 % and 5.0 % at 3.75 m, 4.5 m and 5.25 m depths respectively. These large strain amplitudes were associated with a sharp rise in sand u_e after 1 s of shaking, as mentioned earlier (PC and PB, Fig. 4.3c). As a consequence of these large sand u_e values and the associated loss of stiffness, the silt layer was practically isolated from further input excitation (after about 3.0 s of shaking), and experienced only small stresses and strains thereafter (Figs. 4.5 and 4.6).

The identified stress-strain histories (Fig. 4.6) suggested that stiffness degradation throughout the sand layer started during the first cycle of loading. During the 2–10 s time window, the sand response was characterized by cycles of large strains and small stresses (Figs. 4.5 and 4.6).

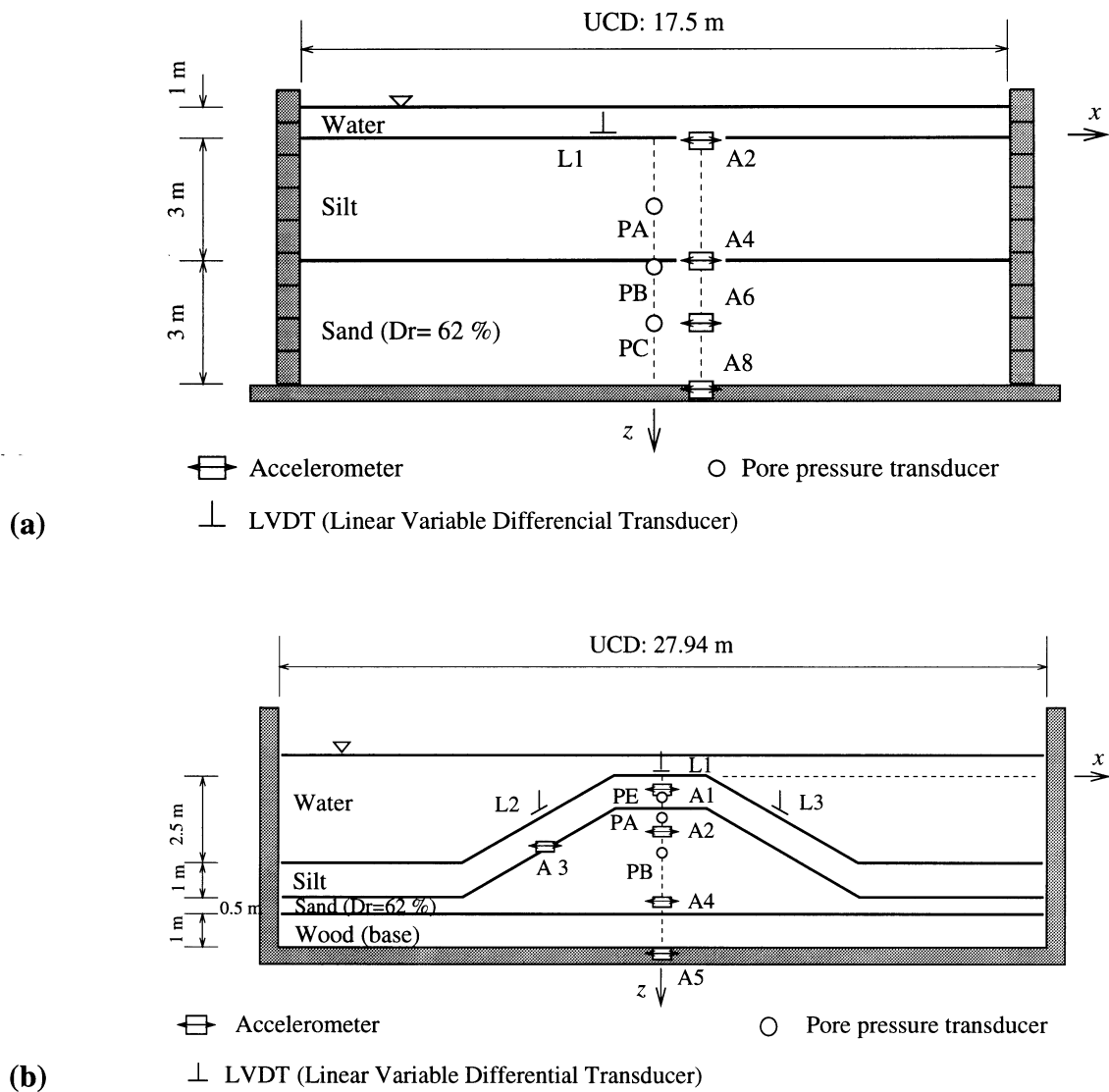


Figure 4.1: Model configurations: (a) VELACS model 4a, and (b) VELACS model 6 (dimensions in prototype units).

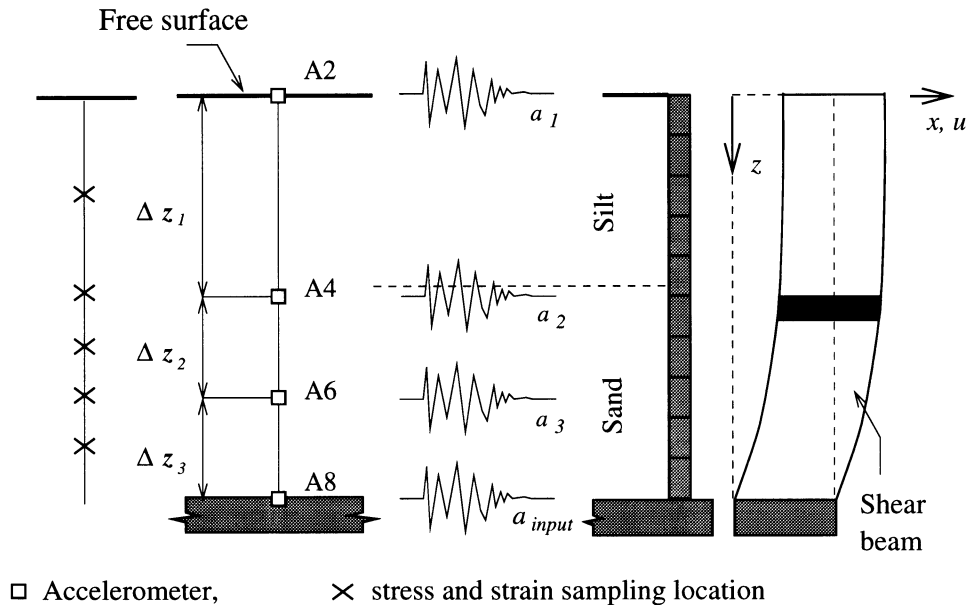


Figure 4.2: Soil-system model and stress-strain sampling locations (model 4a).

Near the end of shaking, at about 19 s, the lower-most sand strata started to gradually regain stiffness and exhibit smaller strains and larger stresses (Figs. 4.5 and 4.6). It may be observed that significant vertical settlement occurred throughout the shaking phase in all tests (Figs. 4.3b and 4.4). This feature of response suggests that the observed regain in stiffness may possibly be due to a densification of the sand layer (increase in relative density), and a resulting increase in interlocking friction forces between the soil particles.

As mentioned earlier, similar dynamic response characteristics (Fig. 4.4) were also observed in three other models including those conducted in rigid boundary containers [39]. For instance, the data recorded along the centerline of model 4b [34] was employed (Eqs. 3-6) to obtain Figure 4.7. Within the sand layer (Fig. 4.7), the loss and gradual regain in stiffness is quite evident. Considering the experimental differences in input motion and other testing details, the similarity of stress-strain response patterns in models 4b (Fig. 4.7) and Model 4a (Fig. 4.6) is notable. This similarity possibly denotes a small influence of boundary effects on the employed centerline acceleration response of model 4b (rigid container test).

Laboratory test results

A similar shear restiffening response pattern was also observed during laboratory tests conducted using the employed Nevada sand [17]. In cyclic stress-controlled direct simple shear tests (at relative densities of $D_r = 40\%$ and $D_r = 60\%$, and a confining pressure of 160 kPa), it was noted that (Figs. 4.8 and 4.9): (1) upon liquefaction, the soil exhibited the typical phase of stiffness reduction and increase in shear strain amplitudes, and (2) during liquefaction, subsequent loading cycles showed a regain of stiffness phase with a gradual decrease in strain amplitudes. This regain of stiffness also coincided with an increase in accumulated vertical strains (or settlements), indicating a possible densification of the soil skeleton.

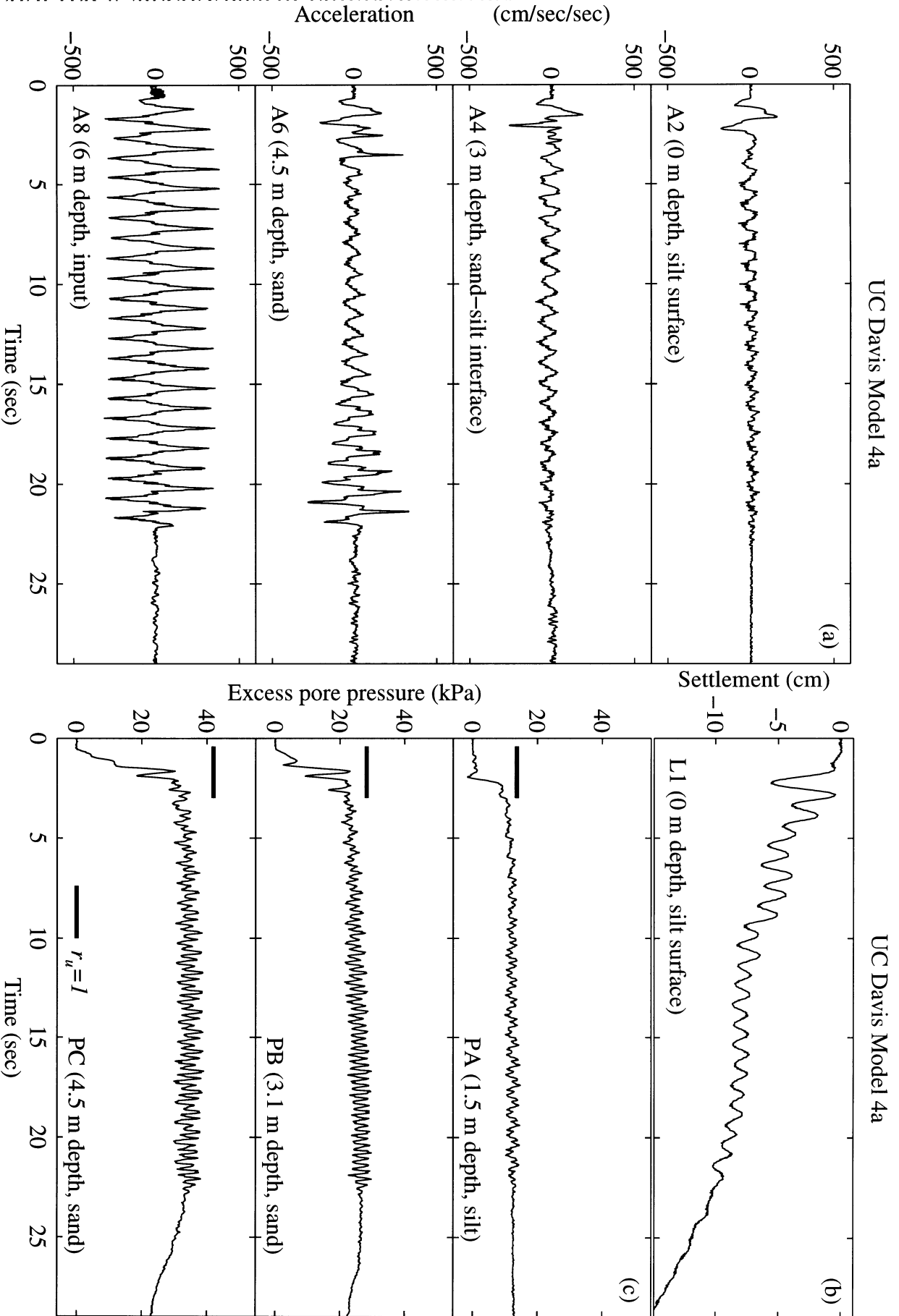


Figure 4.3: UC Davis Model 4a time histories: (a) accelerations at free surface, 3 m depth, 4.5 m depth, and associated input acceleration; (b) settlement at silt layer surface; and (c) excess pore pressures at 1.5 m, 3.1 m, and 4.5 m depths.

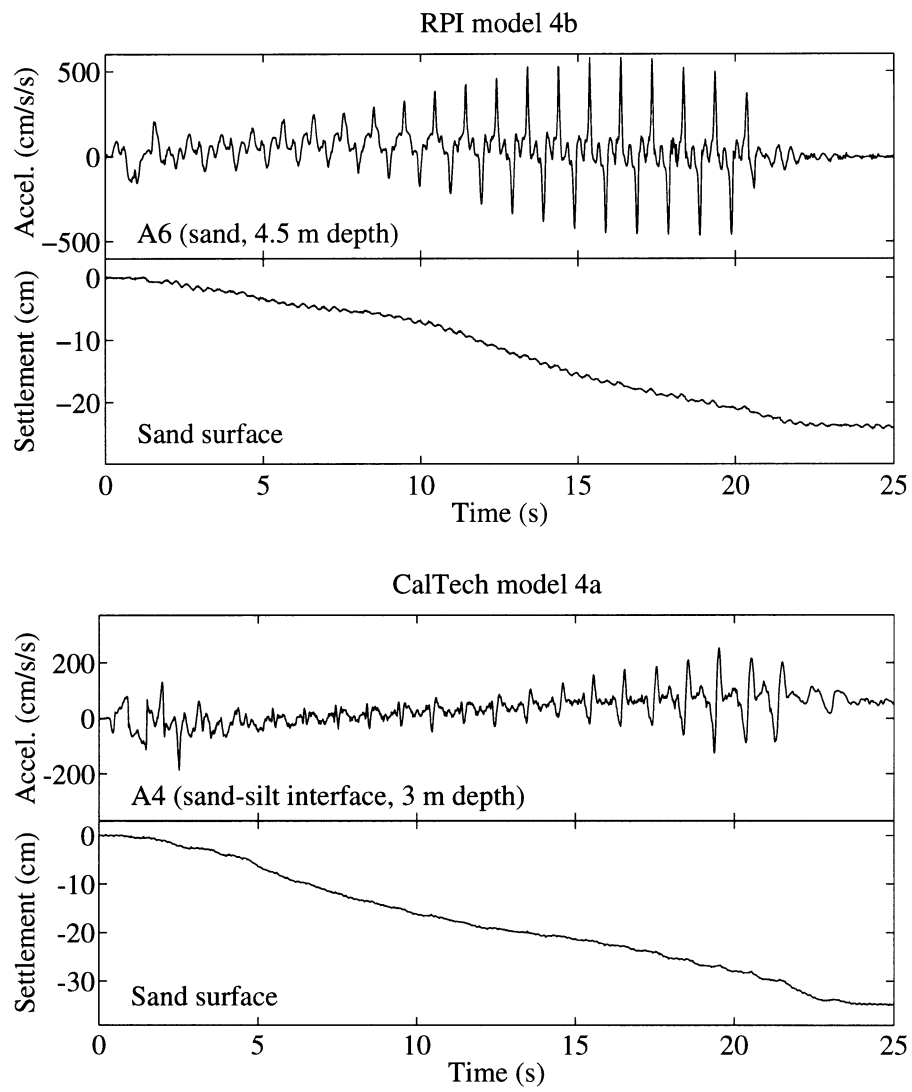


Figure 4.4: Sample acceleration and settlement records of RPI model 4b and CalTech model 4a.

4.4.2 Liquefaction mechanism

After liquefaction, the observed response patterns suggested that a subsequent densification has caused the observed regain in sand stiffness and strength. In the laboratory tests, this regain was also associated with r_u gradually decreasing from a value approaching 1.0 to about 0.8 (Figs. 4.8 and 4.9). However, in the centrifuge experiments (Fig. 4.3), no similar reduction in r_u was observed. Thus, the high shear stresses near the end of shaking at 5.25 m depth are incompatible with u_e at 4.5 m depth. To resolve this inconsistency, one can only speculate that u_e below 4.5 m, closer to the base, must have experienced a level of reduction that allowed for the observed regain in shear stiffness and strength, towards the end of dynamic excitation. This reduction in u_e might have been partially in the form of instantaneous dips leading to instants of dilation and regain in stiffness; as documented during the Wildlife Refuge site case history [20].

4.5 Embankment Response: Model 6

This model was proposed and tested by Arulanandan *et al.* at UCD [16]. It consisted of a submerged Nevada sand embankment overlain by a layer of Bonnie silt (Fig. 4.1, and Tables 4.1 and 4.2).

Time histories of the recorded accelerations (along the central axis), vertical settlement (right slope) and u_e values are shown in Fig. 4.10. Input acceleration was primarily composed of a 1 Hz signal. As observed earlier in models 4a and 4b, the rise in u_e was associated with relatively low amplitude accelerations in the silt layer at the top of the embankment (A1 at 0.3 m depth, Fig. 4.10a). These amplitudes appear to have been reduced further (after about 13 s of shaking) as the recorded sand u_e approached $r_u = 1.0$ at 1.35 m depth near the sand-silt interface (PA, Fig. 4.10c). In the sand, the acceleration recorded by A2 (at 1.5 m depth along the central axis, Figs. 4.1 and 4.10a), exhibited an asymmetric response pattern, with smaller acceleration amplitudes in the negative direction, and large amplitude acceleration spikes in the positive direction. Near the base, the sand acceleration at 3.75 m depth was similar to the input acceleration (A4 and A5 respectively, Fig. 4.10a).

4.5.1 Stress-strain histories

Centrifuge model response

The acceleration histories of Fig. 4.10a were employed in Eqs. 4.6, 4.8 and 4.9 to obtain shear strain and stress histories at 0.9 m and 2.6 m depths, as shown in Fig. 4.11. Selected stress-strain cycles at these locations are shown in Fig. 4.12. The identified stress-strain histories show that:

1. Within the silt layer (at 0.9 m depth), the shear stress-strain response was characterized by cycles of large strains and small stresses (Figs. 4.11 and 4.12). This response pattern which denotes an extremely low shear stiffness and isolation of the silt layer from base excitation, occurred throughout the shaking phase.
2. Within the sand zone, large strains and small stresses occurred at 2.6 m depth during the first loading cycle (Fig. 4.11). After about 10 s, sand strains (at 2.6 m) started to decrease gradually and the corresponding stresses increased in magnitude (Figs. 4.11 and 4.12).

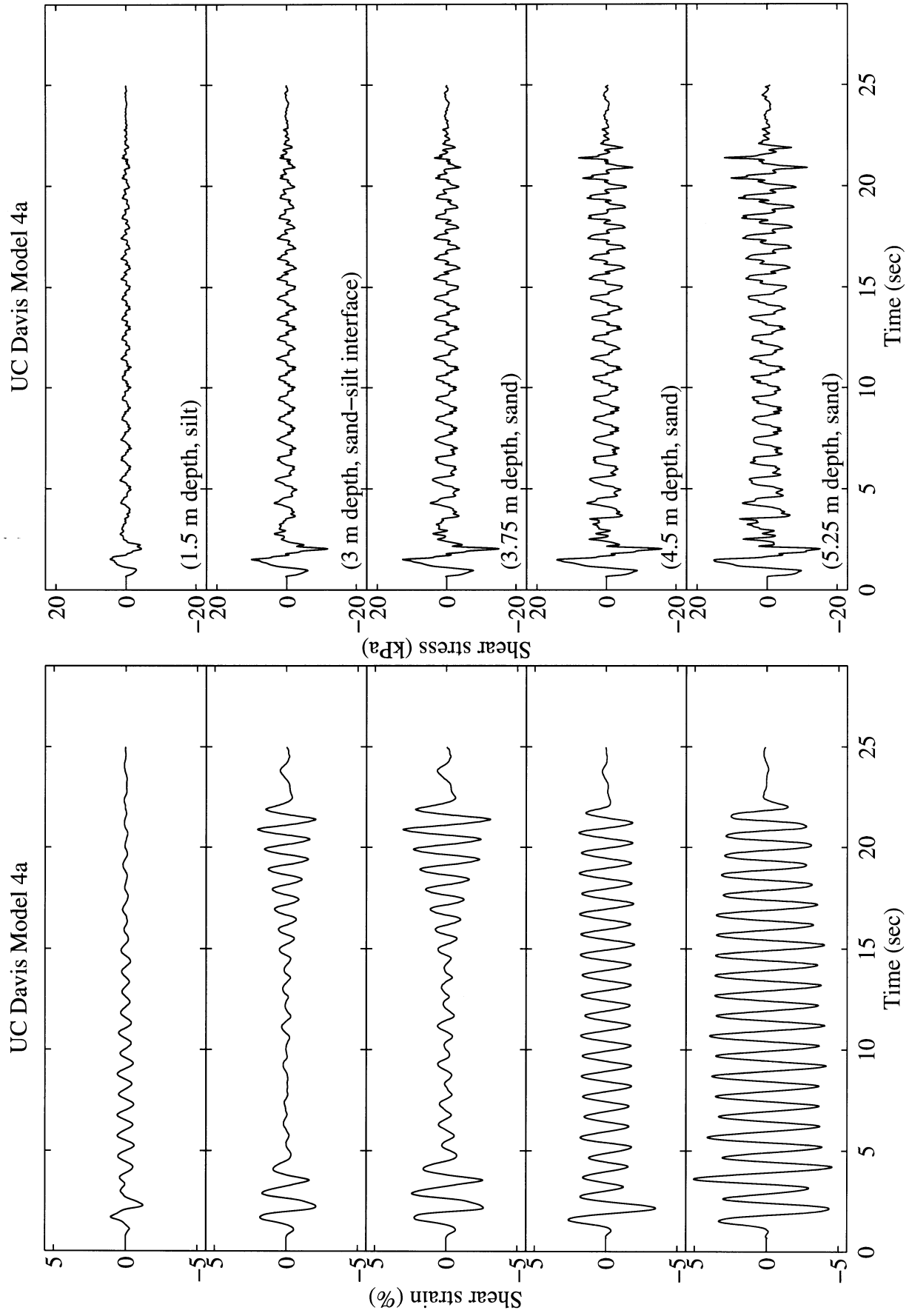


Figure 4.5: UC Davis Model 4a shear stress and strain histories at 1.5 m, 3.0 m, 3.75 m, 4.5 m, and 5.25 m depths.

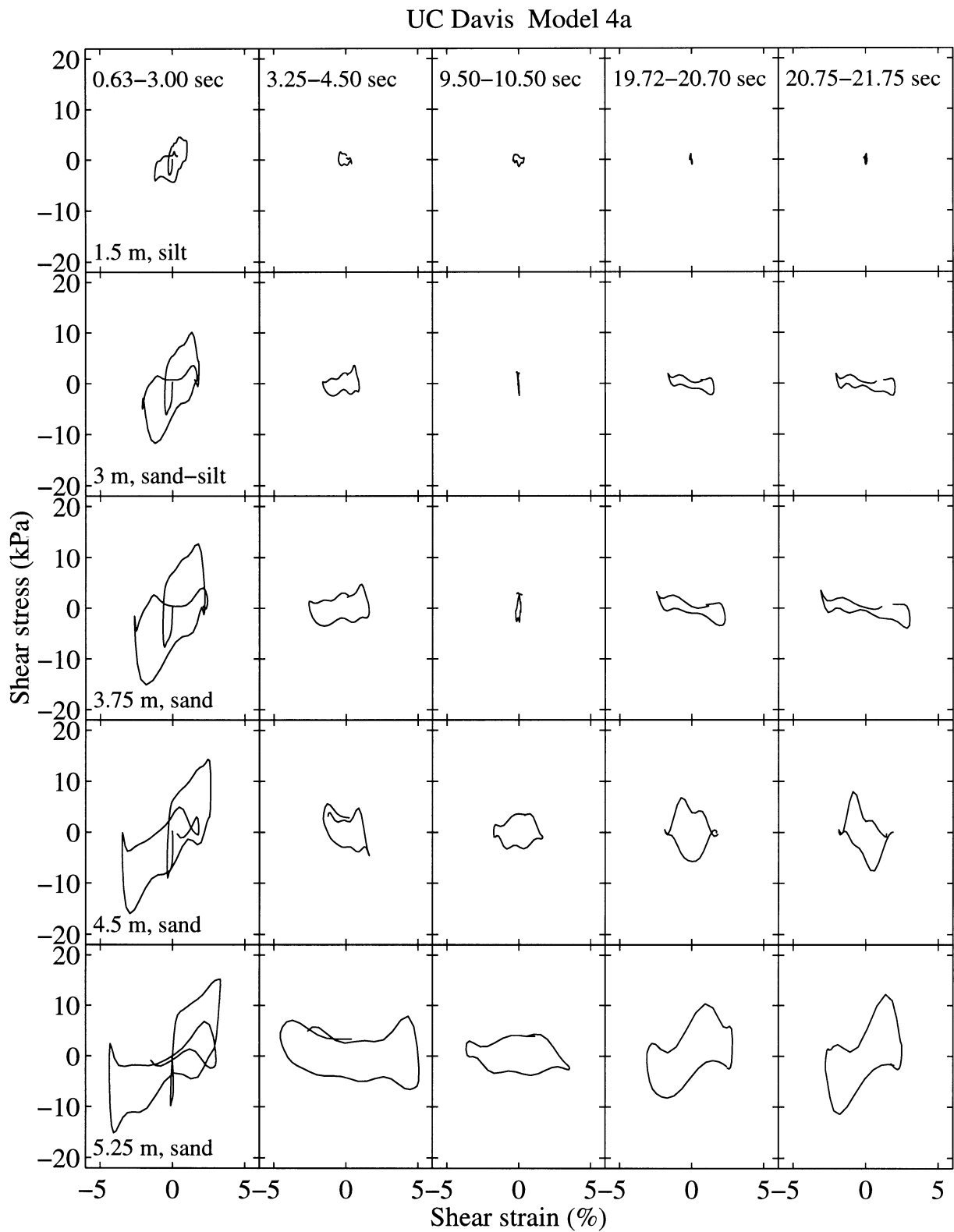


Figure 4.6: Selected cycles of UCD model 4a shear stress-strain histories at 1.5 m, 3.0 m, 3.75 m, 4.5 m, and 5.25 m depths.

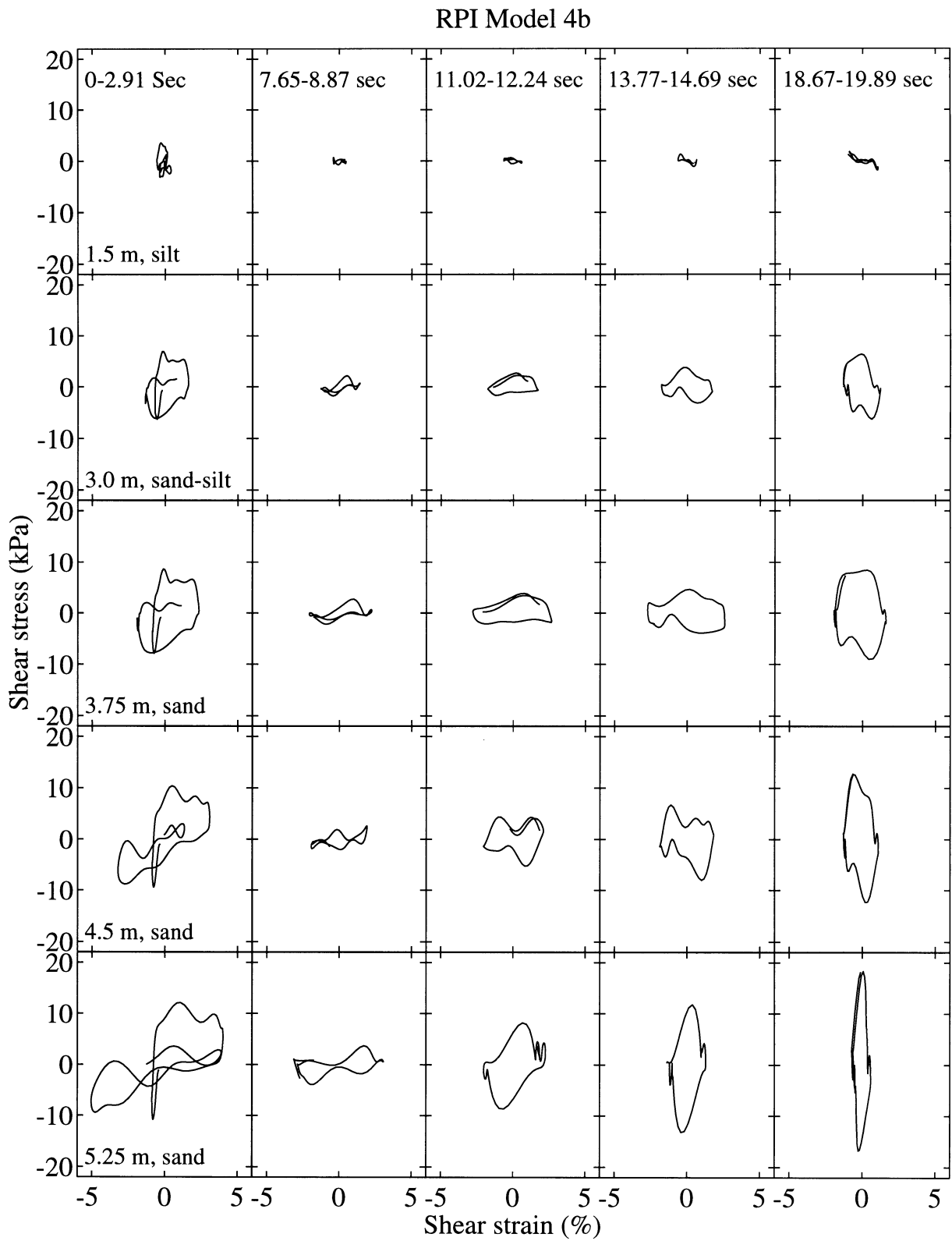


Figure 4.7: Selected cycles of RPI model 4b shear stress-strain histories at 1.5 m, 3.0 m, 3.75 m, 4.5 m, and 5.25 m depths.

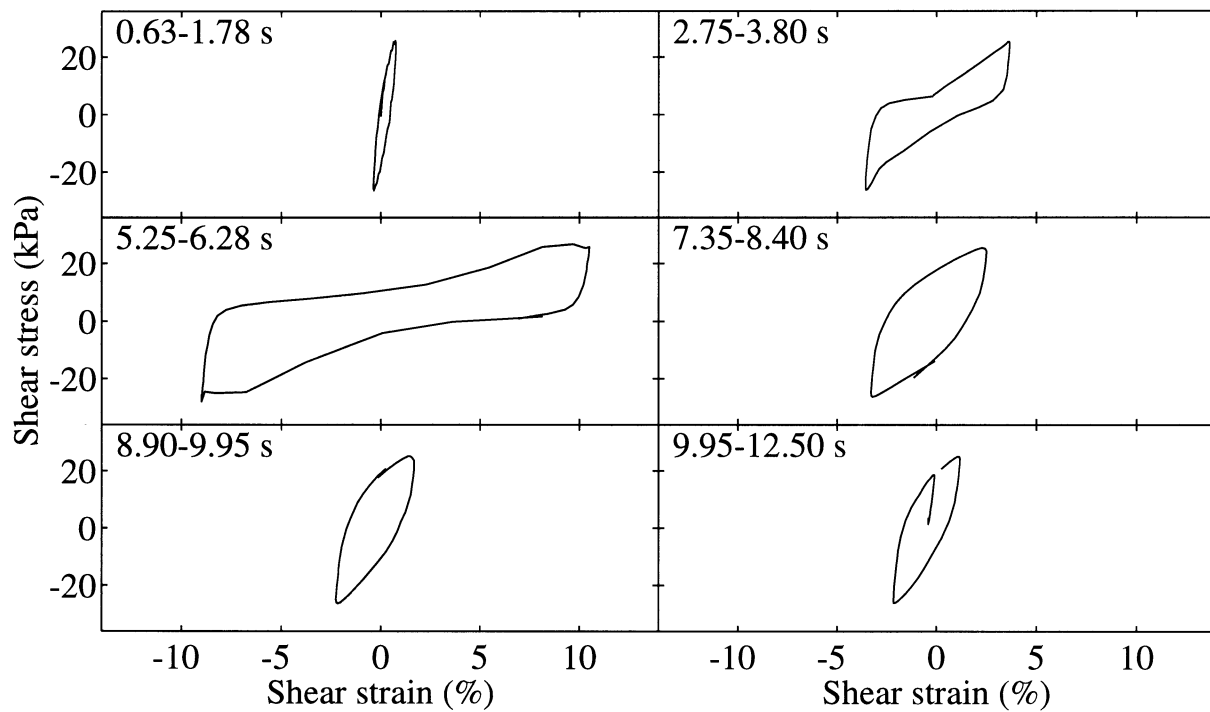
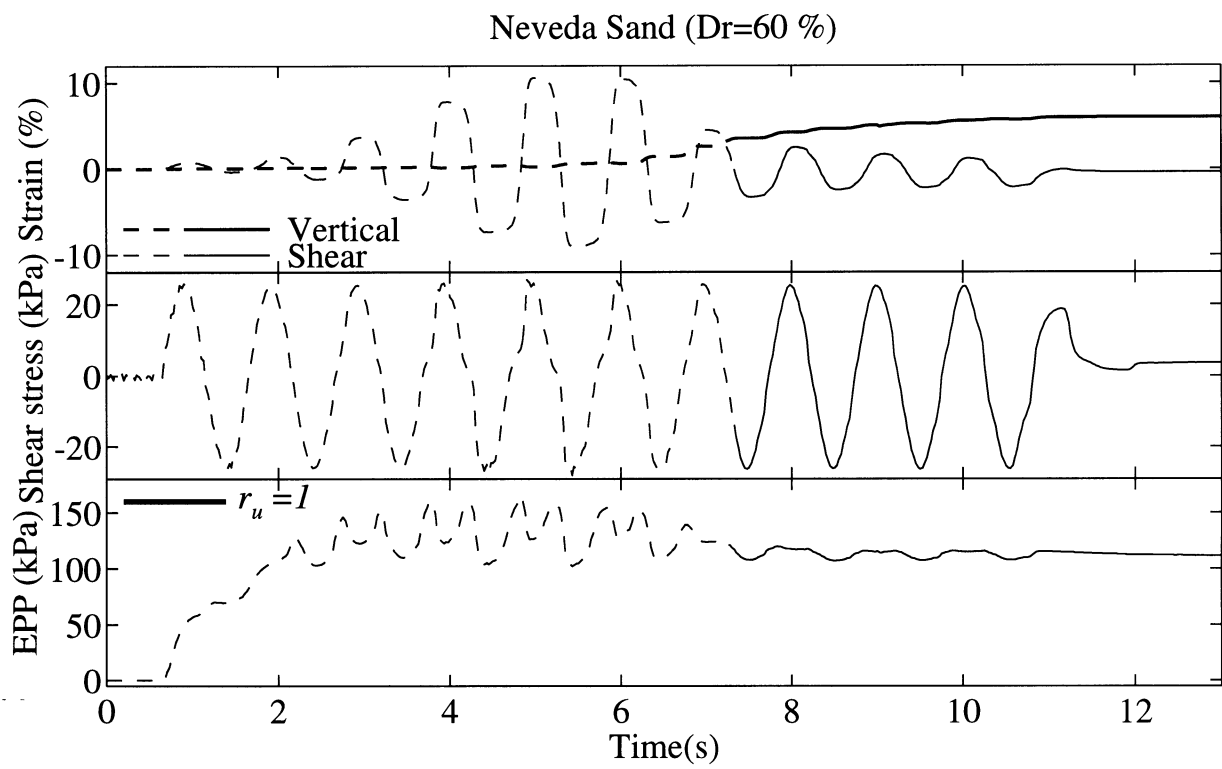


Figure 4.8: Shear stress, shear strain and EPP histories of a Nevada sand sample (at $D_r = 60\%$, and 160 kPa confining pressure) subject to a stress-controlled cyclic direct simple shear test [17].

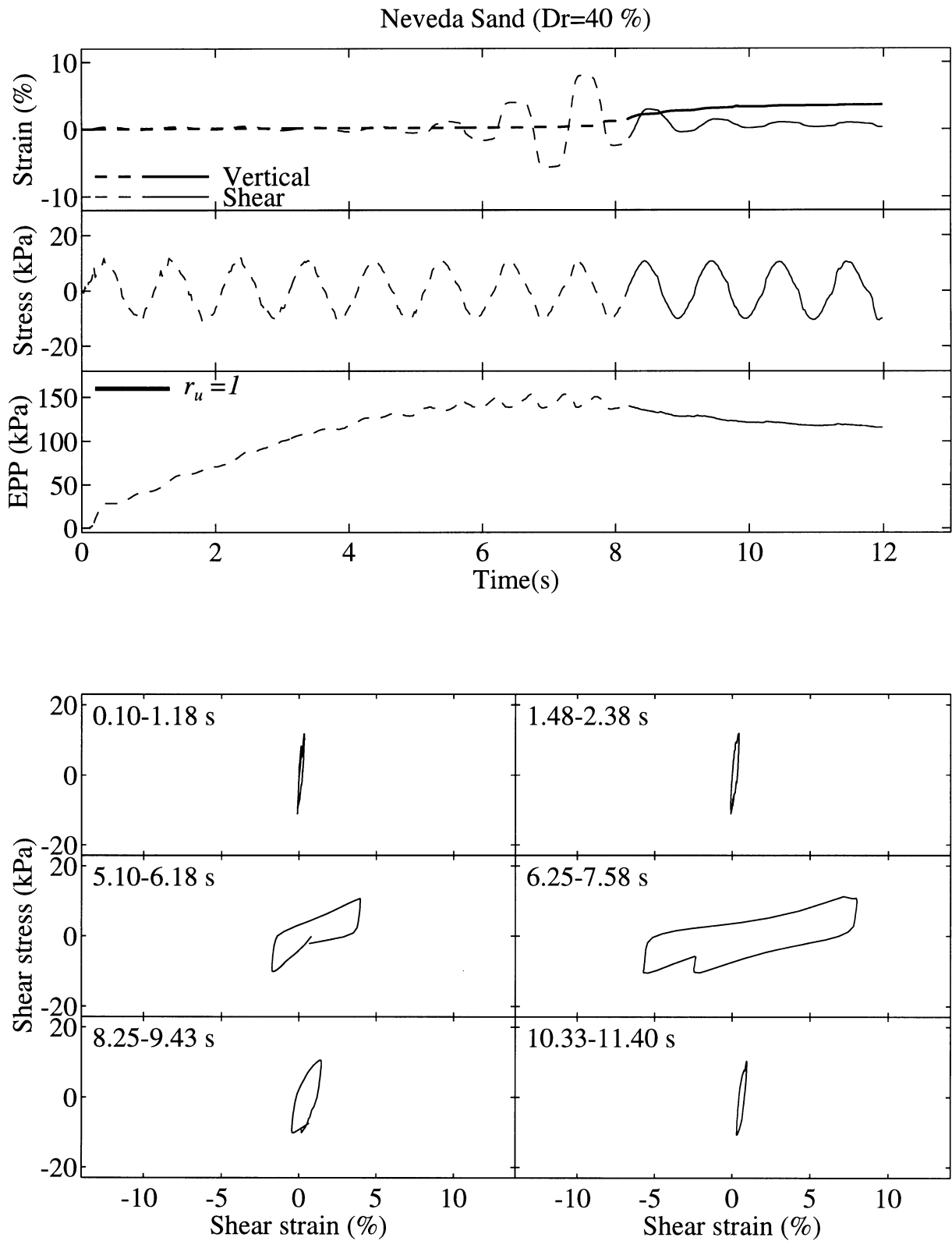


Figure 4.9: Shear stress, shear strain and EPP histories of a Nevada sand sample (at $D_r = 40\%$, and 160 kPa confining pressure) subject to a stress-controlled cyclic direct simple shear test [17].

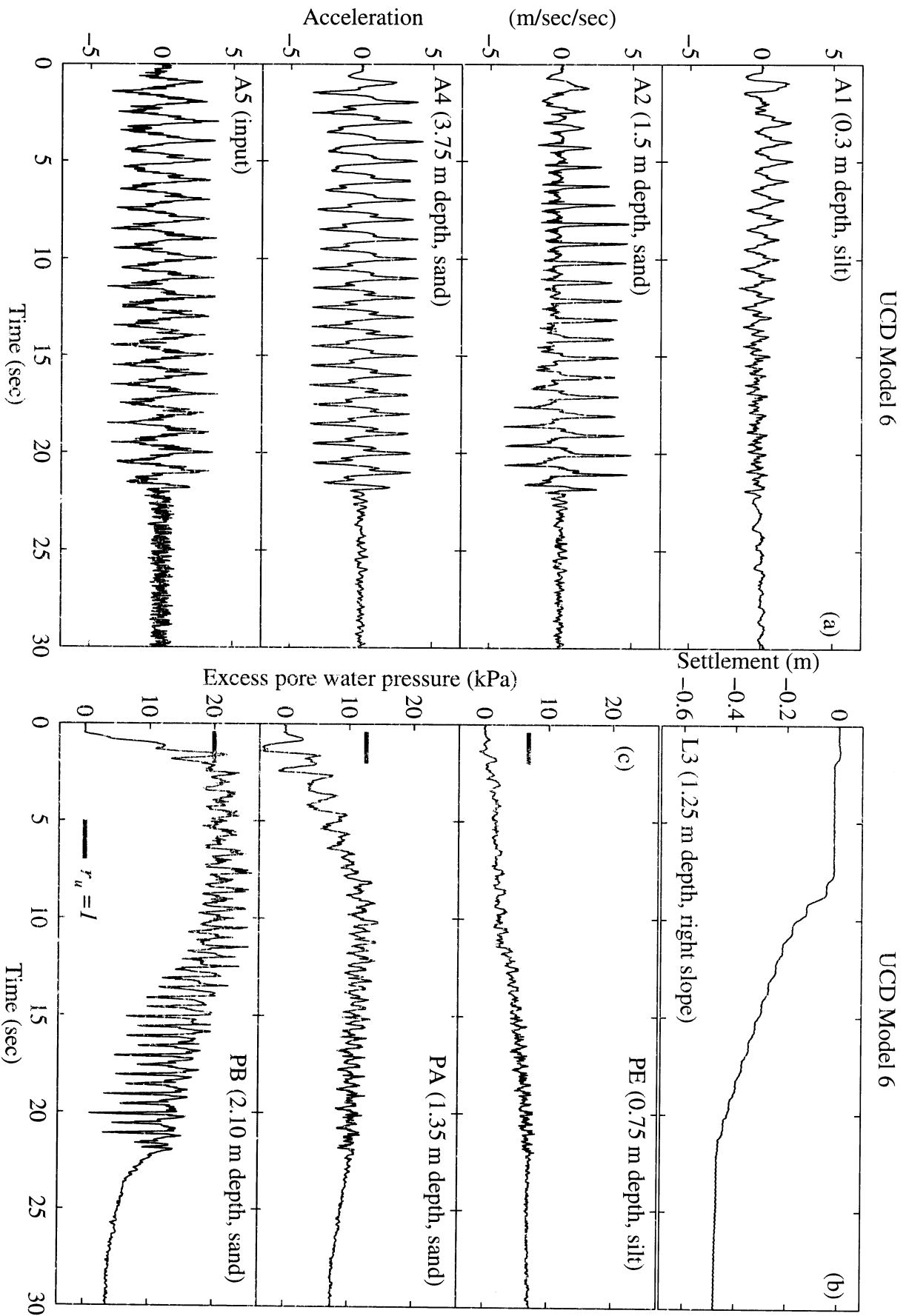


Figure 4.10: Model 6 recorded response: (a) acceleration histories at 0.3 m, 1.5 m, and 3.75 m depths, and associated input acceleration; (b) vertical settlement of the right slope at 1.25 m depth; and (c) excess pore pressure histories at 0.75 m, 1.35 m and 2.10 m depths.

The sand in the neighborhood of this elevation experienced a gradual regain in stiffness that may be attributed partially to: (1) a gradual decrease in sand u_e values at 2.1 m depth from $r_u = 1.0$ at about 10 s to about $r_u = 0.6$ by the end of shaking (PB, Fig. 4.10c), and (2) possible densification of the sand layer as suggested by the observed large settlements (Fig. 4.10b).

3. The shear stress history at 2.6 m (Fig. 4.11) was characterized by an asymmetric response pattern, with large positive spikes that reflect the observed bias in A2 acceleration amplitudes (Fig. 4.10a). These large stress spikes coincided in time with significant instantaneous drops in the sand u_e values at 2.10 m depth (PB, Fig. 4.10c). Such a response pattern denotes the tendency for soil-skeleton dilation at large strain excursions [20, thus causing: (1) instantaneous drops in pore-pressure, and (2) associated increase in soil stiffness and strength (2.6 m depth, Fig. 4.12). The asymmetry in recorded acceleration and calculated stress response may be mainly attributed to a mechanism of biased downslope yielding and large cyclic strain excursions towards the embankment free slope, as described below.

Since no permanent deformation may be evaluated from acceleration records, a crude estimate of permanent lateral shear strain was evaluated using the settlement recorded by LVDT L3 (Figs. 4.1b and 4.10b). The permanent lateral displacement u_p at L3 level was approximated to be proportional to the observed vertical settlement (L3, Fig. 4.10b) and the slope angle α , such as $u_p = l_3(t) / \tan \alpha$ (in which $l_3(t)$ is the permanent vertical settlement at L3 obtained by filtering out the cyclic components, Table 4.3). Thus, an approximate average permanent strain component γ_p for the 1.25 m to 4 m depth sand layer may be evaluated as $\gamma_p = u_p / \Delta z$ (in which $\Delta z = 2.75$ m is the sand layer thickness), and superposed on the 2.6 m depth cyclic strains of Fig. 4.11. This strain only provides a qualitative picture of the involved permanent deformations. The corresponding stress-strain history (Fig. 4.13) demonstrates a stress hardening response in the downslope (positive strain) direction. This observed response pattern shows that accumulation of permanent downslope deformation was influenced significantly by the instantaneous increase in soil stiffness due to soil-skeleton dilation at large cyclic strain excursions, in addition to the regain of stiffness that may be attributed to densification and the reduction in u_e .

Laboratory test results

The observed downslope stress-strain response characteristics of the sand layer were also mimicked in laboratory experiments [17]. During undrained cyclic stress-controlled direct simple shear tests of the employed Nevada sand (at $D_r = 40\%$ and $D_r = 60\%$, and a confining pressure of 160 kPa), with a superposed shear bias to simulate slope induced static stresses (Figs. 4.14 and 4.15 [17]), the soil response was characterized by: (1) an initial reduction in stiffness due to excess pore pressure buildup, (2) stress hardening and accumulation of strains in the direction of imposed static stress bias (or downslope), and (3) with no significant reduction in pore-pressure, a regain in stiffness that coincided in time with a slight reduction in r_u and an accumulation of settlement, reflecting the possible influence of densification.

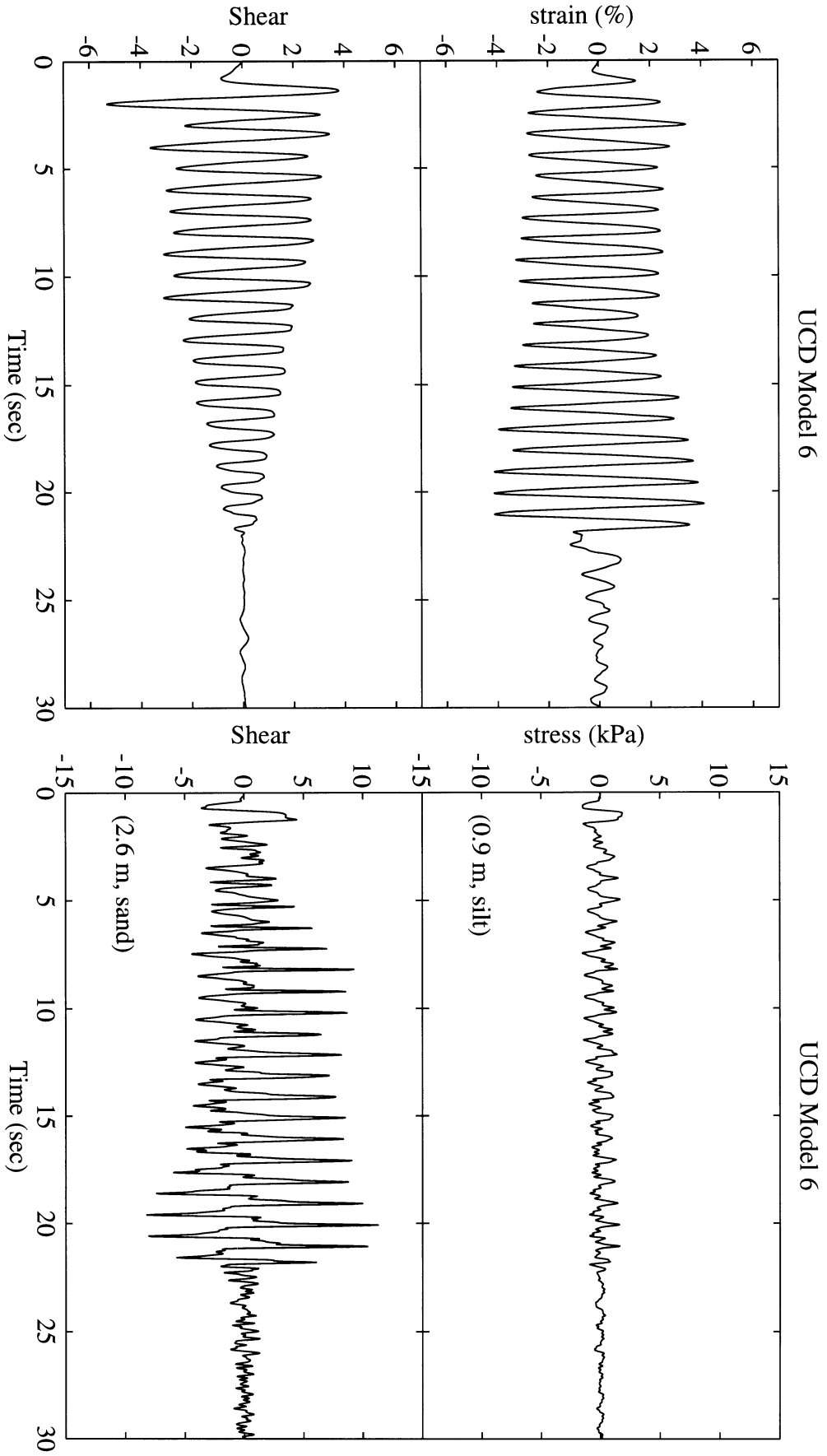


Figure 4.11: Model 6 shear strain and stress histories at 0.9 m and 2.6 m depths.

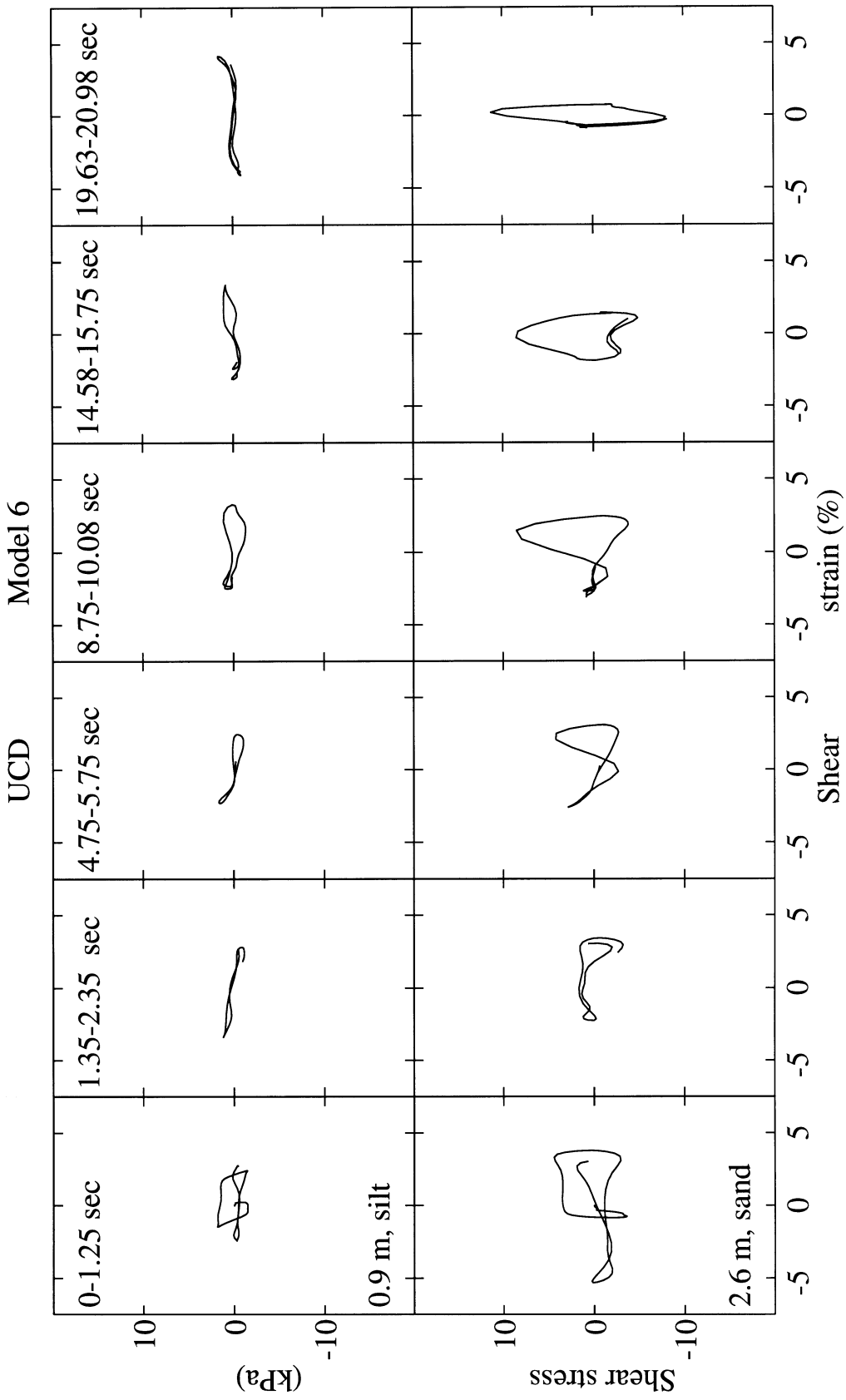


Figure 4.12: Selected cycles of model 6 shear stress-strain histories at 0.9 m and 2.6 m depths.

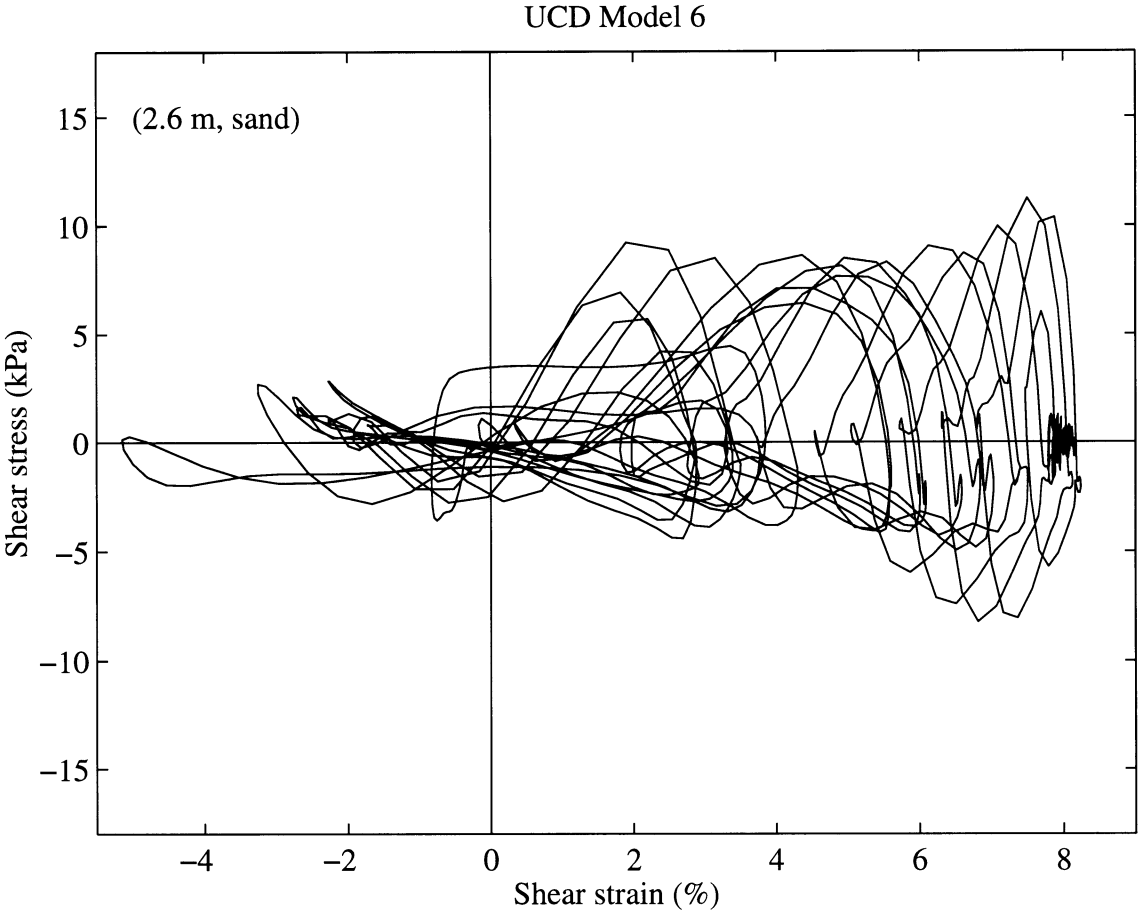


Figure 4.13: Model 6 shear stress-strain history at 2.6 m depth (with superposed permanent deformation evaluated from settlement records).

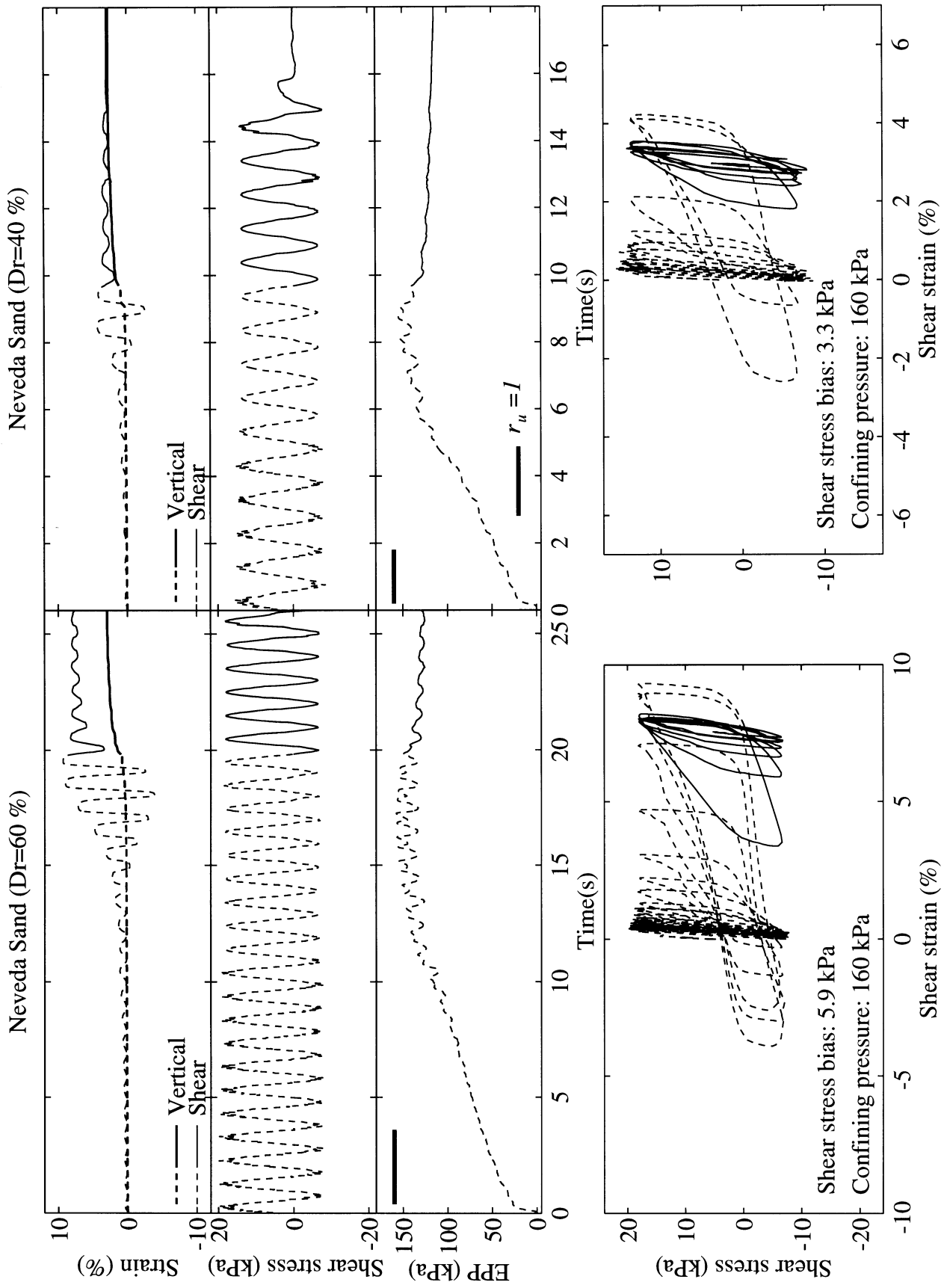


Figure 4.14: Shear stress, shear strain and EPP histories of two Nevada sand samples (at $D_r = 60\%$ and $D_r = 40\%$) subject to a stress-controlled cyclic direct simple shear test and stress bias [17].

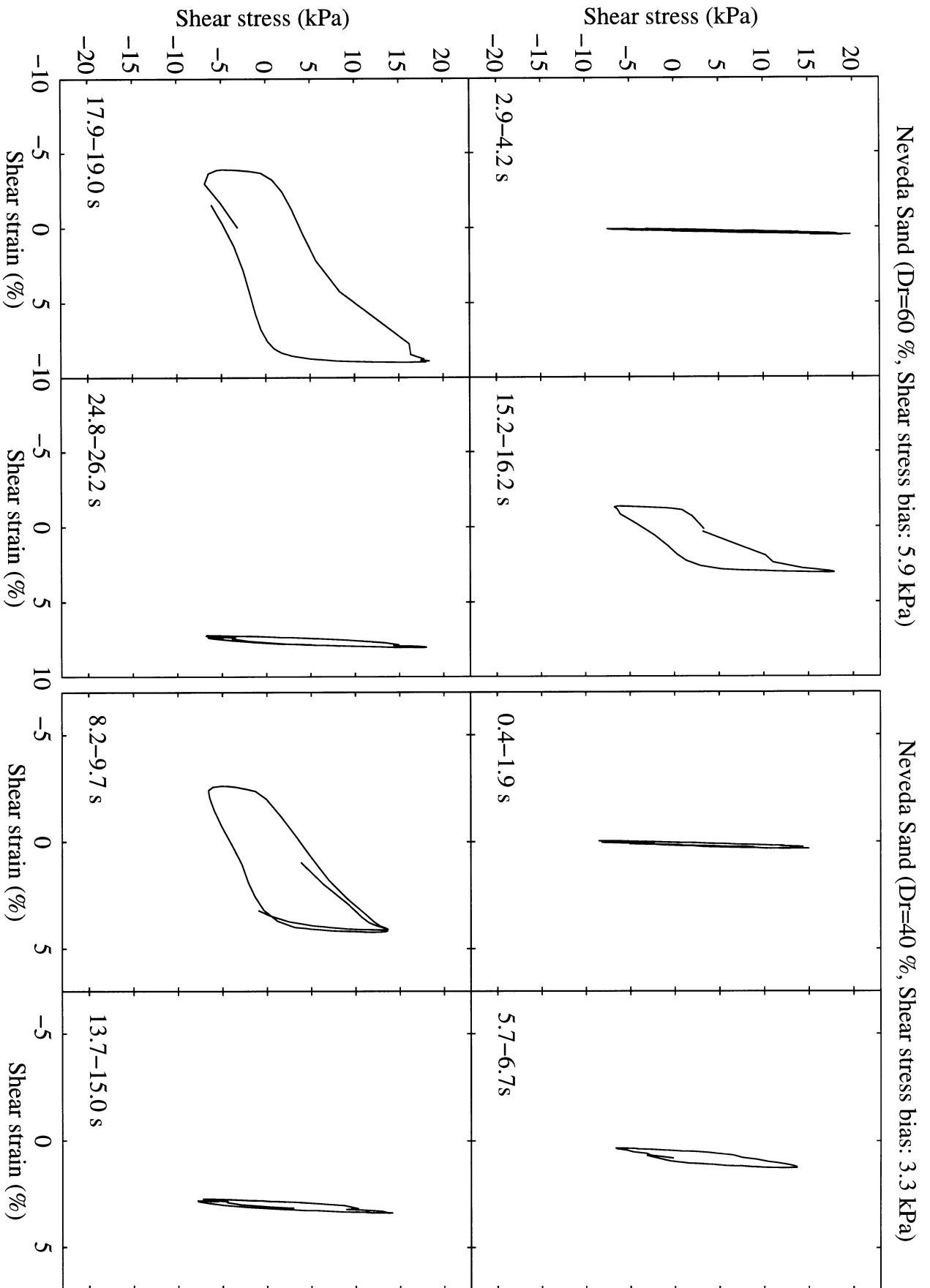


Figure 4.15: Selected shear stress-strain cycles of two Nevada sand samples (at $D_r = 60\%$ and $D_r = 40\%$) subject to a stress-controlled cyclic direct simple shear test and stress bias [17].

4.6 Appendix I: Analysis Approximations

The approximations involved in evaluating stress and strain histories (Eqs. 2.5–4.6, 4.8 and 4.9) stem from the following sources:

- Instrument Configuration: Accuracy of shear stress and strain estimates is a function of: (1) instrument spacing, and (2) acceleration wave-lengths ($\lambda = v_s/f$, where v_s is shear wave velocity and f is frequency). Dynamic energy of UCD models 4a and 6 responses was mainly within the 1.0–2.0 Hz frequency range, and acceleration wave-lengths were about 20–25 m. Within these ranges, approximation errors in shear stress and strain estimates were evaluated to be generally less than 6.0 %. However, note that any strain concentration, which might have occurred at the sand-silt interface during liquefaction, could only be averaged over the spacing between instruments. These approximations were described in detail by Zeghal and Elgamal [19].
- Data Processing: In view of instrument and digitization inaccuracies, shear strain histories (evaluated using integrated accelerations, Eqs. 4.5 and 4.6) include baseline drifts in the form of spurious very low frequency components. These drifts and minor high frequency components were eliminated using low- and high-pass filters [40]. Zero-phase time domain FIR (finite duration impulse response) filters, with the characteristics mentioned in Table 4.3, were utilized. This filtering procedure introduces no phase shifts. As shown in Table 4.3, filter bandwidths were selected to be wide enough so as to conserve the shear stress and strain characteristics.
- Analysis Technique: In view of the relatively close spacing between instruments, and in order to maintain simplicity, first order linear interpolation between accelerations was employed to estimate stresses (Eqs. 2.5, 2.6, 4.8 and 4.9); and second order interpolation between displacements was used to evaluate strains (Eqs. 4.5 and 4.6). These interpolations yield consistent second-order accurate shear stress and strain estimates [19].
- Measurement Errors: For the purpose of illustration, we will assume a case of recorded acceleration response \ddot{u}_1 and input \ddot{u}_2 , where \ddot{u}_1 includes a small amplitude measurement error \ddot{u}_m . Thus, stresses (Eqs. 2.5, 2.6, 4.8, and 4.9) will contain a proportionally small error. However, strains (Eqs. 4.5 and 4.6) will include a relative error proportional to $\ddot{u}_m/(\ddot{u}_1 - \ddot{u}_2)$. Consequently, a small error \ddot{u}_m in recorded accelerations may result in a large error in strains if $(\ddot{u}_1 - \ddot{u}_2) \rightarrow 0$.
- Weight of Model 4a Laminated Container: Additional shear stresses were imposed during shaking due to the inertial forces associated with own weight of the laminates. Consequently, in the adopted shear beam approximations (Eq. 1), the dynamic stresses (Eqs. 3 and 4) were increased by a factor of 16 % due to own weight of UCD laminated container.

4.7 References

1. Seed, H. B., Lee K. L., Idriss, I. M. and Makdisi F. I., "The slides in the San Fernando Dams During the Earthquake of February 9, 1971," *Journal of the Geotechnical Engineering Division*, ASCE, 1975.
2. Seed, R. B., Dickenson, S. E., Riemer, M. F., Bray, J. D., Sitar, N., Mitchell, J. K., Idriss, I. M., Kayen, R. E., Kropp, A., Hander, L. F. Jr., and Power, M. S., "Preliminary Report on the Principal Geotechnical Aspects of the October 17, 1989, Loma Prieta Earthquake," *Report No. UCB/EERC-90/05*, Earthquake Engineering Research Center, University of California, Berkeley, 1990.
3. Bardet, J. P., Oka, F., Sugito, M., and Yashima, A., "The Great Hanshin Earthquake Disaster," *Preliminary Investigation Report*, Department of Civil Engineering, University of Southern California, Los Angeles, California, 1995.
4. Comartin, C. D., Greene, M., and Tubbessing, S. K., eds., "The HyogoKen Nanbu Earthquake, Great Hanshin Earthquake Disaster, January 17, 1995," *Preliminary Reconnaissance Report*, Earthquake Engineering Research Institute, California, 1995.
5. Sitar, N., ed., "Geotechnical Reconnaissance of the Effects of the January 17, 1995, Hyogoken-Nanbu Earthquake Japan," *Report No. UCB/EERC-95/01*, Earthquake Engineering Research Center, Berkeley, California, 1995.
6. Soils and Foundations, "Special Issue on Geotechnical Aspects of the January 17, 1995, Hyogoken Earthquake," *Soils and Foundations*, Japan Geotechnical Society, 1996.
7. Werner, S. D. and Dickenson, S. E., "A Post-Earthquake Reconnaissance of Port Facilities," *Report, Dames and Moore and Oregon State University*, September 1995.
8. National Research Council, *Liquefaction of Soils During Earthquakes*, Committee on Earthquake Engineering, National Academy Press, Washington D. C, 1985.
9. Holzer, T. L., Youd T. L., and Hanks T. C., "Dynamics of Liquefaction During the 1987 Superstition Hills, California, Earthquake," *Science*, Vol. 244, 56-59, 1989.
10. Benoit, J. and de Alba, P., "Catalog of National Geotechnical Experimentation Sites," *Report to the National Science Foundation and the Federal Highway Administration*, University of New Hampshire, April 1993.
11. Arulanandan, K. and Scott, R. F., eds., *Verification of Numerical Procedures for the Analysis of Soil Liquefaction Problems*, Conference Proceedings, Davis, CA, Volume 1, Balkema, 1993.
12. Arulanandan, K. and Scott, R. F., eds., *Verification of Numerical Procedures for the Analysis of Soil Liquefaction Problems*, Conference Proceedings, Davis, CA, Volume 2, Balkema, 1994.
13. Scott, R. F. and Zuckerman, K. A., "Sandblows and Liquefaction in the Great Alaska Earthquake of 1964," *Engineering Publication 1606*, National Academy of Sciences, Washington, D.C., 170-189, 1972.
14. Elgamal, A.-W., Dobry, R., and Adalier, K., "Study of Effects of Clay Layers on Liquefaction of Sand Deposits Using Small-Scale Models," *Proceedings of the 2nd U.S.-Japan Workshop on Liquefaction, Large Deformation and Their Effects on Lifelines*, O'Rourke, T. and Hamada, M., eds., NCEER, Buffalo, NY, 233-245, 1989.
15. Arulanandan, K., Zeng, X., and Rashidi, H., "Experimental Results of Model No. 4a," *Proceedings of the International Conference on the Verification of Numerical Procedures*

- for the Analysis of Soil Liquefaction Problems, Arulanandan, K. and Scott, R. F., eds., Vol. 1, 595-600, Davis, CA, Balkema, 1993.
16. Arulanandan, K., Zeng, X., and Rashidi, H., "Experimental Results of Model No. 6," *Proceedings of the International Conference on the Verification of Numerical Procedures for the Analysis of Soil Liquefaction Problems*, Arulanandan, K. and Scott, R. F., eds., Vol. 1, 737-744, Davis, CA, Balkema, 1993.
 17. Arulmoli, K., Muraleetharan, K. K., Hossain, M. M., and Fruth, L. S., "VELACS: Verification of Liquefaction Analyses by Centrifuge Studies, Laboratory Testing Program, Soil Data Report," *Report, Project No. 90-0562*, The Earth Technology Corporation, Irvine, California, 1992.
 18. Koga, K. and Matsuo, O., "Shaking Table Tests of Embankments Resting on Liquefiable Sandy Ground," *Soils and Foundations*, Vol. 30, No. 4, 162-174, 1990.
 19. Zeghal, M. and Elgamal, A.-W., "Lotung Site: Downhole Seismic Data Analysis," *Report*, Civil Engineering Department, Rensselaer Polytechnic Institute (to be published as an Electric Power Research Institute Report), 1993.
 20. Zeghal, M. and Elgamal, A.-W., "Analysis of Site Liquefaction Using Earthquake Records," *Journal of Geotechnical Engineering*, ASCE, Vol. 120, No. 6, 996-1017, 1994.
 21. Zeghal, M., Elgamal, A.-W., Tang, H. T., and Stepp, J. C., "Lotung Downhole Array. II: Evaluation of Site Nonlinear Properties," *Journal of Geotechnical Engineering*, ASCE, Vol. 121, No. 4, 363-378, 1995.
 22. Hushmand, B., Crouse, C. B. and Scott, R. F., "Centrifuge Liquefaction Tests in a Laminar Box," *Geotechnique*, Vol. 38, 253-262, 1988.
 23. Tan, T. S. and Scott, R. F., "Centrifuge Scaling Considerations for Fluid-Particle Systems," *Geotechnique*, Vol. 35, No. 4, 461-470, 1985.
 24. Cheney, J. A. and Kutter, B. L., "Update on the US National Geotechnical Centrifuge," *Centrifuge 88*, Corte, J., ed., 61-66, Balkema, 1988.
 25. Roesset, J. M., "Soil Amplification of Earthquakes," *Numerical Methods in Geotechnical Engineering*, Desai, C. S. and Christian, J. T., eds., McGraw-Hill, New York, 1977.
 26. Schnabel, P. B. and Lysmer J., "SHAKE-A Computer Program for Earthquake Response Analysis of Horizontally Layered Sites," *Report EERC 72-12*, Earthquake Research Center, University of California Berkeley, 1970.
 27. Pearson, E. C., *Numerical Methods in Engineering and Science*, Van Nostrand Reinhold Company, 1986.
 28. Abdel-Ghaffar, A. M. and Scott, R. F., "Investigation of the Dynamic Characteristics of an Earth Dam," *Report No. EERL 78-02*, Earthquake Engineering Research Laboratory, Pasadena, California, 1978.
 29. Abdel-Ghaffar, A. M. and Scott, R. F., "Shear Moduli and Damping Factors of Earth Dams," *Journal of the Geotechnical Engineering Division*, ASCE Vol. 105, No. Gt12, 1405-1426, 1979.
 30. Taboada, V. M. and Dobry, R., "Experimental Results of Model 4a at RPI," *Proceedings of the International Conference on the Verification of Numerical Procedures for the Analysis of Soil Liquefaction Problems*, Arulanandan, K. and Scott, R. F., eds., Vol. 1, Davis, CA, 611-621, Balkema, 1993.
 31. Scott, R. F., Hushmand, B., and Rashidi, H., "Duplicate Test of Model No. 4a: Horizontally Layered Soil in Laminar Box," *Proceedings of the International Conference on*

Table 4.3: Characteristics of employed filters.

Model	Low frequency cutoff	High frequency cutoff	Frequency range of significant response
4a	0.3 Hz	8.5 Hz	0.7-3.0 Hz
6	0.3 Hz	8.2 Hz	0.7-3.0 Hz

Displacement filter for γ_p	Low frequency cutoff	High frequency cutoff
Model 6	0.0 Hz	0.3 Hz

- the Verification of Numerical Procedures for the Analysis of Soil Liquefaction Problems*, Arulanandan, K. and Scott, R. F., eds., Vol. 1, Davis, CA, 601-609, Balkema, 1993.
32. Arulanandan, K., Zeng, X., and Rashidi, H., "Experimental Results of Model No. 4b," *Proceedings of the International Conference on the Verification of Numerical Procedures for the Analysis of Soil Liquefaction Problems*, Arulanandan, K. and Scott, R. F., eds., Vol. 1, 681-689, Davis, CA, Balkema, 1993.
 33. Dewoolkar, M. M., Ko, H.-Y., and Sture, S., "Experimental Results of Model No. 4b," *Proceedings of the International Conference on the Verification of Numerical Procedures for the Analysis of Soil Liquefaction Problems*, Arulanandan, K. and Scott, R. F., eds., Vol. 1, 701-710, Davis, CA, Balkema, 1993.
 34. Carnevale, R. A. and Elgamal, A.-W., "Experimental Results of RPI Centrifuge Model No. 4b," *Proceedings of the International Conference on the Verification of Numerical Procedures for the Analysis of Soil Liquefaction Problems*, Arulanandan, K. and Scott, R. F., eds., Vol. 1, 691-700, Davis, CA, 1993.
 35. Zorapapel, G. T., and Vucetic, M., "The effect of Pore-Pressure on Ground Motion," *Earthquake Spectra*, Vol. 10, No. 2, 403-438, 1994.
 36. Ishihara, K., "Stability of Natural Deposits During Earthquakes," *Proceeding of the 11th International Conference on Soil Mechanics and Foundation Engineering*, A. A. Balkema Publishers, Rotterdam, Netherlands, 1985.
 37. Hryciw, R. D., Rollins, K. M., Homolka, M., Shewbridge, S. E., and McHood, M., "Soil Amplification at Treasure Island During the Loma Prieta Earthquake," *Proceedings, Second Inter. Conf. on Recent Advances in Geotechnical Earthquake Engineering and Soil Dynamics*, St. Louis, MO, S. Prakash, ed., Vol. II, 1679-1685, 1991.
 38. Elgamal, A.-W., Zeghal, M., and Parra, E., "Liquefaction of an Artificial Island in Kobe, Japan," *Journal of Geotechnical Engineering*, ASCE, Vol. 122, No. 1, 39-49 1996.
 39. Elgamal, A.-W., Adalier, K., and Zeghal, M., "Overview and Relevance of Experimental Data From VELACS Project, Models 4a, 4b and 6," *Proceedings of the International Conference on the Verification of Numerical Procedures for the Analysis of Soil Liquefaction Problems*, Arulanandan, K. and Scott, R. F., eds., Vol. 2, 1681-1702, Davis, CA, Balkema, 1994.
 40. Oppenheim, A. V. and Shafer, R. W., *Discrete-Time Signal Processing*, Prentice Hall, 1989.

Chapter 5

Conclusions

The conducted studies showed that downhole vertical-array records offer a valuable source for: (1) evaluating site seismic shear stress-strain histories, (2) assessing the mechanisms of site amplification, stiffness degradation and liquefaction, and (3) calibrating constitutive models and computational modeling procedures. In this regard, system identification techniques were found to be an effective means to evaluate optimal modeling parameters. At present, downhole seismic records are becoming increasingly available worldwide. Such records are finally providing a growing site response database under a wide range of seismic loading conditions.

At the Wildlife Refuge and Port Island sites, the estimated stress-strain histories showed that: (1) site stiffness and strength decreased steadily with excess pore pressure buildup, (2) at high excess pore pressure levels, site response was characterized by large strains and small stresses, and (3) during liquefaction, significant shear strength may evolve at large shear strains, due to dilation. The employed identification techniques were shown to provide valuable information of direct use for calibration of computational modeling procedures. In this regard, system identification techniques were found to be an effective means of defining the necessary optimal modeling parameters.

Analyses of the dynamically induced liquefaction response in centrifuge models of a level site, composed of a sand layer overlain by a silt deposit, revealed that: (1) liquefaction of the underlying sand rapidly isolated the silt layer from the imparted base excitation, (2) the silt layer experienced relatively low strains during the shaking phase, and was liquefied mainly due to the underlying sand high excess pore pressures, and the resulting upward diffusion of pore-fluid toward the ground surface, and (3) towards the end of shaking, the sand layer exhibited a relative increase in acceleration amplitudes associated with a regain in shear stiffness; a mechanism that was also observed in laboratory experiments. This regain might be partially a result of densification and increased sand skeleton interlocking. The response of a sand-silt embankment showed that: (1) the overlaying silt stratum exhibited extremely low stiffness as the sand stratum liquefied, (2) the sand layer appeared to have partially regained shear stiffness towards the end of shaking, reflecting an observed gradual decrease in sand excess pore pressures and possible densification effects, (3) during liquefaction, large cyclic (downslope) shear strains in the sand layer were associated with an increase in soil strength, manifested in the form of large spikes in shear stress and recorded acceleration, along with drops in pore pressure. This response pattern occurred due to a tendency for soil-skeleton dilation at large strains, and has only appeared during the phases of cyclic deformation towards the embankment free slope, (4) the

sand cyclic dilative response and associated regain in stiffness may be a primary factor in dictating the magnitude of permanent shear strain towards an existing free slope, and (5) the observed deformation mechanisms and stiffness regain were in agreement with data from laboratory experiments.

Chapter 6

Acknowledgments

The research reported herein was supported by the United States Geological Survey (grant No. 1434-97-G-03070), the National Science Foundation (grant No. MSS-9057388), and the National Center for Earthquake Engineering Research (grant No. 90-1503). This support is gratefully acknowledged. The authors are grateful to Professor Kandiah Arulanandan for providing the VELACS data of UCD models 4a and 6.